

AFIT/GA/ENY/92D-08

AD-A258 840



BASELINE EXPERIMENTS ON
COULOMB DAMPING DUE TO
ROTATIONAL SLIP

THESIS

John P. Santacroce, Captain, USAF

AFIT/GA/ENY/92D-08

93-00031



DTIC
S **E** **D**
ELECTE
JAN 07 1993

Approved for public release; distribution unlimited

93 1 04 038

BASELINE EXPERIMENTS ON COULOMB DAMPING
DUE TO ROTATIONAL SLIP

THESIS

Presented to the Faculty of the School of Engineering
of the Air Force Institute of Technology
Air University
In Partial Fulfillment of the
Requirements for the Degree of
Master of Science in Astronautical Engineering

John P. Santacroce, B.S.A.E.
Captain, USAF

December 1992

Accession For	
NTIS CRA&I	<input checked="checked" type="checkbox"/>
DTIC TAB	<input type="checkbox"/>
Unannounced	<input type="checkbox"/>
Justification	
By _____	
Distribution/	
Availability Codes	
Dist	Avail and/or Special
A-1	

Approved for public release; distribution unlimited

UNCLASSIFIED

Acknowledgements

I would like to extend my appreciation to my principal advisor Dr. Torvik for his support, guidance and patience during the research effort. I would also like to extend my thanks to Dr. Leibst and Dr. Hall, both of whom were always willing to listen and give advice.

I also wish to thank Dr. Elrod for putting me in touch with Dr. Rabe of the Propulsion Laboratory, who in turn let me borrow the Surtronic 3 Profile Analyzer.

A special thanks is in order to John Brohas of the AFIT Model Shops for his work in manufacturing the test models, and to Jay Anderson for his help in calibrating the Internally Gauged Bolt Transducers.

I especially want to thank Andy Pitts for his help during the set-up of the experiments. Andy was instrumental in helping me to collect, assemble, and calibrate most of the laboratory equipment required for the experimental set-ups.

Finally, and most importantly, I would like to thank my wife Denise for her continued support and love throughout this entire project.

John

Table of Contents

	Page
Acknowledgments	ii
List of Figures	vi
List of Tables	x
Abstract	xiii
I. Introduction	1-1
1.1 Coulomb Damping Background	1-3
1.2 Problem Statement	1-6
1.3 General Approach and Assumptions	1-6
II. Theory	2-1
2.1 Coulomb Damping Theory	2-1
2.1.1. Simple Spring-Mass Model	2-2
2.1.2. Simple Rotating Circular Surfaces.	2-10
2.1.3. Richardson and Nolle Microslip Model.	2-13
2.1.4. Lieker Macroslip Model	2-19
2.1.5. Macroslip versus Microslip	2-20
2.2 Elementary Beam Theory	2-22
2.2.1. Euler-Bernoulli Beam	2-22
2.2.2. Euler-Bernoulli Beam versus Timoshenko Beam.	2-25
2.3 Theoretical Damping Models	2-26
2.3.1. Mark I Damping Model	2-27
2.3.2. Mark II Damping Model.	2-31
III. Experimental Geometry and Equipment	3-1
3.1 Mark I Beam-Joint Design (Inverted Beam)	3-2
3.1.1. Mark I Test Model.	3-2
3.1.2. Mark I Final Model	3-8

3.2	Mark II Beam-Joint Design (Horizontal Beam)	3-10
3.2.1.	Mark II Test Model	3-10
3.2.2.	Mark II Final Model.	3-12
3.3	Test Equipment	3-16
3.3.1.	Model 5PM Shaker	3-16
3.3.2.	Model TA30 Power Amplifier	3-16
3.3.3.	Oscillator-Servo-Programmer (OSP-4).	3-16
3.3.4.	Accelerometer.	3-17
3.3.5.	Force Transducer	3-17
3.3.6.	Fotonic Sensor	3-17
3.3.7.	Digital Analyzer	3-18
3.3.8.	Surtronic 3 Profile Analyzer	3-18
3.3.9.	Internally Gauged Bolt Transducers	3-18
IV.	Test Procedures and Data	4-1
4.1	Mark I (Free Vibration)	4-1
4.1.1.	Initial Test and Checkout.	4-1
4.1.2.	Test Procedures.	4-8
4.1.2.1.	Pre Testing Assembly and Set-up.	4-8
4.1.2.2.	Testing	4-9
4.1.2.3.	Data Reduction.	4-11
4.1.3.	Test Data.	4-11
4.2	Mark II (Forced Vibration)	4-14
4.2.1.	Initial Test and Checkout	4-14
4.2.2.	Test Procedures	4-24
4.2.2.1.	Pre Testing Assembly and Set-up	4-24
4.2.2.2.	Testing	4-29
4.2.2.3.	Data Reduction	4-31
4.2.3.	Test Data	4-32
4.2.3.1.	Test 1.	4-32
4.2.3.2.	Test 2.	4-34
4.2.3.3.	Test 3.	4-35
4.2.3.4.	Test 4.	4-36
4.2.3.5.	Test 5.	4-36
4.2.3.6.	Test 6.	4-37

4.2.3.7. Test 7.	4-37
4.2.3.8. Test 8.	4-38
V. Results and Discussion	5-1
5.1 Mark I	5-1
5.1.1. Test Results	5-1
5.1.2. Test Set-up.	5-4
5.2 Mark II	5-7
5.2.1. Preliminary Mark II Tests (tests 1 through 7).	5-7
5.2.1.1. Test 1.	5-7
5.2.1.2. Test 2.	5-11
5.2.1.3. Test 3.	5-13
5.2.1.4. Test 4.	5-15
5.2.1.5. Test 5.	5-20
5.2.1.6. Test 6.	5-28
5.2.1.7. Test 7.	5-32
5.2.2. Final Mark II Test (Test 8).	5-36
5.2.3. Mark II Test Set-up	5-41
VI. Conclusions and Recommendations	6-1
6.1 Conclusions	6-1
6.2 Recommendations	6-2
Appendix A: Test Equipment Specifications	A-1
Appendix B: Simple Spring-Mass FRICTION.m Script File	B-1
Appendix C: MATLAB Script.m Files	C-1
Appendix D: Mark II Test Data	D-1
Appendix E: Mark I Damping Model Slope Calculation	E-1
Bibliography	BIB-1
Vita	V-1

List of Figures

Figure	Page
1-1. Simplified Drawing of Mark I Design (Inverted Beam)	1-7
1-2. Simplified Drawing of Mark II Design (Horizontal Beam)	1-8
1-3. Spring-Bolt Assembly	1-9
1-4. Test Set-Up Schematic for Mark II	1-10
2-1. Simple SDOF Spring-Mass System	2-3
2-2. Free Body Diagrams for Spring-Mass System . .	2-4
2-3. Spring-Mass Model Illustration of Harmonic Motion with Friction.	2-9
2-4. Circular Contact Area and Shear Stress Distribution	2-12
2-5. Simplified Rotary Joint	2-13
2-6. Partially Slipped Region	2-16
2-7. Hysteresis Loop	2-18
2-8. Lieker Macroslip Model	2-20
2-9. Clamping Pressure versus Energy Dissipation .	2-21
2-10. Cantilevered Beam with Static Load at Tip . .	2-23
2-11. Mark I Free Body Diagram	2-28
2-12. Mark II Free Body Diagram	2-32
2-13. Displacement and Force Signals from MOMENT.m ($F_o=0.8$ lbs, $F_c=5$ lbs, $\mu=0.0$, 10Hz).	2-38
2-14. Displacement and Force Signals from MOMENT.m ($F_o=0.8$ lbs, $F_c=5$ lbs, $\mu=0.3$, 10Hz).	2-38
2-15. Theoretical Force versus Displacement Hysteresis Loop with Macroslip Friction ($F_o=0.8$ lbs, $F_c=5$ lbs, $\mu=0.3$, 10Hz).	2-39

2-16.	Example of Actual Displacement and Force Signal Data ($F_o \approx 1$ lb, $F_c=40$ lbs, 10Hz) . . .	2-39
2-17.	Example of Actual Displacement versus Force Hysteresis Loop ($F_o \approx 1$ lb, $F_c=40$ lbs, 10Hz) .	2-40
2-18.	Clamping Force versus Energy Dissipated from THEORY1.m ($F_o=0.8$ lbs, $\mu=0.3$, 10Hz).	2-40
3-1.	Mark I Test Model Beam	3-3
3-2.	Spacers and Set Screw Assembly	3-6
3-3.	Mark I Test Baseplates	3-8
3-4.	Mark I Final Assembly	3-9
3-5.	Mark II Beams	3-11
3-6.	Mark II Final Assembly	3-13
4-1.	Ra Measurement Positions for Mark I	4-10
4-2.	Example of Mark I Free Vibration Experimental Displacement versus Time Curve (Clamping Force = 1/4 Turn).	4-12
4-3.	Example of Data Smoothed Incorrectly	4-17
4-4.	Example of Data Smoothed Correctly	4-18
4-5.	Mark II Initial Testing Hysteresis Curves F10 and G10	4-21
4-6.	Ra Measurement Positions for Mark II	4-26
5-1.	Mark I Theoretical Displacement versus Time Curve ($F_c=3$ lbs, $u_o=0.18$ ft, $\mu=0.3$, slope= 0.0392 ft/sec)	5-5
5-2.	Mark I Experimental Displacement versus Time Curve (Clamping Force = 1/2 turn).	5-5
5-3.	Mark I Theoretical Displacement versus Time Curve ($F_c=0.5$ lbs, $u_o=0.18$ ft, $\mu=0.2$, slope= 0.0176 ft/sec)	5-6
5-4.	Mark II Test 1 Results versus Theoretical Energy Dissipation Curve	5-10

5-5.	Mark II Test 3 Results for Low Fo (0.6 lb) with 2nd Order Curve Fit	5-16
5-6.	Mark II Test 3 Results for Mid Fo (0.8 lb) with 2nd Order Curve Fit	5-16
5-7.	Mark II Test 3 Results for Hi Fo (1 lb) with 2nd Order Curve Fit	5-17
5-8.	Mark II Test 3 2nd Order Curve Fits	5-17
5-9.	Mark II Test 4 Results for Low Fo (0.6 lbs) with 2nd Order Curve Fit	5-18
5-10.	Mark II Test 4 Results for Mid Fo (0.8 lbs) with 2nd Order Curve Fit	5-18
5-11.	Mark II Test 4 Results for Hi Fo (1 lb) with 2nd Order Curve Fit	5-19
5-12.	Mark II Test 4 2nd Order Curve Fits	5-19
5-13.	Mark II Test 5A Results for Low Fo (0.6 lbs) with 2nd Order Curve Fit.	5-23
5-14.	Mark II Test 5A Results for Mid Fo (0.8 lbs) with 2nd Order Curve Fit.	5-23
5-15.	Mark II Test 5A Results for Hi Fo (1 lb) with 2nd Order Curve Fit	5-24
5-16.	Mark II Test 5A 2nd Order Curve Fits	5-24
5-17.	Mark II Test 5B Results for Low Fo (0.6 lbs) with 2nd Order Curve Fit	5-25
5-18.	Mark II Test 5B Results for Mid Fo (0.8 lbs) with 2nd Order Curve Fit	5-25
5-19.	Mark II Test 5B Results for Hi Fo (1 lb) with 2nd Order Curve Fit	5-26
5-20.	Mark II Test 5B 2nd Order Curve Fits	5-26
5-21.	Mark II all Results from Test 3 and Test 5A for Mid Fo (0.8 lbs) with 2nd Order Curve Fit . . .	5-27
5-22.	Mark II Test 3 and Test 5A for Mid Fo (0.8 lbs) 2nd Order Curve Fits	5-27

5-23.	Mark II Test 7A Results plotted against Theoretical Energy Dissipation Curve	5-35
5-24.	Mark II Test 7B Results plotted against Theoretical Energy Dissipation Curve	5-35
5-25.	Mark II Test 8A Results plotted against Theoretical Energy Dissipation Curve ($\mu=0.38$)	5-39
5-26.	Mark II Test 8B Results plotted against Theoretical Energy Dissipation Curve ($\mu=0.40$)	5-39
5-27.	Mark II Test 8A Results plotted against Theoretical Energy Dissipation Curve ($\mu=0.43$)	5-40
5-28.	Mark II Test 8B Results plotted against Theoretical Energy Dissipation Curve ($\mu=0.45$)	5-40
5-29.	Mark II Test 8A Results plotted against Upper and Lower Theoretical Energy Dissipation Curves	5-46
A-1.	Schematic of Force Transducer Calibration Set-up	A-8
A-2.	Fotonic Sensor Calibration Curve for Mark II Tests 6,7, and 8	A-15
A-3.	Definition of Ra	A-18
B-1.	MATLAB Friction.m Plot ($m=1$ kg, $k=1$ N/m, $\mu=0.0$, $x_0=1$ m)	B-3
B-2.	MATLAB Friction.m Plot ($m=1$ kg, $k=1$ N/m, $\mu=0.01$, $x_0=1$ m)	B-3
B-3.	MATLAB Friction.m Plot ($m=1$ kg, $k=1$ N/m, $\mu=0.01$, $x_0=1$ m)	B-4
B-4.	MATLAB Friction.m Plot ($m=1$ kg, $k=2$ N/m, $\mu=0.01$, $x_0=1$ m)	B-4

List of Tables

Table	Page
3-1. Mark I Specifications	3-14
3-2. Mark II Specifications.	3-15
4-1. Mass and Physical Dimensions of Mark I	4-1
4-2. Computed versus Measured Moments of Inertia and Natural Frequencies for Mark I	4-4
4-3. Mark I General Test Parameters	4-12
4-4. Mark I Free Vibration Test Data	4-13
4-5. Mark II Initial Testing Grid	4-16
4-6. Mark II Initial Testing Results	4-20
4-7. OSP-4 Front and Back Panel Settings	4-28
4-8. Mark II Test 1 General Parameters	4-33
4-9. Mark II Test 1 AREA.m Data (10Hz)	4-34
4-10. Mark II Test 1 EXPDATA.m Results (10Hz)	4-34
A-1. Model 5PM Shaker Specifications	A-3
A-2. Model TA30 Power Amplifier Specifications	A-4
A-3. Oscillator-Servo-Programmer (OSP-4) Specifications	A-6
A-4. ENDEVCO Accelerometer Model 2235C Specifications.	A-7
A-5. Force Transducer Calibration Data	A-10
A-6. PCB Model No. 208A02 Force Transducer and PCB Model No. 480C06 Power Unit Specifications.	A-11
A-7. Fotonic Sensor Probe/Plug-in Module Specifications	A-12
A-8. Surtronic 3 Specifications	A-19

A-9.	Axial Clamping Forces versus Applied End Loads for fully Clamped Joint (Coefficient of Friction = 0.3)	A-21
A-10.	Internally Gauged Bolt Specifications	A-23
D-1.	Mark II Test 1 General Parameters	D-1
D-2.	Mark II Test 1 AREA.m Data (10Hz)	D-2
D-3.	Mark II Test 1 EXPDATA.m Results (10Hz)	D-2
D-4.	Mark II Test 2 General Parameters	D-3
D-5.	Mark II Test 2A AREA.m Data	D-4
D-6.	Mark II Test 2A EXPDATA.m Results	D-5
D-7.	Mark II Test 2B AREA.m Data (10Hz)	D-6
D-8.	Mark II Test 2B EXPDATA.m Results (10Hz).	D-7
D-9.	Mark II Test 3 General Parameters	D-8
D-10.	Mark II Test 3 AREA.m Data (10Hz)	D-9
D-11.	Mark II Test 3 EXPDATA.m Results (10Hz)	D-10
D-12.	Mark II Test 4 General Parameters	D-11
D-13.	Mark II Test 4 AREA.m Data (15Hz)	D-12
D-14.	Mark II Test 4 EXPDATA.m Results (15Hz)	D-13
D-15.	Mark II Test 5 General Parameters	D-14
D-16.	Mark II Test 5A AREA.m Data (10Hz)	D-15
D-17.	Mark II Test 5A EXPDATA.m Results (10Hz).	D-16
D-18.	Mark II Test 5B AREA.m Data (15Hz)	D-17
D-19.	Mark II Test 5B EXPDATA.m Results (15Hz).	D-18
D-20.	Mark II Test 6 General Parameters	D-19
D-21.	Mark II Test 6A AREA.m Data (10Hz)	D-20
D-22.	Mark II Test 6A EXPDATA.m Results (10Hz).	D-21

D-23.	Mark II Test 6B AREA.m Data (10Hz)	D-22
D-24.	Mark II Test 6B EXPDATA.m Results (10Hz).	D-23
D-25.	Mark II Test 7 General Parameters	D-24
D-26.	Mark II Test 7A AREA.m Data (10Hz)	D-25
D-27.	Mark II Test 7A EXPDATA.m Results (10Hz).	D-26
D-28.	Mark II Test 7B AREA.m Data (10Hz)	D-27
D-29.	Mark II Test 7B EXPDATA.m Results (10Hz).	D-28
D-30.	Mark II Test 8 General Parameters	D-29
D-31.	Mark II Test 8A AREA.m Data (10Hz)	D-30
D-32.	Mark II Test 8A EXPDATA.m Results (10Hz).	D-31
D-33.	Mark II Test 8B AREA.m Data (10Hz)	D-32
D-34.	Mark II Test 8B EXPDATA.m Results (10Hz).	D-33

Abstract

Two experimental pin-type joint models are developed for the purpose of studying the effects of Coulomb Damping due to rotational slip. Model One is an inverted beam with a large mass at the end, allowed to pivot at one end as a pendulum. Model Two is a horizontally mounted beam, allowed to pivot about its center. Model One is a free vibration model, and Model Two is a forced vibration model. The equations of motion for the joint geometries, considering only macro-slip friction, are developed and solved to provide an expression relating the various parameters of the experimental and theoretical models. Theoretical and experimental results for the response of the models in vibration are presented showing energy dissipation versus clamping force for the joint(s).

BASELINE EXPERIMENTS ON COULOMB DAMPING DUE TO ROTATIONAL SLIP

I. Introduction

There are two options for stabilizing and controlling large space structures (LSSs): active and passive control¹. Active control utilizes active elements to maintain stability and to alter the dynamic response of the structure. Passive control relies instead on the inherent structural rigidity and dissipation characteristics of the structure. In a passively controlled structure, the material and structural damping characteristics provide the only means for dissipating vibrational energy. In active control, the structural damping must insure the stability of the uncontrolled modes. Furthermore, a detailed characterization of the origin of structural damping is required for system identification, for optimal estimator based control, and for fault detection¹. In either case, it is necessary to include structural damping in the design, to understand the dissipation mechanisms involved, and be able to experimentally measure and analytically model those mechanisms¹.

The current design of LSSs makes use of low mass materials which reduce the inherent damping mechanisms available, and as a result large complex artificial damping mechanisms are required to provide stability². Many schemes

have been proposed for increasing the passive structural damping of a structure. One in particular is Coulomb damping, or dry friction damping¹. Ninety percent of the damping in most structures is due to the friction damping of the structural joints, and as such it provides the greatest potential for increasing structural damping³. There are several advantages for investigating the friction damping in joints. First, the use of complex active damping systems can be reduced by using friction damping as a source of energy dissipation. Second, friction damping is essentially cost free and, as mentioned previously, has the potential for high energy dissipation. Finally, by using friction damping in joints, the original geometry of a structure can be maintained⁴.

Unfortunately, the analysis of Coulomb damping is not without problems. First, the possibility of wear and corrosion exists, which could ultimately cause failure of the joint and potentially the entire structure. Second, the overall structural stiffness of a system is reduced which may be unacceptable, and finally the nonlinearity of the friction problem presents difficulties in analysis³. However, as the development of LSSs continues, the benefits gained by friction damping in joints can no longer be ignored, and the disadvantages of analysis from allowing friction in the joint can be overcome⁵. The effects of wear and corrosion can be

reduced while still maintaining good energy dissipation characteristics through careful surface preparation⁶. Furthermore, Beards has shown that the overall stiffness characteristics of a structure are better maintained if joints are allowed to slip in rotation and not in translation⁷. It has also been shown that the best environment for friction damping is one in which the cycle frequency is low in order to minimize wear, and the environment is controlled in order to keep corrosion to a minimum¹. LSSs with low vibratory frequencies can provide such an environment.

1.1 Coulomb Damping Background

The understanding of friction damping phenomena, both in analytical studies and experimental verification, can be broken down into two analytical approaches: microslip and macroslip⁸. In macroslip, the entire joint surface is assumed to be totally stuck or totally slipping. The frictional energy dissipation mechanism associated with the joint contact surfaces is assumed to be governed by some form of Coulomb's law of dry friction. In the microslip approach, the joint interface progressively moves from stuck to total slip. The microslip approach is a much more complex approach than the macroslip and requires a relatively detailed analysis of the stress distribution at the contact surface.

Macroslip analytical analysis has been conducted on both single-degree-of-freedom (SDOF) systems, and multi-degree-of-freedom (MDOF) systems. Den Hartog obtained an exact solution for a SDOF system at a steady state stick-then-slip motion⁹. Pratt and Williams extended this type of analysis to a MDOF system with similar results¹⁰. But the macroslip model is not enough to obtain a complete understanding of the damping associated with the slip motion of friction joints¹¹. The energy dissipation of an axial double lapped joint under macroslip and then total slip was analyzed by Earles and Philput¹². Their analysis indicated that the energy dissipated was proportional to the cube of the load and inversely proportional to the coefficient of friction for the partial or macroslip case. Their experiments were conducted on plain stainless steel flat plates with the frictional damping occurring under oscillating tangential loads. They obtained a close agreement for the macroslip region obtained previously by analytical means developed in 1958 by Panovko et al¹³ (for a review of this work in English see Reference 14). Two excellent sources for the latest references concerning both passive and active damping, and the modeling and analysis of LSSs whose behavior is strongly influenced by joints can be found in References 15 and 24. A recent application of dry friction damping analysis that has been applied to a LSS in which a truss structure is made of tubular members was done by

Crawley et al¹. Here a friction damping mechanism was considered that consisted of segmented damping tubes placed end to end inside the tubular load carrying members. A simple microslip Coulomb type friction model was analyzed to determine the energy loss per cycle. The resulting data showed close agreement between experiments and theory.

It can be argued that the analysis conducted by Crawley, as with the analysis on the axial lap joint, dealt with pure translational motion. The other fundamental case of motion is that of pure rotational motion, or slip in a pin-type rotary joint. A common form of a pin-type rotary joint is a bolted or riveted joint.

Beards and Williams conducted an experiment which indicated that a useful increase in the damping of a structure could be achieved by fastening joints tightly to prohibit translational slip, but not tightly enough to prohibit rotational slip⁷. Ferri and Heck analyzed a modified pin-type joint which allowed the normal force to vary with the relative rotation angle²⁴. They concluded that joints designed with amplitude or rate-dependent frictional forces can offer substantial improvements in performance over joints with constant normal forces²⁴. As noted by Ferri and Heck, any passive joint design must be well suited to automated or human space platform construction, and must not adversely affect the structural integrity or weight of the structure. Several

analytical studies on the energy dissipation of simple rotary-type structural joints have been accomplished^{4,5,16}. This paper will deal primarily with energy dissipation by rotational slip in a pin-type rotary joint (bolted joint).

1.2 Problem Statement

The purpose of this thesis is to select an experimental geometry for a representative joint and to measure and analyze damping due to Coulomb friction when rotational slip occurs within that joint.

1.3 General Approach and Assumptions

A bolted joint was selected as the physical model for a pin-type rotary joint. Two different test designs are considered: Mark I and Mark II. The Mark I design is an inverted beam with a bolted joint at the upper end, and the Mark II design is a horizontal beam with a bolted joint located in the middle. The Mark I is a free vibration model, and the Mark II is a forced vibration model. A sketch of these designs can be seen in Figures 1-1 and 1-2. A detailed description of the beam geometries can be found in Chapter 3. The purpose of the beams in both designs is to allow for the application of external moments at the joints. The principal design criteria for the experimental geometry is that when rotation occurs the primary cause of energy dissipation would

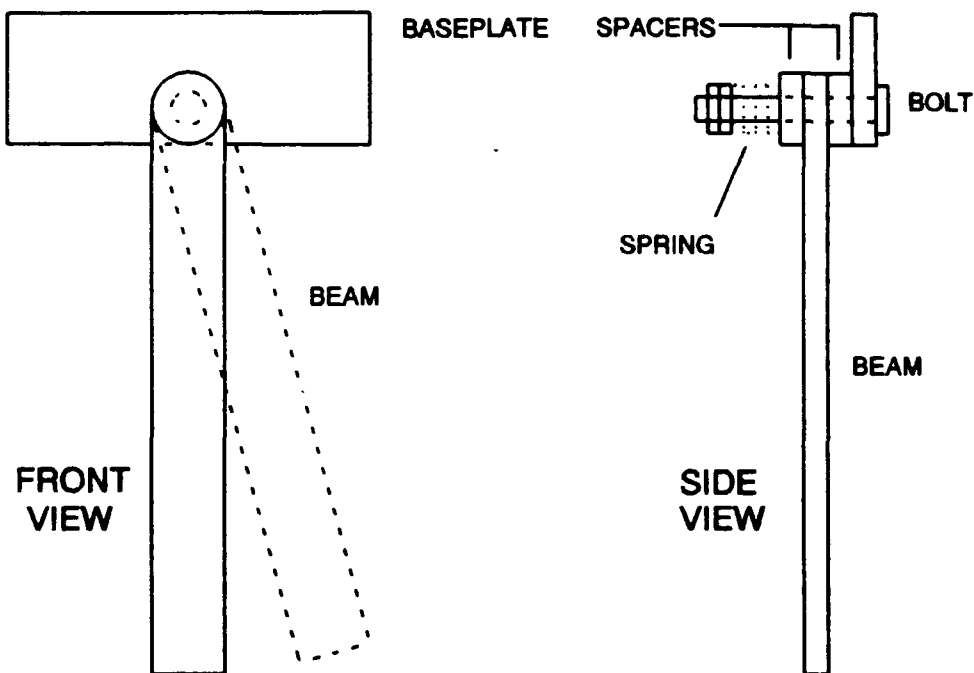


Figure 1-1. Simplified Drawing of Mark I Design
(Inverted Beam)

be due to the rotational slip of the contact areas in the joint. As such, very rigid beams are desired. It is assumed that the energy dissipated by the beams due to bending is negligible compared with the energy dissipated by friction damping at the joint. The test models are constructed from cold rolled stock steel and the final models are constructed from stainless steel. Steel was chosen as a suitable material to meet the requirements for a stiff beam and a twist

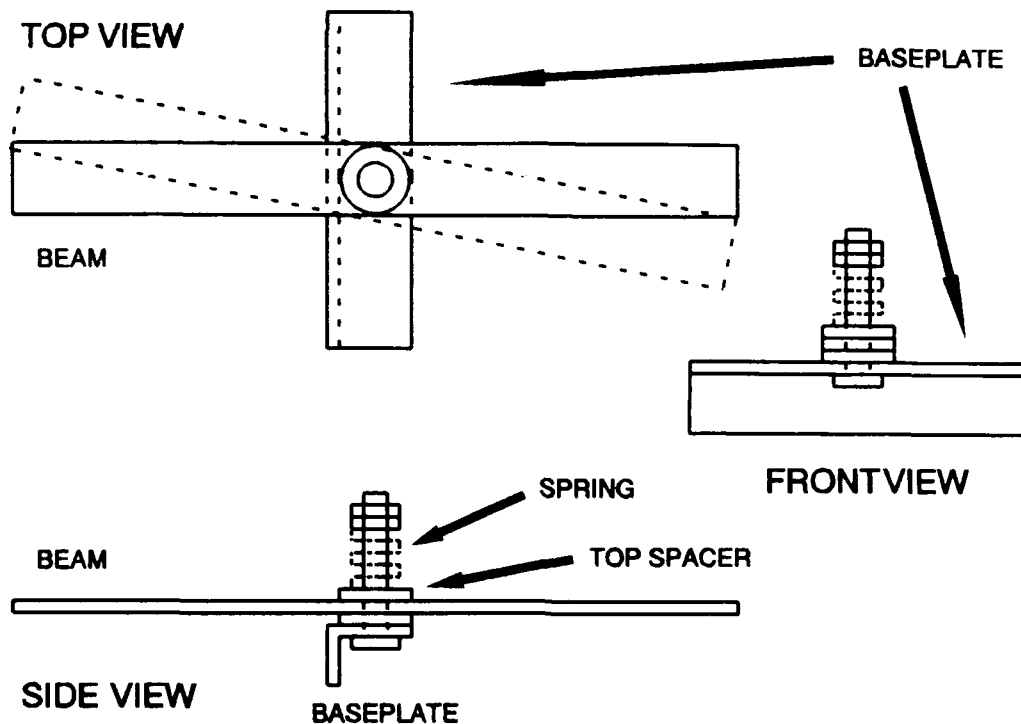


Figure 1-2. Simplified Drawing of Mark II Design
(Horizontal Beam)

resistant friction contact surface. Stainless steel was chosen in an attempt to further control the condition of the friction surface by keeping it free of rust.

The beams in both designs are sandwiched between two thick spacers, or washers, both fixed into place. Under dynamic loading of the beam, the spacers are assumed not to move. The following discussion refers to the Mark II joint design only. (The Mark I design is very similar, except where

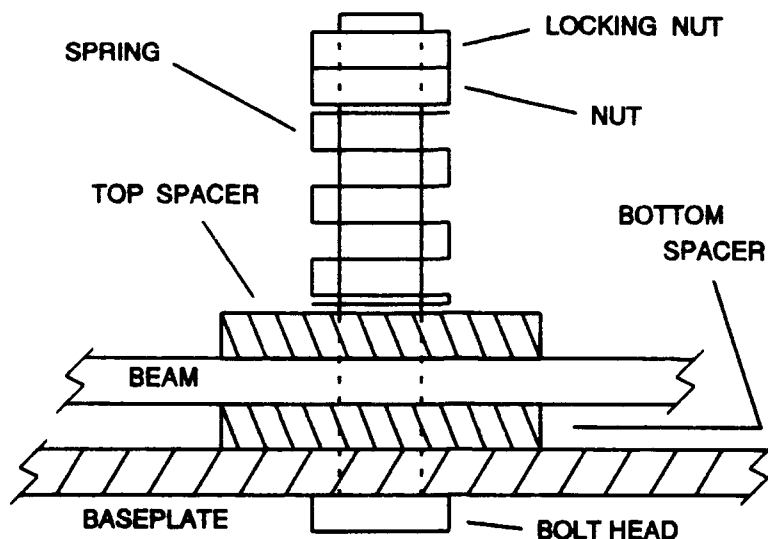


Figure 1-3. Spring-Bolt Assembly

the words "top" and "bottom" are used, replace them with "inner" and "outer"). The bottom spacer is welded into place on top of the baseplate and the top spacer is locked into place with set screws. The clamping pressure of the joint is adjusted via a spring-bolt assembly (see Figure 1-3). It is assumed that the spring-bolt assembly, in conjunction with the relatively thick spacer provides a fairly uniform and constant clamping pressure on the contact surfaces (the top and bottom of the beam). External moments are applied to the joint by attaching a 50lb shaker to the end of the beam. Figure 1-4 is a schematic of a test set-up for the Mark II Beam. Load-deflection (in this case, moment-rotation) hysteresis curves

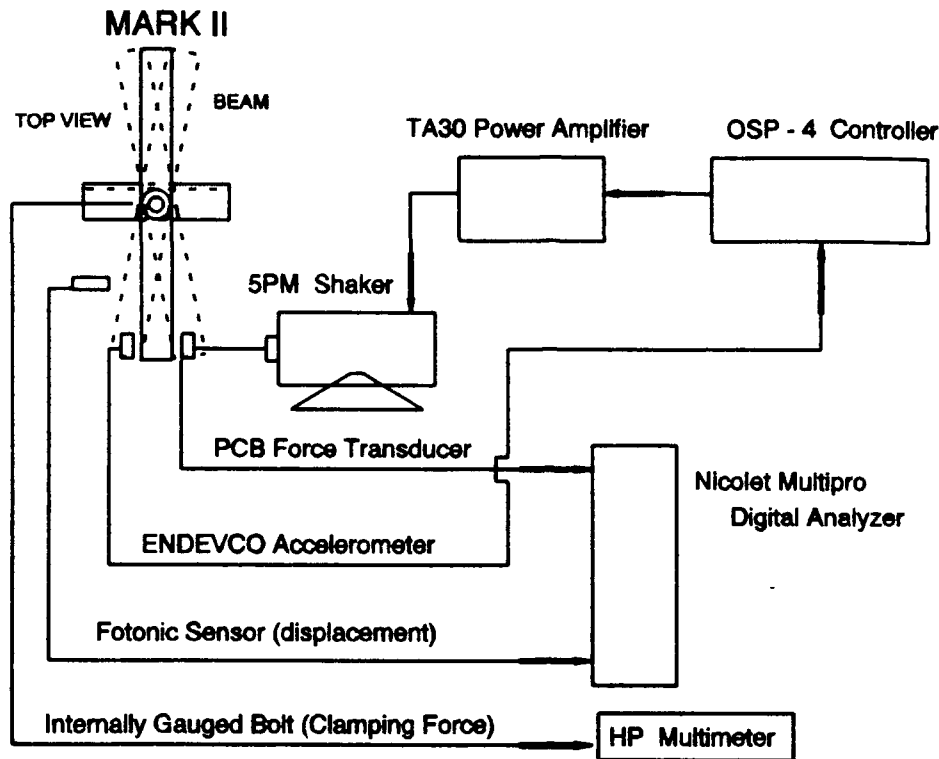


Figure 1-4. Test Set-Up Schematic for Mark II

are integrated over one cycle to give an energy loss per cycle for a constant clamping pressure. The axial clamping pressure of the bolt is measured by an internally mounted strain gage located in the bolt shank. A force transducer between the shaker and the beam, and an optically driven displacement sensor provide a force-displacement history of the system under dynamic loading. A force-displacement hysteresis curve is generated from simple trigonometric relationships assuming small rotations and a rigid beam. An accelerometer collocated with the force transducer provides a feedback signal in order

to control the desired loading or displacement of the beam under cyclic loading. The Mark I is set into free vibration motion, and for various clamping forces at the joint, displacement versus time curves are generated. Energy dissipation at the joint is determined by measuring the slope of the envelope of decay of the displacement peaks as the motion decays to zero.

This thesis is presented in six chapters. The present chapter seeks only to familiarize the reader with the basic problem, the general experimental procedure, and the results of a literature search which showed that interest in the field of friction damping has been around for a long time and has in recent years become a major area of investigation with the advent of LSSs. Chapter 2 sets forth the basic theory and assumptions associated with both translational and rotational Coulomb friction, elementary beam theory, and presents the analytical friction models. Chapter 3 details the experimental geometries of the Mark I and Mark II, and the equipment used in the experiment. Chapter 4 outlines the test procedures and presents the data collected. Chapter 5 discusses the results of the experimental data, and Chapter 6 presents the conclusions and recommendations for further study.

II. Theory

2.1 Coulomb Damping Theory

Coulomb, or dry friction, damping occurs whenever two or more surfaces in contact are allowed to slide relative to one another. For any movement to occur, there must exist some external force strong enough to overcome the resistance caused by the friction between the two surfaces. Two interesting facets of Coulomb damping are significant¹⁷. The first is its extent. All real damping must be partly due to Coulomb damping, since only dry friction damping can stop motion. In viscous damping, motion theoretically continues forever, granted of course at infinitesimally small amplitudes. The second is that Coulomb damping does not alter the natural frequency of the system.

The classical law of sliding friction states that the frictional force is independent of both the contact area and the magnitude of the relative velocity between the surfaces, as long as sliding exists¹⁸. The friction force is parallel to the contact surface and is proportional to the force normal to the contact surface. The friction force is of constant magnitude, and as long as relative motion occurs, it will exist. In order to illustrate some of the concepts about Coulomb damping, a simple SDOF system (translational motion) and a simple rotating circular shaft are discussed below,

followed by a discussion of macroslip and microslip models for rotary joints under dynamic loading.

2.1.1. Simple Spring-Mass Model. Figure 2-1 represents the simplest form of a vibrating system with Coulomb damping. A block of mass, m , translates on a surface and is attached to a linearly elastic helical spring with a spring constant of k . The spring constant, k , represents the force required to produce a unit change in the length of the spring. The spring provides a restoring force against motion away from equilibrium. The block sits on a surface such that a coefficient of sliding friction, μ , exists between the block and the surface. The coefficient of friction is a constant of proportionality between the force acting normal to the contact surface (the weight of the block) and the friction force, f_d . The coefficient of friction depends only on the roughness of the sliding surfaces. The friction force is given as

$$f_d = \pm \mu mg \quad (2-1)$$

where

μ = coefficient of friction
 m = mass of the block
 g = acceleration due to gravity

The friction force always opposes the motion of the block. When the velocity of the block, $\dot{x}(t)$ is positive, f_d is negative, and f_d is positive for a negative velocity. The configuration of the block is determined completely by the translation, $x(t)$, of the block from its equilibrium position,

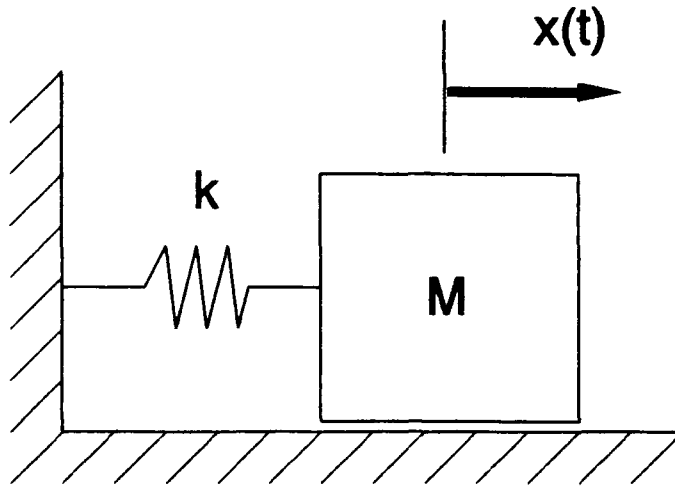


Figure 2-1. Simple SDOF Spring-Mass System

and is measured positive to the right as shown.

Figure 2-2 shows the free body diagrams for the block for positive and negative velocities. The equation of motion for the block is non-linear, due to the switching of the friction force sign, but it can be separated into two linear equations; one for positive velocity and one for negative velocity. From the free body diagrams the equations of motion are:

$$\ddot{x} + \frac{k}{m}x = -\frac{\bar{f}_d}{m} \quad \dot{x} > 0 \quad (2-2)$$

$$\ddot{x} + \frac{k}{m}x = \frac{\bar{f}_d}{m} \quad \dot{x} < 0 \quad (2-3)$$

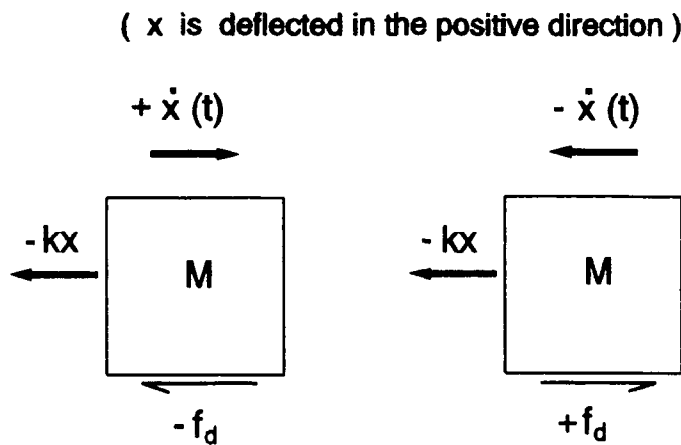


Figure 2-2. Free Body Diagrams for Spring-Mass System

Both Equations (2-2) and (2-3) are valid linear equations of motion for a specific range of velocities, but it should be noted that the switching does not occur as an explicit function of time but is determined by the response of the system and could occur at various times depending on the forcing function (if any) and the initial conditions⁴. Therefore, the solution of the equations of motion must take place over one time interval depending on the sign of $\dot{x}(t)$. A solution for this type of system can be found in several papers and texts, most notably in Den Hartog's classic paper⁹. In the present paper, a solution is derived using Laplace transformations.

Taking the Laplace transformation of Equation (2-2) yields

$$s^2X(s) - sx(0) - \dot{x}(0) + \frac{k}{m}X(s) = -\frac{f_d}{m} \frac{1}{s} \quad (2-4)$$

where $X(s) = x$ in the Laplace Domain
 $x(0) =$ initial value of x at time equal to zero
 $\dot{x}(0) =$ initial value of \dot{x} at time equal to zero

Recall that the friction force, f_d , is a constant force as long as relative motion between the block and the surface exists. In the Laplace domain, this type of force can be represented easily as a unit step. Solving for $X(s)$:

$$X(s) = x(0) \frac{s}{s^2 + \frac{k}{m}} + \dot{x}(0) \frac{1}{s^2 + \frac{k}{m}} - \frac{f_d}{ms} \frac{1}{s^2 + \frac{k}{m}} \quad (2-5)$$

The first two components of Equation (2-5) can be readily inverted back into the time domain but the third component must be reduced first by using partial fractions:

$$\frac{-\frac{f_d}{m}}{s(s^2 + \frac{k}{m})} = \frac{A}{s} + \frac{Bs + C}{s^2 + \frac{k}{m}} \quad (2-6)$$

from which

$$As^2 + A\frac{k}{m} + Bs^2 + Cs = -\frac{f_d}{m} \quad (2-7)$$

where $C=0$ and $A+B=0$. Therefore, $A = -f_d/k$ and $B = f_d/k$. Substituting the solutions for A and B into Equation (2-6), and then into Equation (2-5) gives

$$X(s) = x(0) \frac{s}{s^2 + \frac{k}{m}} + \dot{x}(0) \frac{1}{s^2 + \frac{k}{m}} - \frac{f_d}{k} \left(\frac{1}{s} - \frac{s}{s^2 + \frac{k}{m}} \right) \quad (2-8)$$

Using the Laplace inverse identities for the cosine, sine, and unit step functions¹⁹, Equation (2-8) becomes:

$$x(t) = x(0) \cos \sqrt{\frac{k}{m}} t + \frac{\dot{x}(0)}{\sqrt{\frac{k}{m}}} \sin \sqrt{\frac{k}{m}} t - f_d \left(\frac{1}{k} - \frac{1}{k} \cos \sqrt{\frac{k}{m}} t \right) \quad (2-9)$$

The natural frequency of vibration, ω_n , for the system is defined as the square root of k divided by m ¹⁷, or

$$\omega_n = \sqrt{\frac{k}{m}} \quad (2-10)$$

Substituting Equation (2-10) into Equation (2-9) gives

$$x(t) = x(0) \cos \omega_n t + \frac{\dot{x}(0)}{\omega_n} \sin \omega_n t - f_d \left(\frac{1}{k} - \frac{1}{k} \cos \omega_n t \right) \quad (2-11)$$

Equation (2-11) is a solution to the equation of motion given in Equation (2-2). The solution to Equation (2-3) can be found in a similar fashion and is:

$$x(t) = x(0)\cos\omega_n t + \frac{\dot{x}(0)}{\omega_n}\sin\omega_n t + f_d\left(\frac{1}{k} - \frac{1}{k}\cos\omega_n t\right) \quad (2-12)$$

Note that Equation (2-11) is valid for $\dot{x}(t) > 0$ and Equation (2-12) is valid for $\dot{x}(t) < 0$ only.

Now assume the initial conditions are $x(0) = x_0$ where x_0 is positive, and $\dot{x}(0) = 0$. Since $\dot{x}(t)$ will start off as negative the solution can be found using Equation (2-12). Substituting in the initial conditions gives

$$x(t) = \left(x_0 - \frac{f_d}{k}\right)\cos\omega_n t + \frac{f_d}{k} \quad (2-13)$$

This equation represents harmonic oscillation and is valid for $0 \leq t \leq t_1$, where t_1 is the time at which the velocity reduces to zero and the motion is about to reverse. Differentiating Equation (2-13), the velocity can be found.

$$\dot{x}(t) = -\omega_n\left(x_0 - \frac{f_d}{k}\right)\sin\omega_n t \quad (2-14)$$

The lowest non-trivial solution satisfying the initial condition of $\dot{x}(0)=0$ is $t_1=\pi/\omega_n$. If the restoring force, k times the displacement $x(t_1)$, is large enough to overcome the static friction, the mass will have a positive velocity and then the other equation of motion given by Equation (2-2) must be satisfied. The solution is given by Equation (2-11), or

$$x(t) = (x(t_1) - \frac{f_d}{k}) \cos \omega_n t - \frac{f_d}{k} \quad (2-15)$$

where $x(t_2) = -(x_0 - 2f_d/k)$. Equation (2-15) can then be rewritten as:

$$x(t) = (x_0 - 3 \frac{f_d}{k}) \cos \omega_n t - \frac{f_d}{k} \quad (2-16)$$

Equation (2-16) is valid for the values of $t_1 \leq t \leq t_2$ where t_2 is the value at which the velocity again goes to zero. The value for t_2 can be found in a manner similar to the way t_1 was found above. The value of t_2 is found to be $2\pi/\omega_n$. This procedure is then repeated for $t > t_2$ until motion stops. Motion will eventually stop when the restoring force due to the spring is no longer capable of overcoming the friction force.

A plot showing the decay as a function of time is shown in Figure 2-3. The response of the system consists of a harmonic component and a constant component superimposed on each other much the same way as in viscous damping, however here the decay envelope is linear in time¹⁷. The change in amplitude per cycle is a constant and equal to:

$$x_1 - x_2 = 4 \frac{f_d}{k} \quad (2-17)$$

where, x_1 and x_2 are the amplitudes of successive peaks as seen in Figure 2.3. The $4f_d/k$ term defines the envelope of decay. The duration of every half-cycle is equal to π/ω_n . Also note that the average value of the solutions switches between f_d/k

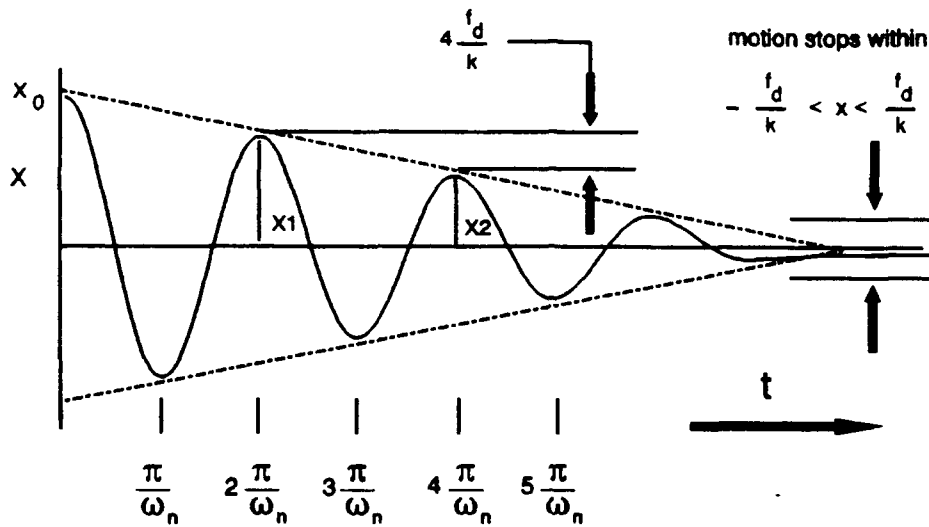


Figure 2-3. Spring-Mass Model Illustration of Harmonic Motion with Friction

and $-f_d/k$, and at the end of each half-cycle the displacement is reduced by $2f_d/k$.

It is interesting to note that for this system, the energy lost per cycle due to the Coulomb damping force is

$$W_d = \oint f_d dx \quad (2-18)$$

which upon integration gives

$$W_d = 2f_d(x_1 + x_2) \quad (2-19)$$

where W_d = energy loss per cycle. The last equation allows for the calculation of amplitude decay per cycle given the energy loss per cycle and the damping force⁵.

A computer program was written in MATLAB to examine the solutions derived above. A SCRIPT.m file was created, and various position versus time, velocity versus time, and position versus velocity plots (phase portraits) were generated to illustrate the concepts discussed here. The program and plots can be found in Appendix B. A sliding block illustrates the most basic ideas about Coulomb damping. The next step is to look at simple rotating surfaces experiencing Coulomb damping.

2.1.2. Simple Rotating Circular Surfaces. Greenwood associates Coulomb friction with rotational slip by looking at the force of sliding friction coming from a frictional shear stress at the contact area that is equal to μ times the normal pressure¹⁸. This gives a result similar to the simpler case of the sliding block, but aids in the analysis of more complicated systems, such as curved contact surfaces, non-uniform pressures, or velocity distributions.

As an example, consider the frictional moment arising from the flat end of a circular rotating shaft of radius R being pressed against a plane surface with a total clamping

force N^{18} . Assuming a uniform normal pressure at the contact area, there is a uniform frictional stress of magnitude

$$\tau_f = \frac{\mu N}{\pi R^2} \quad (2-20)$$

which is everywhere in direction normal to a radial line drawn from the center of the circular contact area¹⁸. Figure 2-4 illustrates the circular contact area and shear stress distribution on that surface. The incremental moment due to an annular element of width dr and area $(2\pi r)dr$ is

$$dM = \frac{\mu N}{\pi R^2} 2\pi r^2 dr \quad (2-21)$$

which when integrated gives the total frictional moment

$$M = \frac{2\pi N}{R^2} \int_0^R r^2 dr = \frac{2}{3} \mu NR \quad (2-22)$$

If the contact surface is perfectly smooth, then $\mu=0$. If on the other hand, the surface is so rough that no slipping can occur, then it can be argued that $\mu=\infty$. The first of these conditions ($\mu=0$) represents a no-clamping case in which the friction force is zero. For values of μ between these two extremes, the static friction force will build up to a peak value, and if the applied load exceeds this peak value then the entire contact surface of the joint begins to slip. This of course, is a description of macroslip or gross slip and is valid for the approximate analysis of simple rotating circular contact areas.

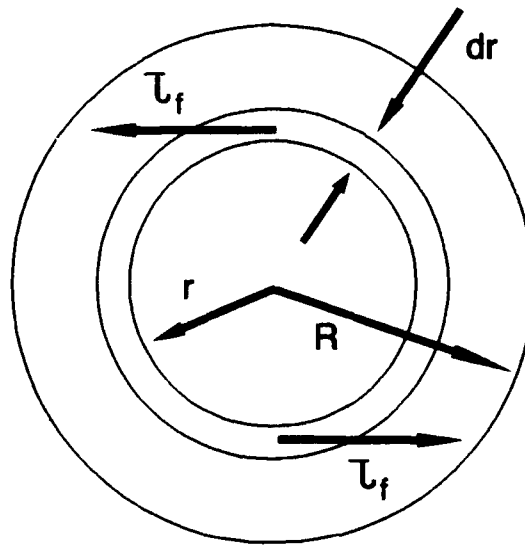


Figure 2-4. Circular Contact Area and Shear Stress Distribution¹⁸

As in the case of the sliding block, when the contact surfaces of the joint move relative to one another, the relative motion is resisted by Coulomb friction forces. For the rotating shaft, the energy lost due to friction can be calculated by multiplying the frictional force on a given elemental area by the relative velocity at that point and integrating over the contact area and over the required time interval¹⁸. No energy is dissipated in friction for either a perfectly smooth or infinitely rough surface. As discussed earlier, a perfectly smooth surface has no friction force, and an infinitely rough surface has no relative velocity.

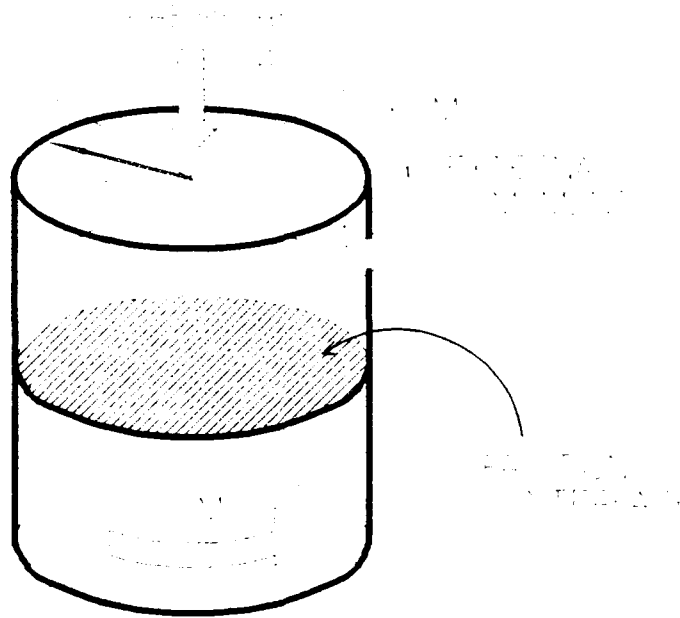


Figure 2-5. Simplified Rotary Joint¹⁶

The analysis of the sliding block and the rotating circular surface were done from the macroslip point of view; the entire contact surface area was assumed to be totally stuck or totally slipping. The next step is to look at macroslip and microslip models for circular contact surfaces under dynamic loading.

2.1.3. Richardson and Nolle Microslip Model. Richardson and Nolle developed a micro-slip model for a rotary joint¹⁶. The micro-slip model allows for partial slip in the outer joint radius while the inner joint radius is assumed to behave like a rigid body. The joint consists of two elastic members

in contact over a circle of radius R , as shown in Figure 2-5. A constant clamping force N is applied normal to the contact surface resulting in a uniform clamping pressure P throughout the joint. Note that the moments are applied about the joint axis. These moments cause friction shear stresses to build up at the interface and microslip between the two members occurs¹⁶. The analysis continues on the basis of the following assumptions as stated by Richardson and Nolle:

1. The friction shear stress is of constant magnitude, given by the product of the coefficient of friction and the normal pressure.
2. The friction shear stress exists only in those parts of the contact surface over which relative slip has occurred.
3. There is no twisting of axial elements (the joint does not resemble that of an elastic shaft in torsion).

The purpose for these assumptions is to relate the externally applied moment to a region of slip in the joint. The frictional shear stresses will build-up and cause slip to occur at the outer radius R and proceed inward to that radius, a , which balances the internal moment caused by the frictional shear stress in the slipped region and the external moment¹⁶. These frictional shear stresses create a shear strain and thus a relative rotation in the joint which will dissipate energy. Figure 2-6 shows the slipped region for a particular value of an externally applied moment⁵. As the external moment is

increased, a will decrease. Similarly, as the external moment is decreased, a will increase.

From equilibrium the external moment, M_{external} , will be balanced by the internal frictional moment M_{friction} , or

$$M_{\text{external}} - M_{\text{friction}} = 0 \quad (2-23)$$

M_{friction} can be found by double integrating the clamping pressure P times μ over the entire area times the moment arm from a to R :

$$M_{\text{friction}} = \int_a^R \int_0^{2\pi} \pi (\mu P \cdot r) r dr d\theta \quad (2-24)$$

which upon integration will yield,

$$M_{\text{friction}} = \frac{2}{3} \pi \mu P (R^3 - a^3) \quad (2-25)$$

substituting Equation (2-24) back into Equation (2-23), then

$$M_{\text{external}} = \frac{2}{3} \pi \mu P (R^3 - a^3) \quad (2-26)$$

The clamping pressure, P , is equal to the normal force, N , per unit area, π/R^2 . Substituting in for P gives

$$M_{\text{external}} = \frac{2}{3} \frac{\mu N}{R^2} (R^3 - a^3) \quad (2-27)$$

which is the external moment in terms of the clamping force. Note that Equation (2-27) is equivalent to Equation (2-22) when $a=0$.

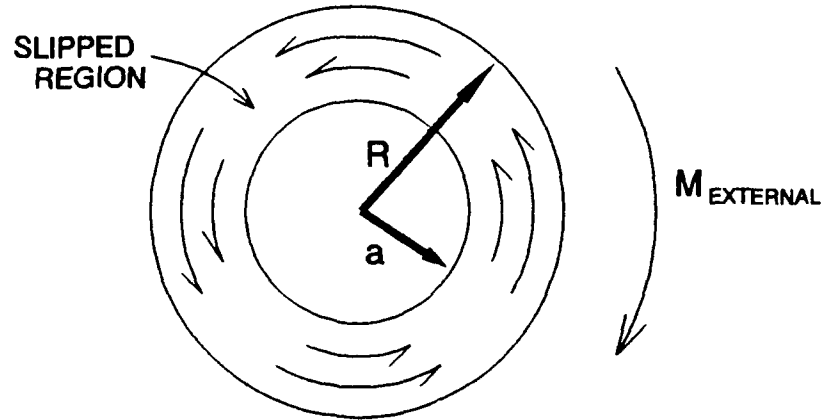


Figure 2-6. Partially Slipped Region¹⁶

The Richardson and Nolle model requires that the external moment applied to the joint be equal to or less than the value for gross slip¹⁶. Once gross slip occurs, the entire joint is slipping. The external moment which causes gross slip can be found by setting $a=0$ and is given by:

$$M_{gross} = \frac{2}{3} \pi \mu P R^3 \quad (2-28)$$

or in terms of the clamping force N :

$$M_{gross} = \frac{2}{3} \mu N R \quad (2-29)$$

Equations (2-28) and (2-29) represent the maximum moment the joint can support before macroslip or gross slip occurs. For

values of moment between 0 and M_{gross} , Richardson and Nolle develop an equation which describes the relative rotation in the joint. Assuming the material which has not slipped behaves like a rigid body, they calculate the net moment acting at any radius r between a and R . Using elasticity equations in polar coordinates, the net moment is equated to a circumferential shear strain which is in turn equated to displacement in the circumferential direction¹⁶.

The Richardson and Nolle model develops three sets of these types of equations for three different parts of a full load cycle: the initial loading, the unloading and the reloading. Each of the 3 regions has its own set of governing equations which relate the applied moment to the region of slip and to the relative rotation¹⁶. Figure 2-7 is a moment-rotation diagram ($M-\theta$ diagram) and the area enclosed by the curve represents the energy dissipated by cyclic loading.

According to Richardson and Nolle, the initial loading need only be considered for the first quarter cycle of the loading and need not be considered again no matter how many cycles are run¹⁶. The external moment is taken from a value of 0 to a value of M_{max} , and as mentioned previously, M_{max} should be less than M_{gross} . The radius associated with the slipped region at M_{max} is designated a_s and $\theta = \theta_{max}$.

During unloading the joint undergoes counterslip from θ_{max} to θ_{in} . The slip region of the joint proceeds again from the

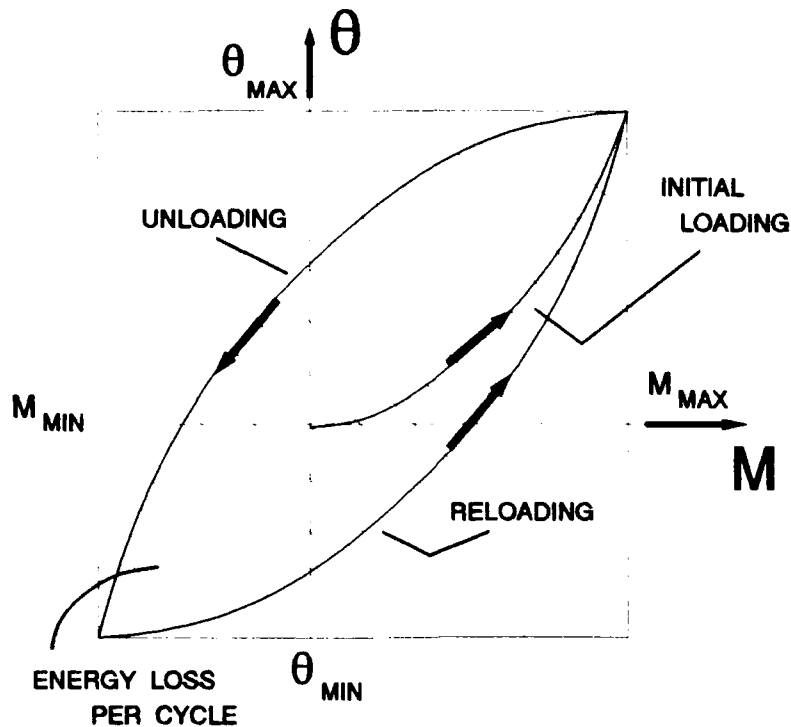


Figure 2-7. Hysteresis Loop ¹⁶

outer radius R inward to some new radius b . At the time when the moment equals M_{min} , the rotation is designated θ_{min} and the radius b_{min} .

During the reloading phase of the cycle, the equation governing the rotation of the joint is dependent on the two previous regions of slip. Richardson and Nolle found that the energy dissipated by the cyclic loading can be determined by calculation of the area enclosed by a M - θ curve as shown in Figure 2-7. The energy dissipated is represented by

$$\Delta E = \int_{M_{\min}}^{M_{\max}} (\theta_{ul} - \theta_{rl}) dM \quad (2-30)$$

Where θ_{ul} and θ_{rl} are the equations governing the rotation of the joint during the unloading and reloading phase of a load cycle. The θ_{ul} and θ_{rl} equations, as well as the initial loading equation for rotation, are developed and defined in the Richardson and Nolle reference¹⁶.

A similar microslip friction model has been developed by Leiker that differs from the Richardson and Nolle model in one major way⁵. Leiker no longer assumes that the unslipped region behaves as a rigid body, but instead it behaves as an elastic circular shaft which twists under any finite level of torque. Leiker believed that the rigid body assumption was too restrictive and a method to account for the moment-carrying capacity of the unslipped region of the joint must be made.

2.1.4. Lieker Macroslip Model. Lieker discusses a method for modeling the behavior of friction in a rotary joint by using a macroslip model, or gross slip model⁵. The model assumes that no rotation occurs between the contact surfaces in a joint until the value of the externally applied moment reaches $-M_{gross}$ as defined in Equation (2-29). During the initial loading, the external moment starts at 0 until it reaches $-M_{gross}$. The negative, in this case, is arbitrary and is dependent only on the sign convention chosen. Once $-M_{gross}$

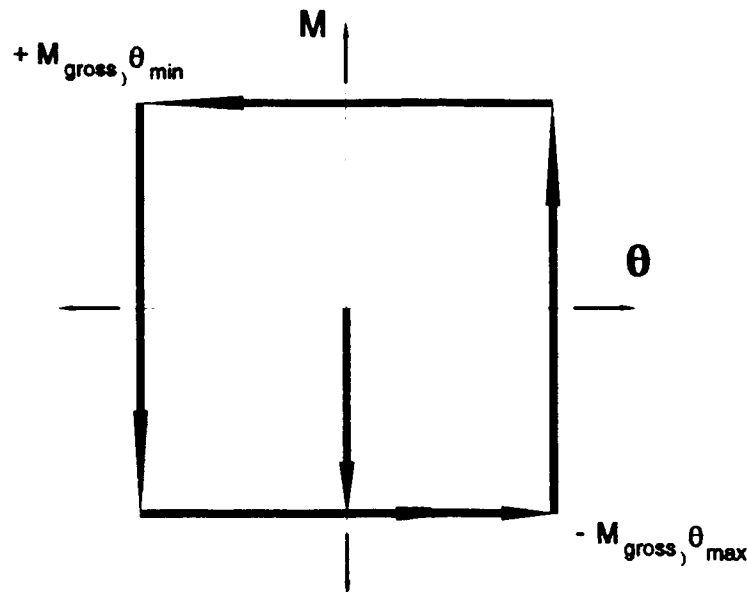


Figure 2-8. Lieker Macroslip Model⁵

is reached, the joint rotates through an angle θ and the moment is limited to a maximum and constant value of $-M_{gross}$ until the cycle reverses itself. During unloading the joint undergoes no further rotation until a value of $+M_{gross}$ is reached, and again the joint rotates to a value of θ_{min} while a value of $+M_{gross}$ is maintained. The process is reversed for the reloading case, and this model produces a square M - θ diagram as shown in Figure 2-8. As mentioned previously, the direction of the cycle can be reversed without loss of generality.

2.1.5. Macroslip versus Microslip. As previously shown, for any applied moment below M_{gross} the relative slip will be in microslip. Donnelly shows the relationship between damping

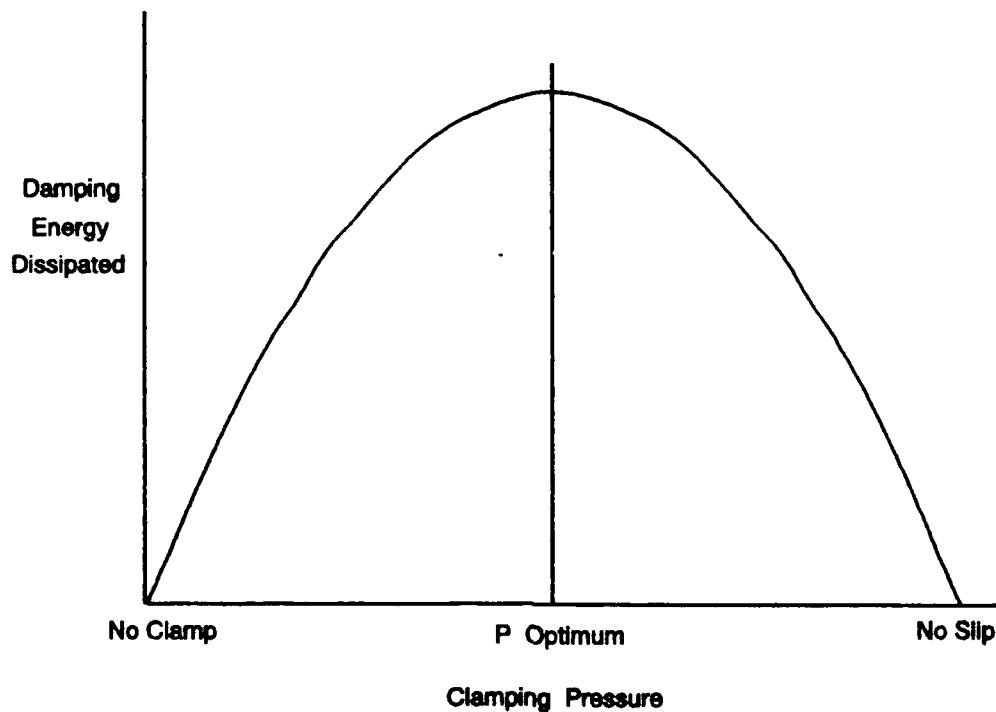


Figure 2-9. Clamping Pressure versus Energy Dissipation⁴

and clamping pressure graphically in Figure 2-9. As seen in Equation (2-27), the value of M_{gross} can be varied as a function of clamping pressure. The low end of the macroslip region occurs at low clamping forces and is known as the no-clamp case. As the moment increases, the amount of damping increases until M_{gross} is reached. Above M_{gross} , damping will begin to decrease in the microslip region until the clamping pressure is so great that no relative slip occurs. Damping is maximized at some clamping pressure just above that required to prevent gross slip⁴.

2.2 Elementary Beam Theory

One way in which an external torque or moment can be applied to a rotary joint is by means of a moment arm. For the purposes of this paper, an external moment will be applied to a joint by exerting a force at the end of a beam. It is desirable to transfer as much of the applied force as possible to the joint, and not in to the bending of the beam. A completely rigid beam would be ideal, but in reality no beam is truly rigid. It is therefore necessary to investigate the equations of motion of beams in order to select a beam geometry that is sufficiently rigid for the experiment.

2.2.1. Euler-Bernoulli Beam. For the purposes of this thesis, when the joint is completely clamped (no-slip condition) the connecting beam can be thought of as a cantilevered beam fixed at one end and free at the other as shown in Figure 2-10. Euler-Bernoulli Beam Theory assumes that the cross-sectional dimensions of the beam are small compared with its length, and that the lines originally drawn perpendicular to the beam center line remain perpendicular to the center line after beam deformation²⁰.

The equation of motion for the Euler-Bernoulli beam is given by:

$$q(x, t) = \rho A \ddot{w}(x, t) + EI w''''(x, t) \quad (2-31)^{23}$$

where

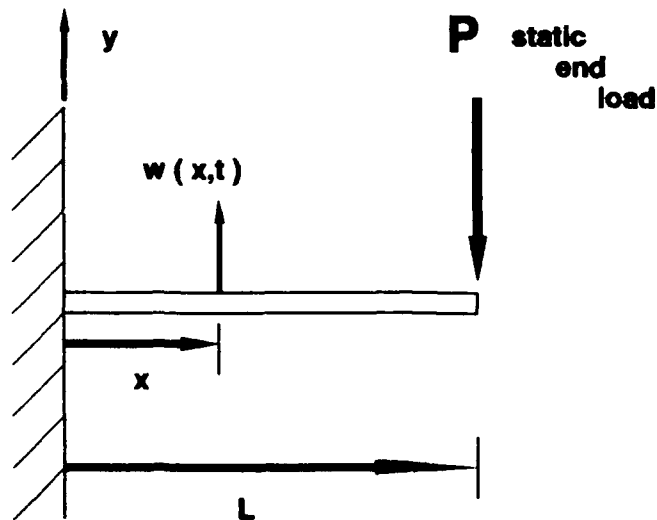


Figure 2-10. Cantilevered Beam with Static Load at Tip

$q(x,t)$ = distributed load as a function of position and time

ρ = mass density per unit length

A = cross-sectional area of the beam

E = modulus of elasticity

I = cross-sectional moment of inertia

$w(x,t)$ = transverse displacement of beam as a function of position and time

Assuming the problem is a cantilevered beam with an end load in static equilibrium (note that in this case, time is no longer a variable), then Equation (2-31) reduces to

$$EIw(x)'''' = 0 \quad (2-32)$$

with natural boundary conditions given by

$$w'''(L) = \frac{P}{EI} \quad (2-33)$$

$$w''(L) = 0 \quad (2-34)$$

and geometric boundary conditions given by

$$w(0) = 0 \quad (2-35)$$

$$w'(0) = 0 \quad (2-36)$$

Equation (2-33) represents the shear at the end of the beam. Equation (2-34) states that no moment exists at the end of the beam, and Equations (2-35) and (2-36) state that there is no displacement or bending respectively at the wall. Assuming E and I to be constant throughout the length of the beam, and integrating Equation (2-32) four times results in

$$w(x) = \frac{1}{6}C_1x^3 + \frac{1}{2}C_2x^2 + C_3x + C_4 \quad (2-37)$$

Where C_1 , C_2 , C_3 , and C_4 are arbitrary constants. Solving Equation (2-37) using the four boundary conditions leads to

$$C_1 = \frac{P}{EI} \quad (2-37a)$$

$$C_2 = -\frac{PL}{EI} \quad (2-37b)$$

$$C_3 = C_4 = 0 \quad (2-37c)$$

Substituting back into Equation (2-37) gives the transverse displacement as a function of x :

$$w(x) = \frac{1}{6} \frac{P}{EI} x^3 - \frac{1}{2} \frac{PL}{EI} x^2 \quad (2-38)$$

The maximum deflection of the beam is at the tip and is given by

$$w(L) = -\frac{1}{3} \frac{PL^3}{EI} \quad (2-39)$$

As a check, Equation (2-39) was compared against the tabulated results for a cantilevered beam compiled by Griffel²¹. As expected Equation (2-39) matches the result given by Griffel.

2.2.2. Euler-Bernoulli Beam versus Timoshenko Beam.

Omitted from Euler-Bernoulli beam theory are the effects of rotary inertia and of shear deformation. For static analysis, to avoid shear deformation effects it is required that long and slender beams be used. In the dynamic case, an additional restriction of relatively long wave length is necessary in order for the simpler Euler-Bernoulli beam theory to give results in agreement with observation. Both high-frequency motions and problems involving short deep beams require a more exact theory of bending, such as the Timoshenko beam. Euler-Bernoulli beam theory is of most utility in those cases involving somewhat lower frequencies and relatively longer and more slender beams, such as the beam proposed for this thesis²⁰.

Reference 22 shows the influence of shear and rotary motion on the natural frequencies of a uniform cantilever

beam. It can be seen that as the ratio of the radius gyration of the cross section, r , divided by the length, L , of the beam decreases (the beam becomes longer with respect to its thickness), the Euler-Bernoulli beam theory compares quite well with the Timoshenko beam for the first mode. For the purpose of this paper a ratio of r/L less than 0.1 will be considered reasonable to assume a long slender beam. The ratio is given by

$$\frac{r}{L} = \frac{\sqrt{\frac{I}{A}}}{L} = \frac{\sqrt{\frac{bh^3}{12bh}}}{L} = \frac{h}{\sqrt{12}L} \quad (2-40)^4$$

where

- r = radius of gyration
- L = length of beam
- I = cross-sectional moment of inertia
- A = cross-sectional area
- b = cross-sectional base of beam (beam thickness)
- h = cross-sectional height of beam (beam width)

See Chapter 3 for the detailed analysis concerning the design of the beams.

2.3 Theoretical Damping Models

Macrosliip models were developed for comparison against the experimental data. Because the beams used in the experiment are assumed to be sufficiently rigid, no dissipation due to bending of the beams will be considered. Furthermore, since the contact surfaces are hard steel on hard steel, they are considered to be free of any twisting during rotation.

2.3.1. Mark I Damping Model. The Mark I beam is a pendulum with distributed mass with a large weight at the end as shown in Figure 2-11. The center of mass of the system can be found using

$$X_{cm} = \frac{mass_1 X_1 + mass_2 X_2}{mass_{total}} \quad (2-41)$$

with x_1 , x_2 , and x_{cm} defined as shown in Figure 2-11. The mass moment of inertia of the entire system is given by

$$I_o = I_1 + I_2 \quad (2-42)$$

where I_1 is the moment of inertia of the beam and is given by

$$I_1 = \frac{1}{12} mass_1 (h^2 + L^2) + mass_1 (x_1)^2 \quad (2-43)$$

where

h = beam width
L = length of beam from pivot point to tip

I_2 is the moment of inertia of the weight assembly and is given by

$$I_2 = 2 \left(\frac{1}{12} \frac{mass_2}{2} (a^2 + b^2) + \frac{mass_2}{2} (x_2)^2 \right) \quad (2-44)$$

where a and b are the height and width (not thickness) of the two plates. Note that there are 2 plates attached at the beam tip. The equations of motion for the system are

$$I_o \ddot{\theta} = -W x_{cm} \sin \theta \pm M_{gross} \quad (2-45)$$

which for small rotations ($\theta \leq 10^\circ$) can be written as

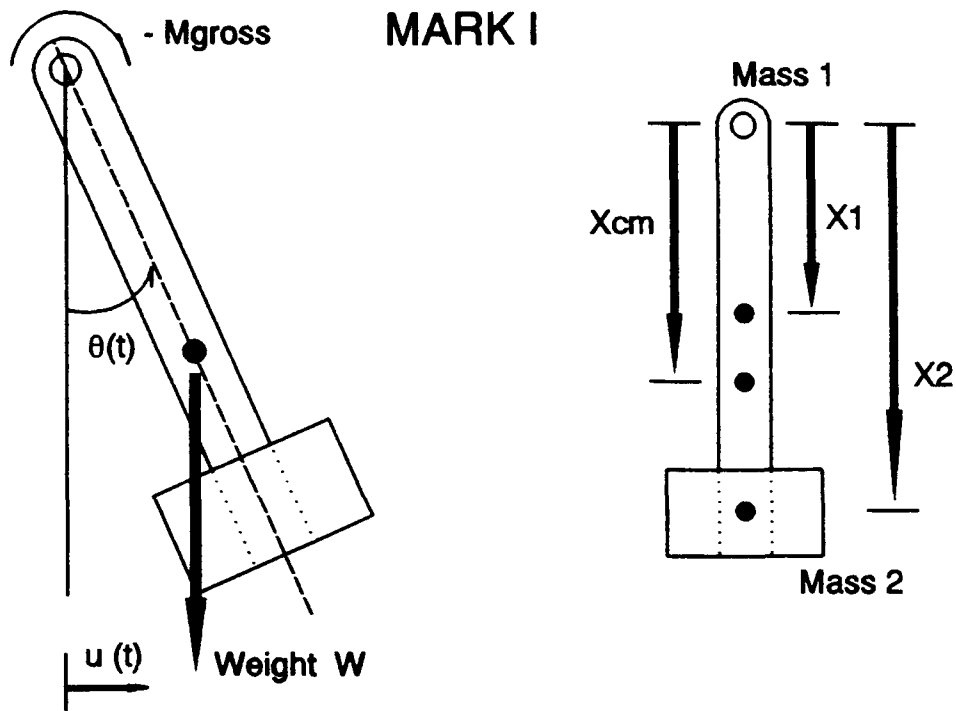


Figure 2-11. Mark I Free Body Diagram

$$\ddot{\theta} = -\frac{W X_{cm}}{I_o} \theta \pm \frac{M_{gross}}{I_o} \quad (2-46)$$

where M_{gross} is the friction moment at the pivot point as a function of the clamping force at the joint. M_{gross} can be written as

$$M_{gross} = \frac{4}{3} \mu F_c \left(\frac{R^3 - R_{hole}^3}{R^2 - R_{hole}^2} \right) \quad (2-47)$$

where

- F_c = Clamping force (lbs)
- μ = coefficient of friction
- R = outer radius of joint
- R_{hole} = Radius of the bolt hole

Equation (2-47) is fully developed in Appendix A.9, and is different from the Richardson and Nolle M_{gross} equation discussed previously in that it accounts for 2 frictional contact surfaces with a hole in the center. The solutions to Equation (2-46) can be found in the same manner as for the simple spring-mass system presented in Section 2.1.1. The natural frequency of the system is given by

$$\omega_n = \sqrt{\frac{W x_{cm}}{I_o}} \quad (2-48)$$

Substitution into Equation (2-46) yields

$$\ddot{\theta} = -\omega_n^2 \theta \pm \frac{M_{gross}}{I_o} \quad (2-49)$$

Recall that the solutions to this type of equation are piecewise solutions since for positive θ , the frictional moment is negative, and for negative θ , the frictional moment is positive. Assuming positive θ , and taking the Laplace transform of Equation (2-49) then

$$\theta(s) s^2 - s\theta_0 - \dot{\theta}_0 = -\omega_n^2 \theta(s) - \frac{M_{gross}}{I_o s} \quad (2-50)$$

which can be rewritten as

$$\theta(s) = -\frac{M_{gross}}{I_o \omega_n^2} \left(\frac{1}{s} - \frac{s}{s^2 + \omega_n^2} \right) + \theta_0 \frac{s}{s^2 + \omega_n^2} + \dot{\theta}_0 \frac{1}{s^2 + \omega_n^2} \quad (2-51)$$

The Laplace inverse of Equation (2-51) gives

$$\theta(t) = -\frac{M_{gross}}{I_o \omega_n^2} (1 - \cos \omega_n t) + \theta_0 \cos \omega_n t + \frac{\dot{\theta}_0}{\omega_n} \sin \omega_n t \quad (2-52)$$

Differentiation gives $\dot{\theta}$ as

$$\dot{\theta}(t) = -\frac{M_{gross}}{I_o \omega_n} \sin \omega_n t - \theta_0 \omega_n \sin \omega_n t + \dot{\theta}_0 \cos \omega_n t \quad (2-53)$$

When $\dot{\theta}$ is negative the solutions are

$$\theta(t) = \frac{M_{gross}}{I_o \omega_n^2} (1 - \cos \omega_n t) + \theta_0 \cos \omega_n t + \frac{\dot{\theta}_0}{\omega_n} \sin \omega_n t \quad (2-54)$$

$$\dot{\theta}(t) = \frac{M_{gross}}{I_o \omega_n} \sin \omega_n t - \theta_0 \omega_n \sin \omega_n t + \dot{\theta}_0 \cos \omega_n t \quad (2-55)$$

For small angles, θ can be represented as

$$\theta = \frac{u}{L} \quad (2-56)$$

where $u(t)$ is defined positive as shown in Figure 2-11. Assuming positive velocities and substituting Equation (2-56) into Equations (2-52)-(2-55) gives:

$$u(t) = -\frac{M_{gross} L}{I_o \omega_n^2} (1 - \cos \omega_n t) + u_0 \cos \omega_n t + \frac{\dot{u}_0}{\omega_n} \sin \omega_n t \quad (2-57)$$

$$\dot{u}(t) = -\frac{M_{gross} L}{I_o \omega_n} \sin \omega_n t - u_0 \omega_n \sin \omega_n t + \dot{u}_0 \cos \omega_n t \quad (2-58)$$

and for negative velocities

$$u(t) = \frac{M_{gross}L}{I_o\omega_n^2} (1 - \cos\omega_n t) + u_0 \cos\omega_n t + \frac{\dot{u}_0}{\omega_n} \sin\omega_n t \quad (2-59)$$

$$\dot{u}(t) = \frac{M_{gross}L}{I_o\omega_n} \sin\omega_n t - u_0 \omega_n \sin\omega_n t + \dot{u}_0 \cos\omega_n t \quad (2-60)$$

Equations (2-57)-(2-60) were used to predict the motion of the Mark I beam for free vibration and small rotations (less than 10 degrees). A MATLAB script file, MARKPLOT.m, can be found in Appendix C.

Note that Equations (2-57)-(2-60) do not consider the friction of the beam on the bolt shank, or M_{shank} . M_{shank} is a constant moment whenever there is motion and is assumed to be independent of the clamping force, F_c , at the joint. M_{shank} is the weight of the beam on the bolt shank times μ_{shank} times the radius of the bolt hole, and is included in M_{gross} as

$$M_{gross} = \frac{4}{3} \mu F_c \left(\frac{R^3 - R_{hole}^3}{R^2 - R_{hole}^2} \right) + M_{shank} \quad (2-61)$$

2.3.2. Mark II Damping Model. The Mark II beam will be subjected to a shaker force $F(t)$ as shown in Figure 2-12. The equation of motion for the beam is:

$$I\ddot{\theta} = F(t)L\cos\theta \pm M(t) \quad (2-62)$$

where I is the mass moment of inertia of the beam and is given by

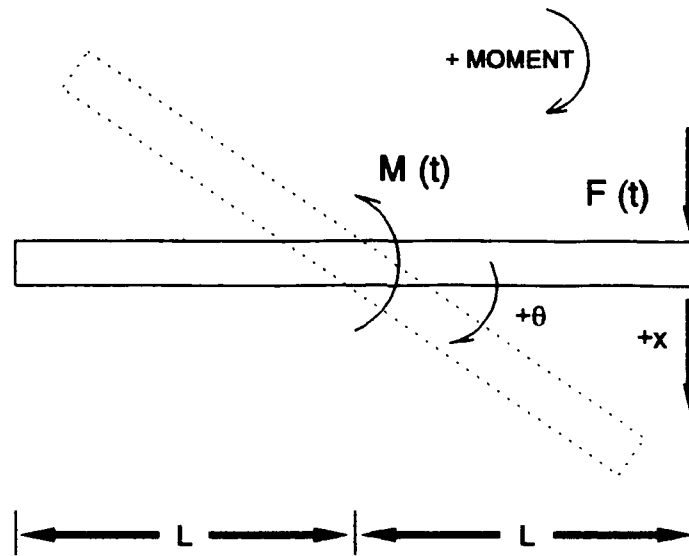


Figure 2-12. Mark II Free Body Diagram

$$I = \frac{1}{12} \text{mass} (h^2 + (2L)^2) \quad (2-63)$$

where

h = width of the beam
 2L = overall length of the beam

Assuming small rotations, Equation (2-62) reduces to

$$\ddot{x} = \frac{F(t)L^2}{I} \pm \frac{M(t)L}{I} \quad (2-64)$$

where x is measured positive as shown in Figure 2-12. The following discussion assumes that the beam only moves when $|F(t)*L| > M_{\text{gross}}$, where M_{gross} is the maximum moment the joint can support before slipping. When $|F(t)*L| < M_{\text{gross}}$, there is

no motion, and no energy is dissipated by the joint. When $|F(t) \cdot L| < M_{gross}$, then the equations of motion are

$$\ddot{x} = \frac{F(t) L^2}{I} - \frac{M_{gross} L}{I} \quad \text{for } \dot{x} > 0 \quad (2-65)$$

$$\ddot{x} = \frac{F(t) L^2}{I} + \frac{M_{gross} L}{I} \quad \text{for } \dot{x} < 0 \quad (2-66)$$

The force $F(t)$ applied at the tip is often represented as

$$F(t) = F_0 \sin \omega t \quad (2-67)$$

F_0 = peak magnitude of the forcing function
 ω = angular frequency

However, attempts at solving Equations (2-65) and (2-66) using Equation (2-67) without first prescribing the peak magnitude of x were unsuccessful. Assuming $F(t) = F_0 \sin \omega t$ and a positive velocity, then the equation of motion is

$$\ddot{x} = \frac{F_0 L^2}{I} \sin \omega t - \frac{M_{gross} L}{I} \quad \dot{x} > 0, |F(t) \cdot L| > M_{gross} \quad (2-68)$$

Where the solutions are

$$x = \frac{F_0 L^2}{I \omega} \left(t - \frac{1}{\omega} \sin \omega t \right) - \frac{M_{gross} L}{2 I} t^2 + x(0) + \dot{x}(0) t \quad (2-69)$$

$$\dot{x} = \frac{F_0 L^2}{I \omega} (1 - \cos \omega t) - \frac{M_{gross} L}{I} t + \dot{x}(0) \quad (2-70)$$

But for the case where $M_{gross} = 0$ (i.e. no friction), Equation (2-70) never goes negative, and x is always increasing. Since a shaker will turn the beam around every 1/2 cycle, Equation

(2-67) is not a valid model of the force for this system without first defining the limit of x .

A solution can be found by thinking of the shaker as a displacement mover instead of a force generator. In these terms, the shaker will use whatever force is necessary to move the tip of the beam a fixed distance. Therefore, for steady state motion, the tip of the beam will move according to

$$x = D \sin \omega t \quad (2-71)$$

where D is the magnitude of the peak displacement. The velocity and acceleration can be found by differentiating Equation (2-71):

$$\dot{x} = D \omega \cos \omega t \quad (2-72)$$

$$\ddot{x} = -D \omega^2 \sin \omega t \quad (2-73)$$

Now for $|F(t) \cdot L| > M_{gross}$ the equations of motion become

$$-D \omega^2 \sin \omega t = \frac{F(t) L^2}{I} \pm \frac{M_{gross} L}{I} \quad (2-74)$$

Solving for $F(t)$:

$$F(t) = -\frac{D I \omega^2}{L^2} \sin \omega t \pm \frac{M_{gross}}{L} \quad (2-75)$$

Assuming $F(t)$ is $F_0 \sin \omega t$, then the peak magnitude of $F(t)$ is F_0 , which can be found by

$$F_0 = \left| \frac{-DI\omega^2}{L^2} - \frac{M_{gross}}{L} \right| = \left| \frac{DI\omega^2}{L^2} + \frac{M_{gross}}{L} \right| \quad (2-76)$$

where

$$D = (F_0 - \frac{M_{gross}}{L}) (\frac{L^2}{\omega^2 I}) \quad (2-77)$$

Now when there is no friction, F_0 becomes

$$F_0 = \frac{D\omega^2 I}{L^2} \quad (2-78)$$

which is the steady state solution for the peak force magnitude. A MATLAB script file, MOMENT.m, was written to demonstrate the model. An overview of the logic is as follows:

For a given

F_0 = sinusoidal peak force magnitude
 F_c = clamping force at joint
 μ = coefficient of friction
 cycle = shaker cycle in Hz

1. Compute maximum distance D the shaker will move using Equation (2-77).
2. Compute x and \dot{x} using Equations (2-71) and (2-72).
3. Compute $F(t)$ using Equations (2-75), depending on the sign of \dot{x} .

A copy of the script file MOMENT.m can be found in Appendix C. See Figures 2-13, 2-14, and 2-15 for examples of output from MOMENT.m. Figure 2-13 shows steady state displacements and forces on the beam assuming no friction. Figure 2-14 represents steady state displacements and forces on the beam

with friction. Notice that the beam does not move as far in 1 cycle as with no friction. Also note the discontinuity in the force signal. With this model, the force is made to be discontinuous every 1/2 cycle in order to keep up with the beam displacements. In actuality, the force signal is not discontinuous but rounds off sharply. Figure 2-16 is an example of actual force versus time and displacement versus time curves. Figure 2-15 illustrates a force-displacement curve as a result of the data generated with friction. Assuming a rigid beam, and small rotations, this is a representation of the energy dissipated at the joint. The shape of the hysteresis curves are similar to Donnelly's and Lieker's Macroslip Models, except in this paper the energy dissipation, both theoretically and experimentally, will be computed using force-displacement curves instead of moment-rotation curves. Figure 2-17 is a force versus displacement plot of the experimentally measured signals seen in Figure 2-16. Note that the resulting hysteresis curve looks like a trapezoid.

In order to test the validity of the model, another script file was written, THEORY1.m, to compute the force-displacement curves and their enclosed areas for varying clamping pressures with a given sinusoidal peak magnitude and coefficient of friction. Figure 2-18 illustrates the results for a particular case. The resulting curve produces the

expected shape as outlined in Section 2.1.5. Note that THEORY1.m does not account for the weight of the beam on the bottom frictional surfaces. The weight of the beam is assumed to add to M_{gross} by

$$M_{gross} = \frac{4}{3} \mu (F_c + \frac{1}{2} W_{beam}) \left(\frac{R^3 - R_{hole}^3}{R^2 - R_{hole}^2} \right) \quad (2-79)$$

because the full weight of the beam is applied to only 1/2 of the total frictional contact area in the joint. See Appendix C for copies of the MOMENT.m and THEORY1.m script files.

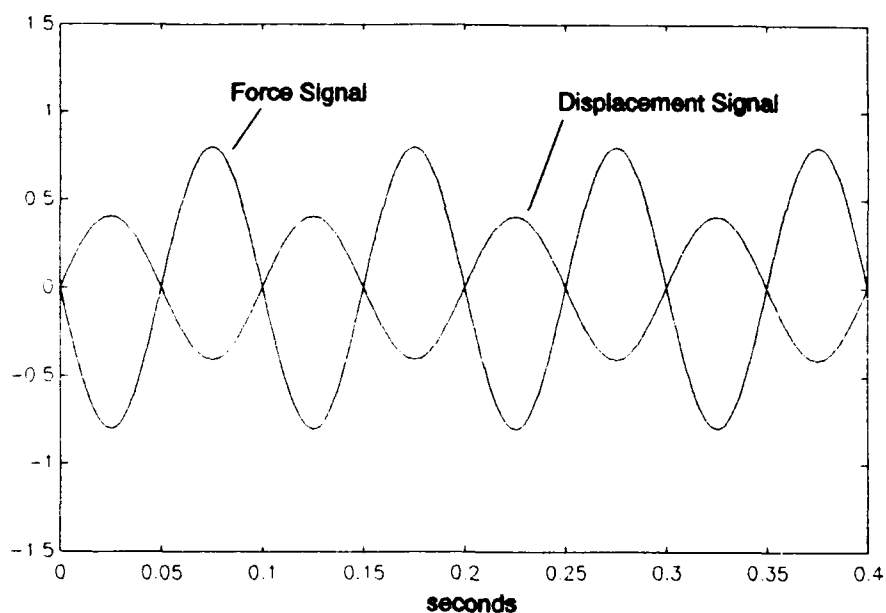


Figure 2-13. Displacement and Force Signals from MOMENT.m
 ($F_o=0.8$ lbs, $F_c=5$ lbs, $\mu=0.0$, 10Hz)

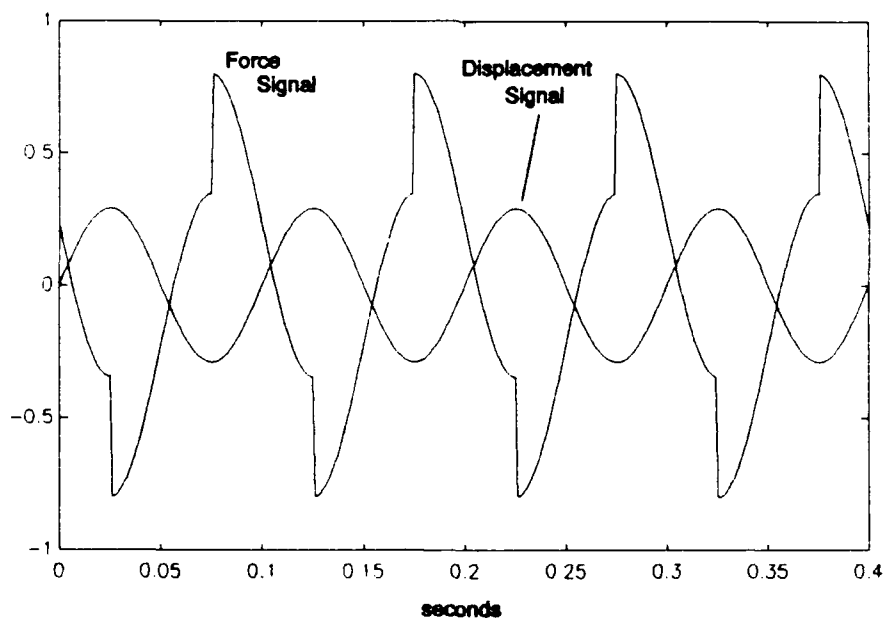


Figure 2-14. Displacement and Force Signals from MOMENT.m
 ($F_o=0.8$ lbs, $F_c=5$ lbs, $\mu=0.3$, 10Hz)

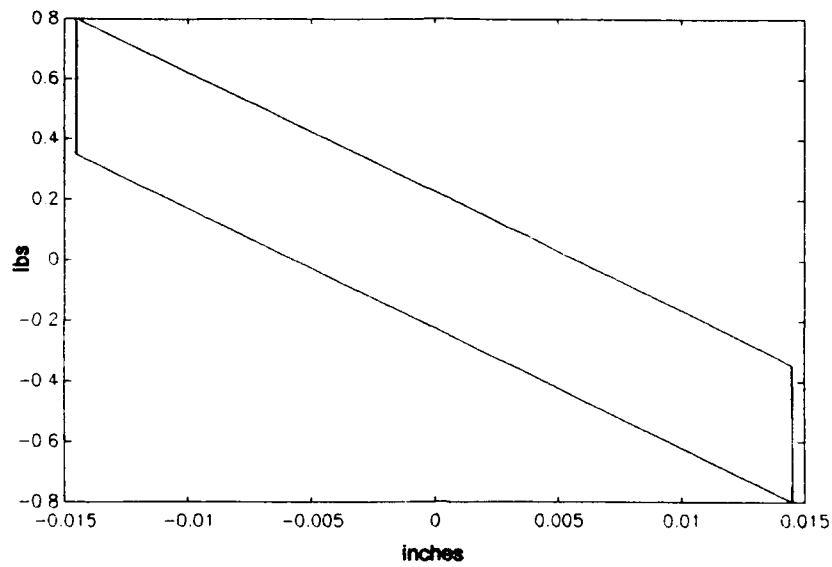


Figure 2-15. Theoretical Force versus Displacement Hysteresis Loop with Macroslip Friction ($F_o=0.8$ lbs, $F_c=5$ lbs, $\mu=0.3$, 10Hz)

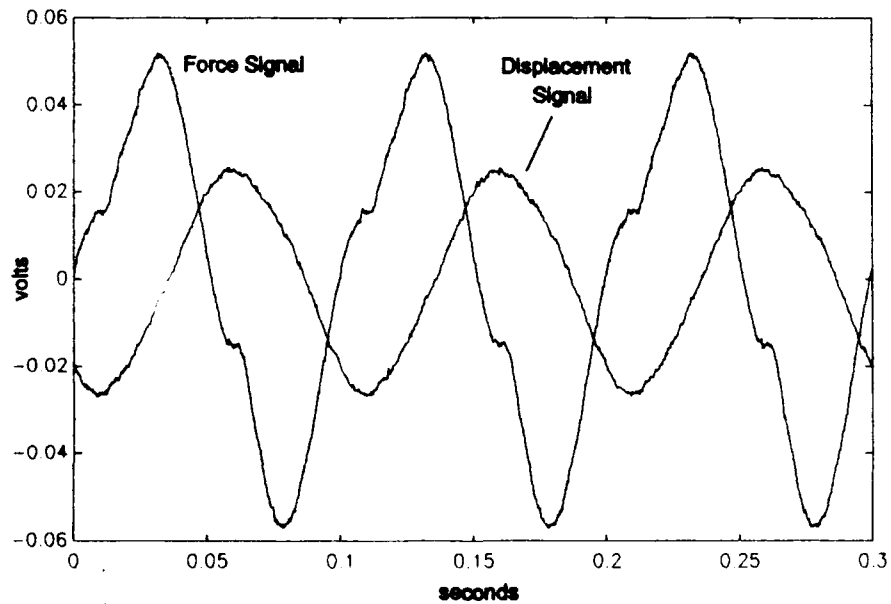


Figure 2-16. Example of Actual Displacement and Force Signal Data ($F_o \approx 1$ lb, $F_c=40$ lbs, 10Hz)

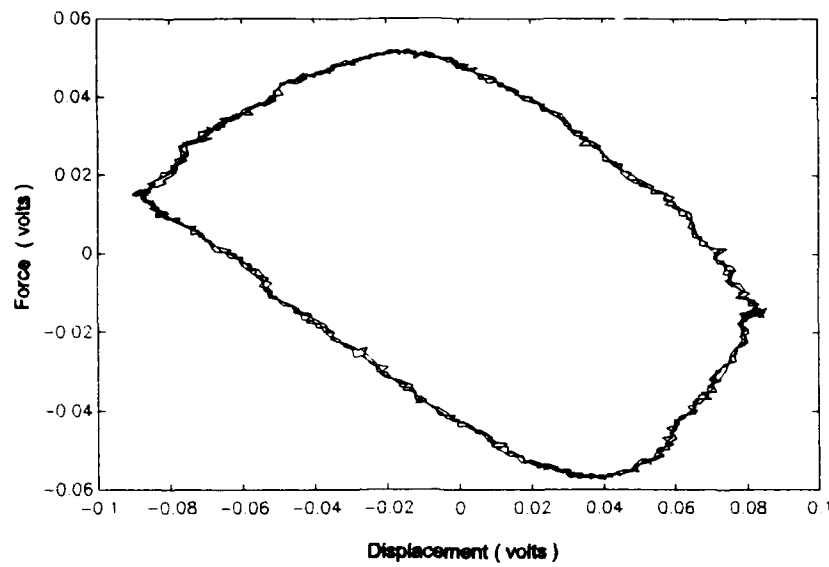


Figure 2-17. Example of Actual Displacement versus Force Hysteresis Loop ($F_o \approx 1$ lb, $F_c=40$ lbs, 10Hz)

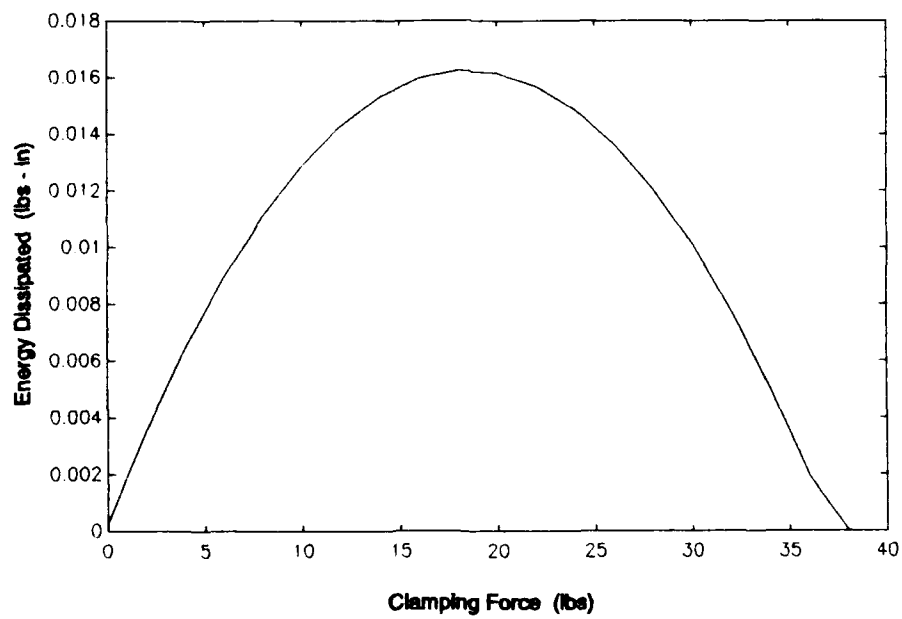


Figure 2-18. Clamping Force versus Energy Dissipated from THEORY1.m ($F_o=0.8$ lbs, $\mu=0.3$, 10Hz)

III. Experimental Geometry and Equipment

A bolted joint was selected as the physical model for a pin-type rotary joint. Two different test designs were considered: Mark I and Mark II. The Mark I is an inverted beam with a bolted joint at the upper end, and the Mark II design is a horizontal beam with a bolted joint located in the middle. A sketch of these designs can be seen in Figures 1-1 and 1-2. For a brief description of the beam-joint geometries, see Section 1.3 General Approach and Assumptions. Originally, the Mark I design was the only design considered for the experiment. It would allow for both free and forced vibration testing. A test model fabricated from cold-rolled stock steel would permit test and checkout of the design before the final model was fabricated from stainless steel. However, once the Mark I test model was built and mounted to the 2-girder-plate vibration isolation stand located in room 150 of the AFIT Aeronautical Laboratory, it was noted that the weight of the beam on the bolt shank presented itself as a significant frictional surface, and had been overlooked as such. That led to the Mark II design, which eliminated the problem. However, the Mark II design was not suitable for free vibration testing. It was decided to proceed with both designs; the Mark I being principally for free vibration testing, and the Mark II design as a forced vibration model.

The following sections discuss the development and design of the Mark I and Mark II models.

3.1 Mark I Beam-Joint Design (Inverted Beam)

3.1.1. Mark I Test Model. A test model was fabricated out of cold rolled stock steel. The purpose of the model was to test the overall suitability of the design for experimental work. Cold rolled stock steel was chosen for two reasons: (1) availability, and (2) the requirement for a stiff beam and twist resistant surfaces. The following is a description of each part of the Mark I test model.

Beam: The Mark I beam was fabricated out of cold rolled stock steel. The beam is 1.5 inches wide by 0.5 inches thick. The overall length of the beam is 21.25 inches. The beam has a 0.5 inch hole at the top as shown in Figure 3-1. There are two 10-32 tapped holes near the bottom of the beam to serve as accelerometer and force transducer attachment points. The distance from the center of the 0.5 inch bolt hole at the top to the attachment points is 19.5 inches. Two additional holes were drilled near the bottom to allow for the attachment of two rectangular lead weights. The purpose of the lead weights is to add mass to the beam in order to facilitate the free vibration testing of the system. Assuming the following values:

$$\begin{aligned} E &= 2.9 * 10^7 \text{ lb/in}^2 \\ b &= 0.5 \text{ in} \end{aligned}$$

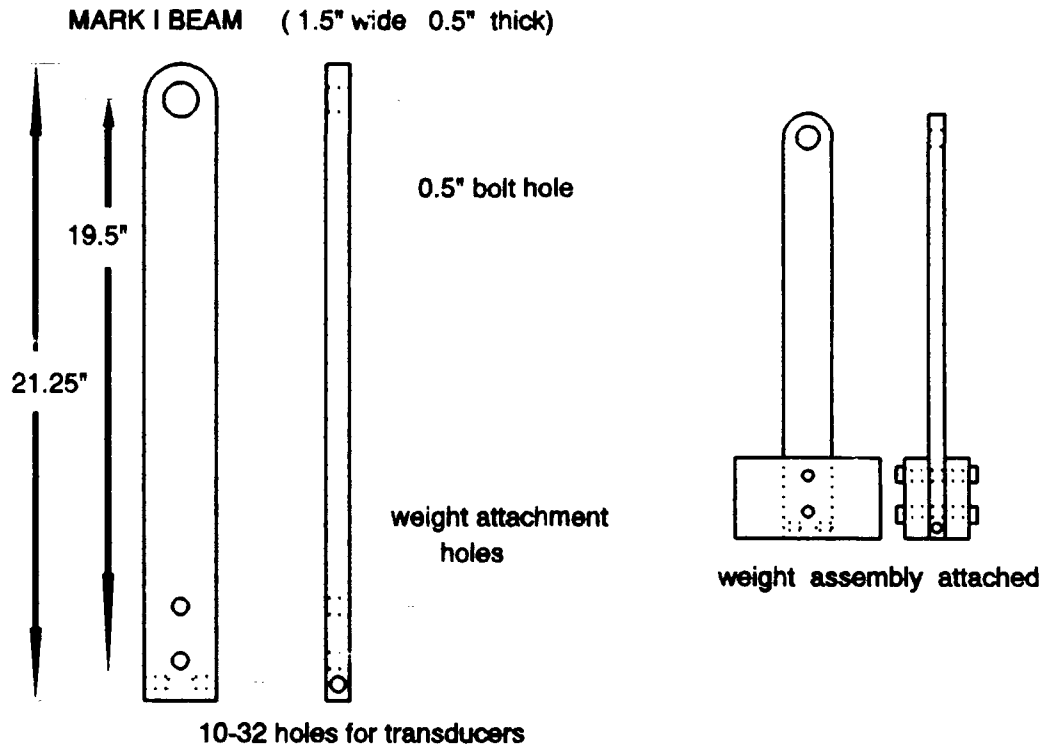


Figure 3-1. Mark I Test Model Beam

$$\begin{aligned}
 h &= 1.5 \text{ in} \\
 L &= 19.5 \text{ in} \\
 I &= bh^3/12 = 0.1406 \text{ in}^4 \\
 P &= 50 \text{ lb (maximum output load of shaker)}
 \end{aligned}$$

and using Equations (2-39) and (2-40) then,

$$w(x)|_{x=L} = -\frac{1}{3} \frac{PL^3}{EI} = -0.0303 \text{ inches} \quad (3-1)$$

and,

$$\frac{r}{L} = \frac{h}{\sqrt{12}L} = 0.022 \quad (3-2)$$

Equation (3-1) represents the maximum static tip deflection of

the beam (when fully clamped) with a 50lb end load, and Equation (3-2) validates the Euler-Bernoulli beam theory assumption of a long and slender beam. Assuming the full 0.0303 inch deflection of the beam is transmitted to a joint rotation, the corresponding angle of rotation would be

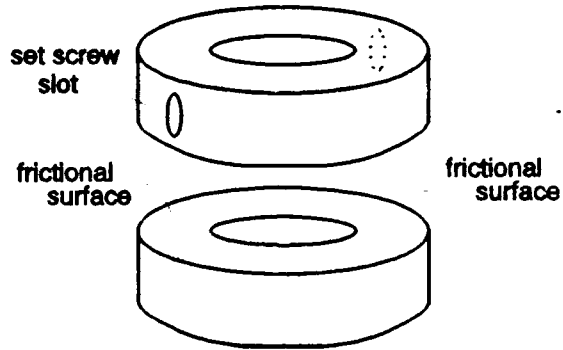
$$\text{maximum } \theta = \sin^{-1}\left(\frac{\text{max tip deflection}}{L}\right) = 0.089^\circ \quad (3-3)$$

or less than one tenth of a degree. Since it is expected that the magnitude of the sinusoidal force inputs on the beam will be under 10lbs (with a corresponding degree rotation of 0.018 degree or less), and the joint will be allowed to slip (i.e. a true cantilevered beam condition will not exist), then any bending of the beam near the joint is negligible compared to a joint rotation measurement. As an example, assume an optical sensor measures displacement along the edge of the beam 3 inches from the joint location. The magnitude of the maximum static deflection of the beam (fully clamped) at that point for a 10lb load is given by Equation (2-38) to be 0.0002 inches. The corresponding angle rotation of the joint (again, assuming the joint is allowed to rotate under this condition) is 0.004 degrees and is considered to be negligible. As discussed in Section 2.1.5, and seen in Figure 2-9, the optimum clamping pressure for maximum energy dissipation is somewhere below the fully clamped condition. Therefore, the displacement of the beam due to bending below a fully clamped

joint condition will be considered negligible when measuring the joint rotation along the edge of the beam as discussed above. For the purposes of this paper then, the beams are considered to be rigid. Any measured displacement of the beam while the beam is not fully clamped will be directly proportional to an angular displacement of the joint.

Spacers: The spacers were fabricated from the same cold rolled steel stock as the beam. Each spacer has a diameter of 1.5 inches with a 0.5 inch hole in the middle for the bolt. The principal design criteria for the experimental geometry is to isolate the frictional surfaces to either side of the beam and the corresponding spacer surfaces facing the beam at the joint location. The inner spacer is welded to the baseplate and can not move. The outer spacer, because of its thickness and applied clamping pressure was originally thought to be sufficiently immobilized. However, a simple dynamic test for varying bolt clamping pressures over a wide range of sinusoidal end loads provided by the shaker showed that the outer spacer was prone to slip; even at high clamping pressures. Two set screw towers were welded onto the baseplate on either side of the joint location in order to lock the outer spacer into place. See Figure 3-2. As a result the outer spacer was slotted to allow for the insertion of the set screws. Subsequent testing showed no visible signs of the outer spacer moving.

OUTER SPACER fixed into position with set screws



INNER SPACER welded into place

For the MARK II design replace
"outer and inner" with
"top and bottom"

NOTE: The beam is clamped between
the spacers

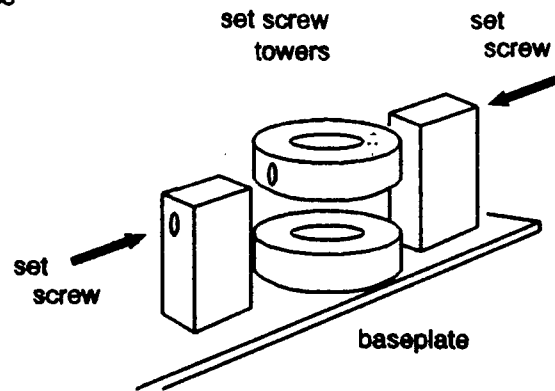


Figure 3-2. Spacers and Set Screw Assembly

Spring-Nut Assembly: The purpose of the spring is to allow for some sensitivity when tightening down the bolt. The spring also serves as a mechanism which, in conjunction with the relatively large size of the spacer, provides a means by which the clamping pressure can be more uniformly distributed over the contact areas than with a basic bolt-washer fastener. Once the first nut is in position, a second nut is backed securely down onto the first. This is done to keep the first nut in a fixed position during testing. A single nut, without any locking mechanism, may not provide a constant clamping

pressure under cyclic loading conditions²⁵. See Figure 1-3 for a simplified schematic of the spring-nut assembly.

Base Plate: Two test baseplate assemblies were fabricated for the Mark I. The first baseplate was 0.5 inch thick and was fabricated from the same material as the beam and the top spacer. The first baseplate essentially served as the bottom spacer. See Figure 3-3. However, as discussed earlier, the need for set screw towers was discovered, and this baseplate was discarded. A second test baseplate was constructed to permit the placement of the set screw towers. The second baseplate was constructed out of 0.25 inch flat plate stock steel. The only dimensional requirements for the baseplate design was that it be sufficiently rigid enough to support the entire beam-joint assembly, and allow enough room for attachment to the 2-girder-plate vibration isolation stand. The test baseplates were clamped to the 2-girder-plate vibration isolation stand with large c-clamps (the final model was bolted down).

Weight Assembly: Two lead weights were fastened to the end of the Mark I beam in order to facilitate free vibration testing over a wide range of bolt clamping pressures. Each weight is a rectangular flat lead plate (1" x 4" x 6.75"). The weights are bolted to the beam as shown in Figure 3-1.

Bolt: Common 0.5 inch diameter steel bolts were used in the test models. The only requirement was that the bolt shank

TEST BASEPLATES FOR MARK I

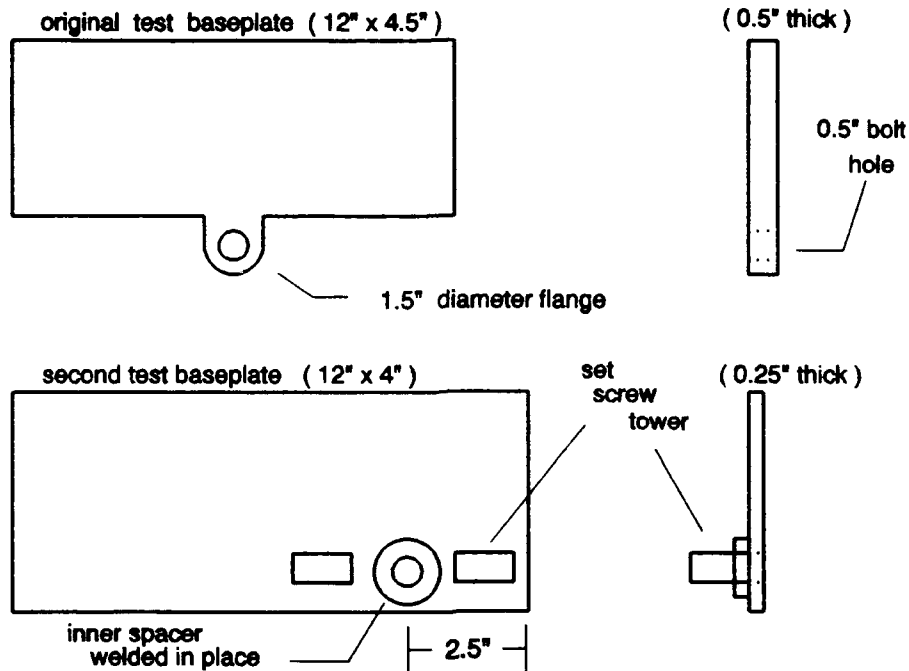


Figure 3-3. Mark I Test Baseplates

length be long enough to clear the spacers, beam and baseplate combined thicknesses. Refer to Section 3.3.8 for a complete description of the bolts used for final testing.

3.1.2. Mark I Final Model. The final model, illustrated in Figure 3-4, is very similar to the first except for three major differences. The beam and spacers are made from a 2 inch by 0.5 inch beam of stainless steel, and the baseplate is designed to be bolted securely to the 2-girder-plate vibration isolation stand with two 1 inch diameter bolts. Stainless steel was chosen as a suitable material for the final design in an attempt to control the condition of the friction

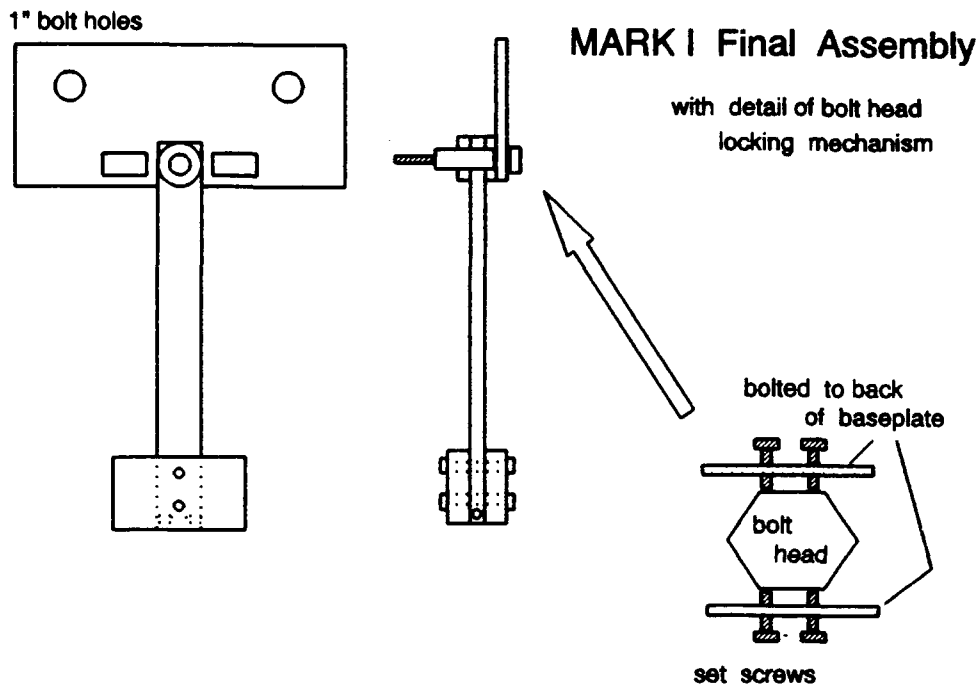


Figure 3-4. Mark I Final Assembly

surfaces by keeping them free from rust. The third difference is that a bolt head locking mechanism has been added in order to ensure the bolt is locked into a fixed position during final testing. With the addition of the bolt head locking mechanism, it is now assumed that the only frictional dissipative surfaces are the sides of the beam facing the spacers. Also note that the top of the beam on the final model is not rounded. Table 3-1 lists the specifications for the Mark I and Mark II test and final models.

3.2 Mark II Beam-Joint Design (Horizontal Beam)

3.2.1. Mark II Test Model. The design of the Mark II Beam-Joint model evolved from the Mark I design in an attempt to remove the weight of the beam from the bolt shank. In doing so, the weight of the beam has been added to the force normal to the frictional surfaces of the joint. This is not considered to be a problem, since the weight of the beam is measurable. The other noticeable difference between the Mark I and Mark II beams is that the Mark II beam is approximately twice as long as the Mark I beam. This was done in order to balance the beam on the frictional surface of bottom spacer. As with the Mark I design, a test model was fabricated out of cold rolled stock steel in order to test the overall suitability of the design for experimental work. The following is a description of each part of the Mark II test model.

Beam: The Mark II test beam was fabricated out of cold rolled stock steel. The beam is 1.5 inches wide by 0.5 inches thick. The overall length of the beam is 39.375 inches. the beam has a 0.5 inch hole in the center as shown in Figure 3-5. There are two 10-32 tapped holes near one end of beam to serve as accelerometer and force transducer attachment points. The distance from the center of the 0.5 inch diameter bolt hole in the center to the attachment points is 19.25 inches. When the joint is fully clamped, then the beam can be thought of as a

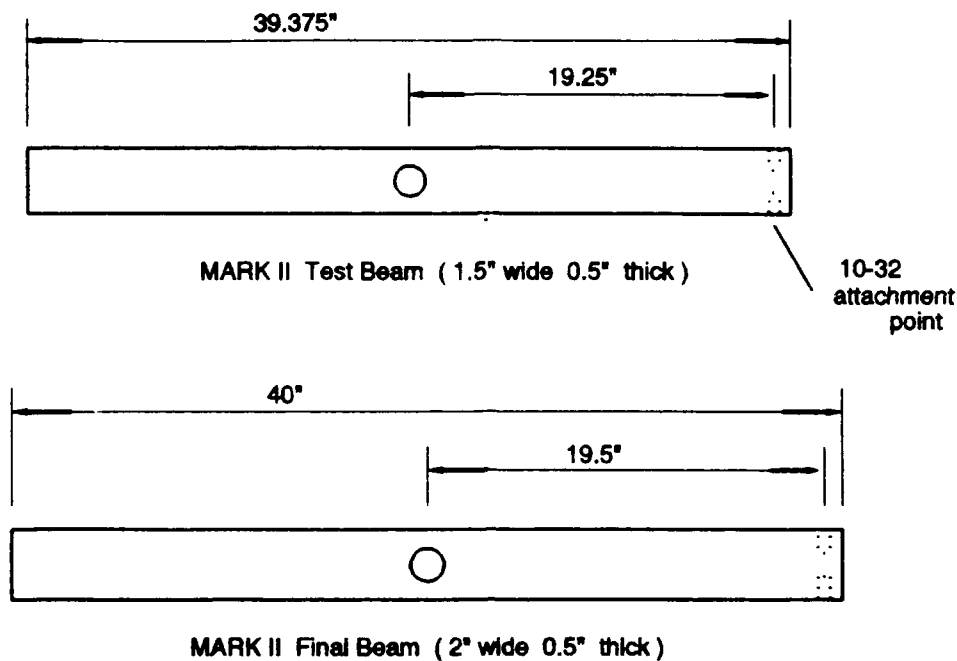


Figure 3-5. Mark II Beams

cantilevered beam, very similar in design to the Mark I beam. Based on the discussion in Section 3.1.1. for the Mark I design, the Mark II beam is assumed to be rigid, and any measured linear displacement of the beam below the fully clamped condition will be approximately proportional to the angular displacement of the joint.

Spacers: The spacers were fabricated from the same cold rolled steel stock as the beam. The design of the spacers is nearly identical to the Mark I design, except the inner spacer is now the bottom spacer, and the outer spacer is now the top spacer. See Figure 3-2.

Spring-Nut Assembly: The spring nut assembly is identical to the spring-nut assembly for the Mark I, and is in fact, interchangeable with the Mark I. See Figure 1-3.

Baseplate: Only one test baseplate was fabricated for the Mark II. The baseplate was made from a 24 inch long piece of angle iron. The angle iron is 0.25 inches thick with 2.5 inch and 1.5 inch sides. See Figure 3-6. Set screw towers were welded onto the baseplate to secure the top spacer. The test baseplate was clamped to the 2-girder-plate vibration isolation stand for testing (the final model was bolted down).

Bolt: Common 0.5 inch diameter steel bolts were used in the test model. The only requirement was that the bolt shank length was long enough to clear the spacers, beam and baseplate combined thicknesses. See Section 3.3.8. for a complete description of the bolts used for final testing.

3.2.2. Mark II Final Model. The final model, illustrated in Figure 3-6, is very similar to the first except for three major differences. The beam and spacers are made from a 2 inch wide by 0.5 inch thick beam of stainless steel, and the baseplate is designed to be bolted securely to the 2-girder-plate vibration isolation stand with 1 inch diameter bolts. Stainless steel was chosen as a suitable material for the final design of the beam in an attempt to control the condition of the friction surfaces by keeping them free from rust. The third difference is that a bolt head locking

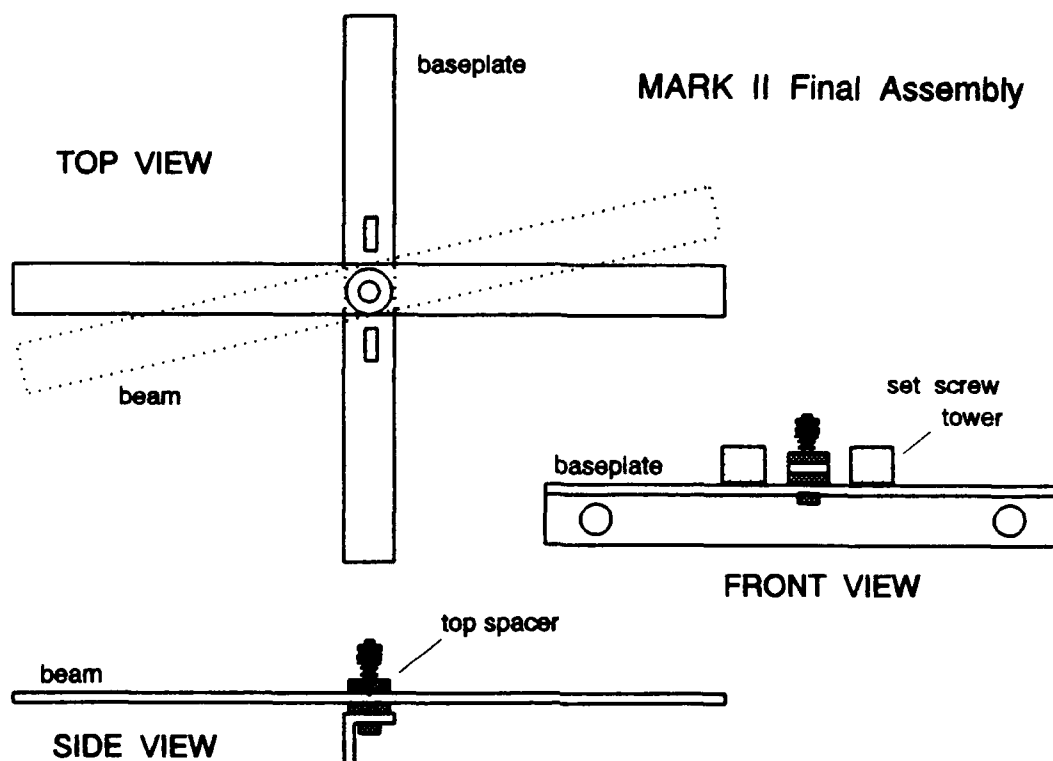


Figure 3-6. Mark II Final Assembly

mechanism has been added in order to ensure the bolt is locked into a fixed position during final testing. With the addition of the bolt head locking mechanism, it is now assumed that the only frictional dissipative surfaces are the sides of the beam facing the spacers. Tables 3-1 and 3-2 list the specifications for the Mark I and Mark II test and final models.

Table 3-1
Mark I Specifications

MARK I			
	Test Model	Final Model	
Beam Dimensions	21.25" x 1.5" x 0.5"	21.5" x 2" x 0.5"	
Beam Material	Cold Rolled Stock Steel	Stainless Steel(304)	
Distance L from bolt hole center to shaker	19.5"	19.5"	
Area Moment of Inertia, $I=(bh^3)/12$	0.1406 in ⁴ (b=thick) (h=width)	0.3333 in ⁴	
Young's Modulus, E	2.9E07	2.9E07	
Max Static Deflection for cantilevered beam with tip loads			
x=L :	50lb	30.30 mils	12.79 mils
	10	6.06	2.56
	5	3.03	1.28
	1	0.61	0.26
x=3":	50lb	1.02 mils	0.43 mils
	10	0.20	0.09
	5	0.10	0.04
	1	0.02	0.01
r/L ratio	0.089	0.089	
Beam Wgt	4.25 lbs	5.75 lbs	
Lead Wgt	20.25 lbs	20.25 lbs	
Total Wgt	24.5 lbs	26 lbs	
Spacer Dimensions	1.5" dia 0.5" hole 0.5" thick	2" dia 0.5" hole 0.5" thick	
Mass Moment of Inertia (slug-ft ²)	(not computed)	1.683 (measured)	

Table 3-2

Mark II Specifications

MARK II			
	Test Model	Final Model	
Beam Dimensions	39.375" x 1.5" x 0.5"	40" x 2" x 0.5"	
Beam Material	Cold Rolled Stock Steel	Stainless Steel(304)	
Distance L from bolt hole center to shaker	19.25"	19.5"	
Area Moment of Inertia, $I=(bh^3)/12$	0.1406 in ⁴ (b=thick) (h=width)	0.3333 in ⁴	
Young's Modulus,E	2.9E07	2.9E07	
Max Static Deflection for cantilevered beam with tip loads			
x=L :	50lb	29.16 mils	12.79 mils
	10	5.83	2.56
	5	2.92	1.28
	1	0.58	0.26
x=3":	50lb	1.01 mils	0.43 mils
	10	0.20	0.09
	5	0.10	0.04
	1	0.02	0.01
r/L ratio	0.090	0.089	
Beam Wgt	8 lbs	11 lbs	
Lead Wgt	N/A	N/A	
Total Wgt	8 lbs	11 lbs	
Spacer Dimensions	1.5" dia 0.5" hole 0.5" thick	2" dia 0.5" hole 0.5" thick	
Mass Moment of Inertia (slug-ft ²)	0.223 (computed)	0.317 (computed)	

3.3 Test Equipment

The following is a list of the equipment used during the experiment. A brief description of each item is provided, but a more detailed description including calibration methods and data, can be found in Appendix A. A schematic of the test setup for the Mark II beam can be seen in Figure 1-4. All of the equipment listed below were used during Mark II forced vibration testing. Only the Fotonic sensor, the Surtronic 3 profile analyzer and Nicolet Digital Analyzer were used during Mark I testing (free vibration).

3.3.1. Model 5PM Shaker. A Unholtz-Dickie Corporation Model 5PM shaker was used to supply sinusoidal loads during testing. The maximum force output of the shaker is 50 lbs. Refer to Appendix Section A.1 for more details.

3.3.2. Model TA30 Power Amplifier. A Unholtz-Dickie Corporation Model TA30 Power Amplifier was used to drive the shaker. The TA30 Power Amplifier can drive the shaker to full performance anywhere from 2-10,000 Hz. Refer to Appendix Section A.2 for more details.

3.3.3. Oscillator-Servo-Programmer (OSP-4). A Unholtz-Dickie Oscillator-Servo-Programmer (OSP-4) Sine Vibration Controller was used to provide the signal generation and control during the sinusoidal vibration testing of the Mark II beam. The OSP-4 is designed to maintain constant set values of displacement or acceleration during frequency sweeping

anywhere from 5-5000 Hz. The OSP-4's system sensitivity to the input acceleration signal was calibrated when the ENDEVCO accelerometer calibration was performed. Refer to Appendix A.3 for more details.

3.3.4. Accelerometer. An ENDEVCO Piezoelectric accelerometer model 2235C was used to provide the acceleration signal for the OSP-4. The accelerometer has a frequency response of 4-5000 Hz. The accelerometer was calibrated against the AFIT laboratory's standard accelerometer at 10 mv/g. Refer to Appendix A.4 for more details.

3.3.5. Force Transducer. A PCB Piezotronics Quartz Force Transducer was used to measure the force on the beam. The rated capacity of the transducer is ± 100 lbs with a manufacturer's calibration of 50mv/lb, with an in-house calibration of approximately 49.94 mv/lb (a calibration constant of 50 mv/lb is used throughout testing). The transducer has a frequency response of .15-100,000 Hz. Refer to Appendix A.5 for more details.

3.3.6. Fotonic Sensor. A fiber optic measurement system, the MTI 1000 Fotonic sensor performs non-contact displacement/vibration measurements. For this thesis, a Fotonic sensor Model KD-320 was used. The Fotonic sensor was used to measure displacements of the beam. The Fotonic sensor has a frequency response from dc to 100kHz. The Model KD-320 sensor (with the optical extender) has a linear operating

range of approximately 100 mils over a 4-5 volt range with a standoff distance of approximately 0.45 inches. The KD-320 can measure displacements as low as 18 microinches. Refer to Appendix A.6 for more details.

3.3.7. Digital Analyzer. A Nicolet Multipro Digital Analyzer was used for data acquisition during testing. The Nicolet was used to digitize analog signals from the force transducer and Fotonic sensor. In addition, the Nicolet SMOOTHING function was used to smooth the acquired signals by computing a weighted running average to eliminate high frequency noise. The Nicolet system was also used when calibrating the Fotonic sensor and force transducer. Refer to Appendix A.7 for more details.

3.3.8. Surtronic 3 Profile Analyzer. The Surtronic 3 is a profile analyzer which provides a numerical measurement of the roughness (but not the waviness or curvature) of a surface by what is known as the Ra (Rough average) method. The Surtronic 3 was used in an attempt to monitor the surface finish of the beam and spacer frictional surfaces. The Surtronic 3 can accurately measure surface irregularities as small as 2-8 microinches (0.05-0.2 microns) high. Refer to Appendix A.8 for more details.

3.3.9. Internally Gauged Bolt Transducers. In order to measure the clamping force at the joint, four 0.5 inch diameter stainless steel (Grade 8) bolts were purchased, each

with a 4-bridge strain gauge internally mounted into the shank of each bolt. The bolts are designed to measure clamping forces from 0-4000 lbs with a maximum error of 1.5% at full strength. The bolts were calibrated to 1 mv/lb. Refer to Appendix A.9 for more details.

IV. Test Procedures and Data

4.1 Mark I (Free Vibration)

4.1.1. Initial Test and Checkout. The purpose of the initial testing for the Mark I was to calculate the moment of inertia and natural frequency of the system, and then to experimentally verify the results. Table 4-1 lists the mass and physical dimensions required to calculate the system mass moment of inertia, I_o , and x_{cm} as outlined in Section 2.3.1.

Table 4-1

Mass and Physical Dimensions of Mark I

Mass:

$$\begin{aligned}m_1 &= (5.75\text{lbs}) / (32.2 \text{ ft/s}^2) = 0.1786 \text{ slugs} \\m_2 &= (20.25\text{lbs}) / (32.2 \text{ ft/s}^2) = 0.6289 \text{ slugs} \\m_t &= \phantom{(20.25\text{lbs}) / (32.2 \text{ ft/s}^2)} = 0.8075 \text{ slugs}\end{aligned}$$

Physical Dimensions:

for I_1 calculation:

$$\begin{aligned}x_1 &= \text{pivot to beam c.g.} = 9.75" \\h &= \text{beam width} = 2" \\L &= \text{overall beam length} = 21.5"\end{aligned}$$

for I_2 calculation:

$$\begin{aligned}x_2 &= \text{pivot to plate c.g.} = 18.5" \\a &= \text{plate height} = 4" \\b &= \text{plate width} = 6.75"\end{aligned}$$

x_1 , x_2 , and x_{cm} are defined as shown in Figure 2-11. First, x_{cm} is calculated using Equation (2-41). Note that x_1 , x_2 ,

and x_{cm} are measured from the pivot point, and not the top of the beam, which is 1 inch further out. Therefore Equation (2-41) becomes

$$x_{cm} + 1'' = \frac{m_1(x_1 + 1'') + m_2(x_2 + 1'')}{m_t} \quad (4-1)$$

which gives $x_{cm} = 16.57$ inches. Recall that the mass moment of inertia for the beam is I_1 , and can be found by using Equation (2-43),

$$\begin{aligned} I_1 &= \frac{.1786}{12} \left(\left(\frac{2}{12} \right)^2 + \left(\frac{21.5}{12} \right)^2 \right) + .1786 \left(\frac{9.75}{12} \right)^2 \quad (4-2) \\ &= 0.1661 \text{ slugs-ft}^2 \end{aligned}$$

I_2 is found using Equation (2-44),

$$\begin{aligned} I_2 &= \frac{.6289}{12} \left(\left(\frac{4}{12} \right)^2 + \left(\frac{6.75}{12} \right)^2 \right) + .6289 \left(\frac{18.5}{12} \right)^2 \quad (4-3) \\ &= 1.5171 \text{ slugs-ft}^2 \end{aligned}$$

and I_o is

$$I_o = I_1 + I_2 = 1.6834 \text{ slugs-ft}^2 \quad (4-4)$$

The natural frequency of the system is then computed using Equation (2-48) to give

$$\omega_n = \sqrt{\frac{Wx_{cm}}{I_o}} = \sqrt{\frac{(26) \left(\frac{16.57}{12} \right)}{1.6834}} = 4.62 \frac{\text{rad}}{\text{sec}} \quad (4-5)$$

and the vibration frequency of the system is

$$f = \frac{\omega_n}{2\pi} = 0.735 \frac{\text{cycles}}{\text{sec}} \quad (4-6)$$

In order to check the computed center of mass, several attempts were made in balancing the beam on a center punch clamped vertically with a table mounted vise. The beam appeared to balance at the computed position, but was unstable, and kept toppling over. However, the computed x_{cm} appeared to be correct. In order to measure the moment of inertia, a knife edge support was fashioned out of a small piece of steel about 4 inches long using a grinder. The knife edge was securely clamped to the edge of a table. The Mark I was suspended from the knife edge and set into motion. A stopwatch was used to count 10 cycles. On the average, 10 cycles were counted every 13.76 seconds. The measured vibration frequency is

$$f_{meas} = \frac{10 \text{ cycles}}{13.76 \text{ seconds}} = 0.727 \frac{\text{cycles}}{\text{seconds}} \quad (4-7)$$

Table 4-2 lists the computed and experimentally measured mass moment of inertias and frequencies. The measured values are considered more accurate since the computed values did not take into consideration the various holes or roundness of the corners of the lead weight plates (which would affect inertia calculations) in the beam and plates.

Table 4-2

Computed versus Measured
Moments of Inertia and Natural Frequencies for Mark I

Computed	Measured
$I_o = 1.6834 \text{ slugs-ft}^2$	$I_o = 1.7218 \text{ slugs-ft}^2$
$\omega_n = 4.62 \text{ rad/sec}$	$\omega_n = 4.57 \text{ rad/sec}$
$f = 0.735 \text{ Hz}$	$f = 0.727 \text{ Hz}$

Two major problems were noted with the experimental set-up during the initial test and checkout phase: (1) the internally gauged bolt transducer was not capable of accurately measuring the clamping forces at the joint, and (2) the Fotonic Sensor's calibration could not be considered reliable under the full range of free vibration motion. Both problems are discussed below.

As discussed in Appendix A, the internally gauged bolt transducers are not capable of accurately measuring clamping forces when subjected to off-axis loading, or torsional bending. The weight of the beam on the bolt shank under free vibration motion produced wide fluctuations in the clamping force readings, sometimes as much as 10 lbs. Once the beam was placed onto the bolt shank, the calibration gain was no longer considered to be reliable. In an attempt to control the amount of clamping force, a method was developed using quarter turn rotations of the spring-nut assembly. The outside spacer was brought into contact with the beam due to

a slight pressure from the spring-nut assembly. This position was called the zero clamping position, although a slight clamping force was present. The clamping force was then increased by 1 quarter turn positions of the nut. Under static conditions (i.e. no movement of the beam), several attempts were made to determine the clamping force for the quarter turn positions using the calibrated bolt. This was accomplished by trimming the bolt amplifier to zero at the zero clamping force position described above, and then recording clamping force readings as the nut was turned in 1 quarter increments. The clamping force values listed in Table 4-4 are averaged over 8 trials. However the clamping force data from trial to trial were not repeatable, mostly because the zero position is poorly defined and difficult to duplicate by hand. For example, the one half turn position averaged to 20 lbs, but ranged between 12 to 30 lbs over 8 trials. The calibrated bolts were useless in terms of measuring clamping forces under these conditions. A more accurate representation of a repeatable clamping force was found by measuring the time to decay for a set clamping force as determined by the quarter turn method. Once a clamping force is set and the beam is set into motion, then the time for the motion to completely stop (as measured by the digital analyzer) is recorded. Since the beam is displaced the same amount for every test, then the time to decay should be the same under the same clamping force

condition. This method (time to decay) was used for the Mark I testing. Refer to Mark I test procedures in Section 4.1.2. for details.

The second problem with the experimental set-up was with the Fotonic sensor calibration. As discussed in Appendix A, the Fotonic sensor is targeting a polished aluminum disc mounted near the top of the beam. The target disc is superglued to the beam, and the Fotonic Sensor signal hits the target at a distance of approximately 1.25 inches above the pivot point of the beam. The Fotonic Sensor could be mounted closer to the pivot point, but doing so would limit access to one of the set screw towers. The maximum initial displacement of the beam is physically limited to a rotation of approximately 10 degrees, because of the placement of the Fotonic sensor equipment near the beam. The 10 degree rotation equates to an approximate horizontal tip displacement of ± 3.6 inches from the vertical, and an approximate target disc horizontal displacement of ± 0.22 inches from the vertical. This means that the Fotonic sensor signal will bounce back off the target disc at different angles as the beam cycles back and forth. Although 10 degrees is considered small enough to assume linear analysis of rotational motion (which is assumed throughout this thesis), 10 degrees is a relatively large angle when a light source less than an one eighth of an inch is expected to reflect back to the source off

of a target rotating that much. Since the Fotonic Sensor is designed to measure linear displacements, smaller angle rotations are desired for linear analysis. It was hoped that a solution to the problem would be to only include the measured displacements near the end of a free vibration test. Unfortunately, with no clamping force and an initial tip displacement of 3.6 inches, the motion of the beam would completely stop under 30 seconds, and with $3/4$ to 1 full turn of the nut, the motion would stop after only 2-3 cycles. This meant that the number of peaks available for determining the envelope of decay (which is a measure of the amount of damping present) was low. Furthermore, it was difficult to calibrate the Fotonic Sensor against tip displacements of more than 1 inch, because the table top micrometer pushed the beam up and away during calibration. (Although the Mark II was calibrated using the same method as the Mark I, the Mark II was physically limited to maximum tip displacements of ± 0.25 inches, and rarely exceeded tip displacements of ± 0.15 inches during testing.) For this reason, only three successive positive displacement peak positions and magnitudes were recorded during testing, usually beginning with the fourth peak back from the steady state zero volt position. The peaks closest to the steady state zero position are considered to be more representative of linear decay. The response of the Fotonic sensor signal did display nonlinear characteristics

(which will be discussed in Section 5.1), and is not considered to be reliable enough to be included in a detailed damping analysis. However, the experimental data (which is presented in Section 4.1.3. and discussed in Section 5.1) appears to be generally linear over the entire range of displacements, and tends to experimentally verify the estimated calibration constant of 8.3 volts per foot (refer to Figure 4-2). A Linear Displacement Voltage Transducer (LDVT) was considered as a way in which to measure the displacements of the beam. This idea was abandoned because the same problems that the Fotonic Sensor has in measuring larger rotations are inherent with the LDVT, plus the LDVT adds undesired friction to the system.

4.1.2. Test Procedures. The testing procedures for the Mark I are listed below. Note that all of the Mark II testing preceded the Mark I testing. The testing procedures are broken into three general areas:

1. Pre Testing Assembly and Set-up
2. Testing
3. Data Reduction

4.1.2.1. Pre Testing Assembly and Set-up.

Step 1: An internally gauged bolt is inserted through the baseplate and locked into place using the bolt head locking mechanism.

Step 2: The Mark I baseplate is bolted to the 2-girder-isolation stand using 1" bolts.

Step 3: The bolt is connected to the Measurements Group 2310 Signal Conditioning Amplifier. Refer to Step 3 in Section 4.2.2.1.

Step 4: The frictional surfaces are Ra measured using the Surtronic 3 profile analyzer. Figure 4-1 illustrates the measurement locations. Refer to Step 4 in Section 4.2.2.1.

Step 5: The beam is placed over the bolt shank.

Step 6: The Fotonic Sensor is calibrated. See Step 6 in Section 4.2.2.1., and refer to the previous section for a discussion on the reliability of the calibration.

4.1.2.2. Testing. Once the Pre Testing Assembly and Set-up is completed, the actual testing phase begins. Note that the step numbering begins where it left off in the previous section.

Step 7: The Nicolet Multipro Digital Analyzer is configured with a TIMEBASE of 10-30 seconds, depending on the clamping force, with a 6 volt scale. The Fotonic Sensor output is fed into channel 1A.

Step 8: Balance (trim) the Fotonic Sensor and bolt gauge readings. Be sure that the beam is in a vertical position. The bolt gauge is unreliable under torsional loading (see Appendix A). Clamping forces were set by quarter turns of the first nut. Refer to Table 4-4 and see step 15 in Section 4.2.2.1.

Step 9: Set the desired clamping force and record it.

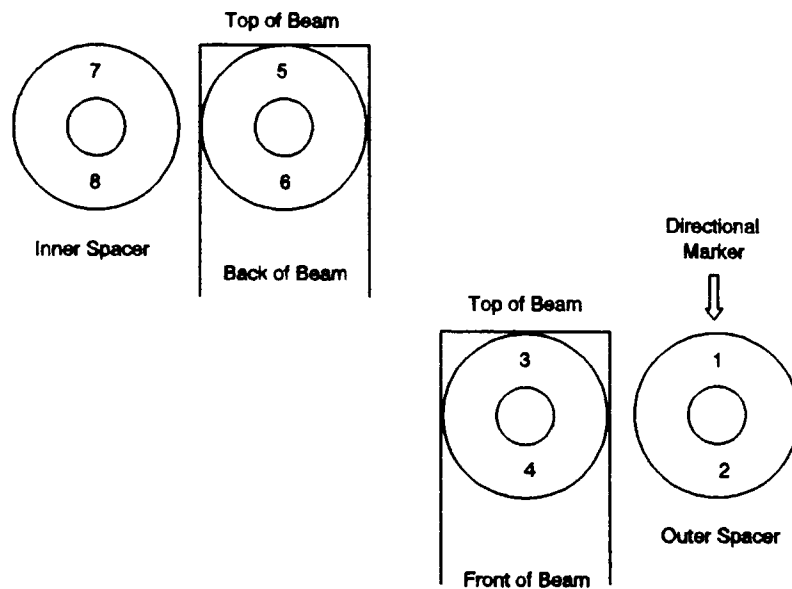


Figure 4-1. Ra Measurement Positions for Mark I

Clamping forces were set by quarter turn positions of the nut as described in Section 4.1.1. The second locking nut was not required for Mark I testing, because the set screw towers sufficiently immobilized the outer spacer. Refer to step 16 in Section 4.2.2.1.

Step 10: Set a positive TRIGGER near 0.2 volts and select AUTO TRIGGER on the Nicolet Digital Analyzer. Displace the beam (to the left when facing the front of the beam) to the stop position (3.6 inches) and release. Note that the Fotonic Sensor was positioned in such a manner that a displacement to the left produced a negative voltage signal. The AUTO TRIGGER would not trigger until the beam was released from the stop position and passed through the zero position which was determined in Step 8. Therefore, all the experimental data

begins with an initial displacement near zero and an initial velocity other than zero.

Step 11: Record time (seconds) and magnitude (volts) of three positive peaks in the displacement curve, usually beginning with the 4th peak back from the zero (stopped) position of the beam. Save the digitized data. Refer to Step 26 in Section 4.2.2.3.

Step 12: Repeat steps 9-11 until the full range of clamping forces has been reached.

4.1.2.3. Data Reduction. The data recorded in step 11 is sufficient for the envelope of decay calculations, which is computed using the script.m file MARK1MU.m. MARK1MU.m also computes the coefficient of friction μ .

4.1.3. Test Data. Table 4-3 lists the general parameters for the Mark I free vibration tests. No forced vibration testing was conducted on the Mark I. The test data are presented in Table 4-4. Figure 4-2 is representative of the type of displacement versus time curves that were collected. For a discussion of the results and comparisons against the theoretical model, refer to Section 5.1.

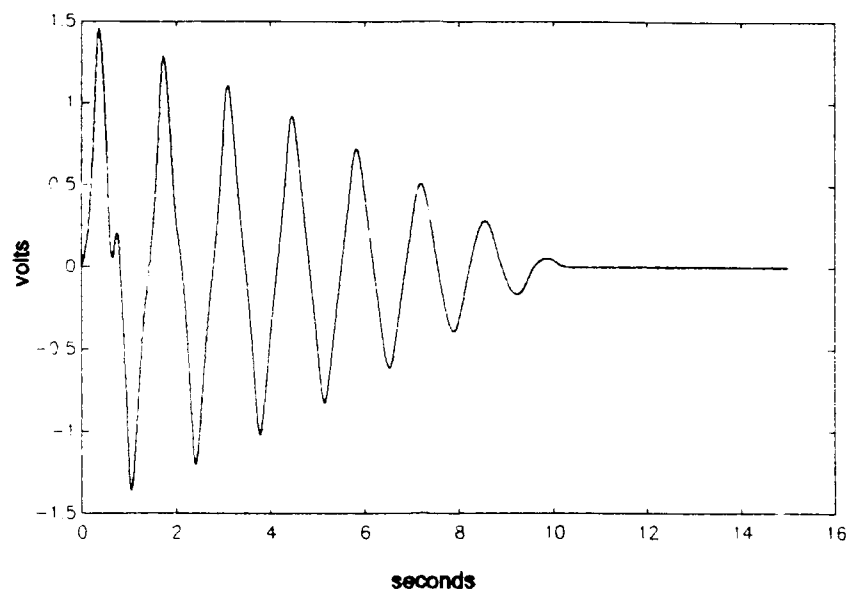


Figure 4-2. Example of Mark I Free Vibration Experimental Displacement versus Time Curve (Clamping Force = 1/4 Turn)

Table 4-3

Mark I General Test Parameters

Bolt: 572E
 Sweep Time: 10-30 seconds
 Fotonic Sensor Calibration: ≈ 8.6 volts/foot

Ra Measurements (microinches)								
(position)	(1)	(2)	(3)	(4)	(5)	(6)	(7)	(8)
before:	26	27	21	30	31	37	32	35
after:	26	26	22	31	31	36	xx	xx

Table 4-4

Mark I Free Vibration Test Data

Clamping Force ¹	Peak 1	Peak 2	Peak 3	Damping Time to 0 volts ⁴
	(sec,volts)	(sec,volts)	(sec,volts)	(sec)
0 turn ²	15.36, .621	16.70, .520	18.08, .422	23.4
(0 lbs) ³	16.70, .520	16.70, .525	18.08, .437	24.3
	15.36, .603	16.70, .504	18.05, .397	24.3
1/4 turn	4.48, 0.907	5.81, 0.722	7.18, 0.509	10.2
(1 lbs)	4.48, 0.912	5.85, 0.712	7.20, 0.501	10.2
	4.46, 0.925	5.81, 0.726	7.18, 0.512	10.2
1/2 turn	1.75, 1.045	3.11, 0.645	4.45, 0.200	4.9
(20 lbs)	1.75, 1.046	3.12, 0.643	4.46, 0.203	5.0
	1.75, 1.051	3.11, 0.656	4.48, 0.221	4.9
3/4 to 1 full turn	Less than 2-3 full cycles			

Note 1: Under dynamic torsional loading the gauged bolts could not produce a steady clamping force reading. Readings varied as much as 10 lbs.

Note 2: Tests were performed at 1/4 turns of the locking nut, beginning with a zero position where the outside spacer was just touching the beam under a slight clamping tension produced by the spring-nut assembly.

Note 3: Static testing of the 0, 1/4,... turn positions of the nut produced these avg clamping force readings (lbs). Note that at the zero turn position, a small non-zero clamping force exists, but the bolt amp is trimmed to zero.

Note 4: This time begins when the beam passes through the vertical line for the first time once it is released from the stop position.

4.2 Mark II (Forced Vibration)

4.2.1. Initial Test and Checkout. Initial testing was performed using the Mark II test set-up. The purpose of the initial testing phase was to learn how to operate the test equipment and to develop procedures for collecting and analyzing data. The internally gauged bolts were not available for initial testing, so tests were done using no clamping pressures and arbitrarily chosen high clamping pressures. The high clamping pressures were chosen below a clamping pressure which would totally lock up the beam. The purpose in choosing two different clamping pressures was to be sure two different hysteresis curves would be produced.

The Mark II Test beam was attached to the 2-girder-beam-plate assembly in room 150 of the AFIT Laboratory as already discussed in Section 3.2. The accelerometer and force transducer were attached to one end of the beam using 10-32 studs. The force transducer was connected to the shaker via a shaker stinger. The Fotonic sensor was arbitrarily placed along the edge of the beam, about midspan, with a standoff distance of approximately 0.5 inches. Neither the Fotonic sensor or force transducer were calibrated for initial testing (although the force transducer is factory calibrated at 50mv/lb), since all force versus displacement measurements would be in volts. Again, only the shape and relative magnitudes of the force versus displacement curves were of

interest. The accelerometer was calibrated as discussed in Appendix A. The test beam and test beam attachment plates were tested for levelness using a level, and care was taken to ensure the stinger mount was level when the beam and shaker were fastened together. All initial testing was done at an arbitrarily chosen load controlled value of 0.2g from the OSP-4. The outputs of the Fotonic sensor and force transducer were fed simultaneously into the Textronic oscilloscope and the Nicolet Multipro Digital Analyzer. The accelerometer signal was fed directly into the OSP-4. No special preparation of the frictional surfaces was performed, other than to wipe them off with a dry cloth prior to mating. All the attachments, bolts, set screws, and clamps were checked for tightness periodically.

All initial tests were run with a sweep time of 200 ms with a data point being sampled every 200 microseconds. This number was chosen to ensure that at least 2 cycles of force and displacement were captured at every test frequency. The test frequencies were at 10, 20, 30 and 40 Hz. A test grid is shown in Table 4-5.

Table 4-5

Mark II Initial Testing Grid

Frequency	No Clamping Force	Higher Clamping Force
10 Hz	F10A F10B	G10A G10B
20 Hz	F20A F20B	G20A G20B
30 Hz	F30A F30B	G30A G30B
40 Hz	F40A F40B	G40A G40B

F(G) = No Clamping (Higher Clamping) Force Designator
 # = cycle frequency in Hz
 A = Channel 1A: Force (volts) vs time (sec)
 B = Channel 1B: Displacement (volts) vs time (sec)

F10A is a data file containing a volt versus time signal acquired by the Nicolet Digital analyzer. The Prefix F is a designator for no clamping pressure, and the number 10 is for 10 Hz. The letter A is a designator for channel 1A, which is always the force transducer signal. Channel 1B is always the Fotonic sensor signal. Channel 1A and 1B were always captured simultaneously.

Once the data was captured, it was smoothed using the Nicolet Multipro SMOOTHING function. The SMOOTHING function performs a weighted running average in order to eliminate high frequency noise on the signals. The Fotonic sensor signal was especially noisy (20mv plus). This was attributed to the fact that the Fotonic sensor was not calibrated nor was it

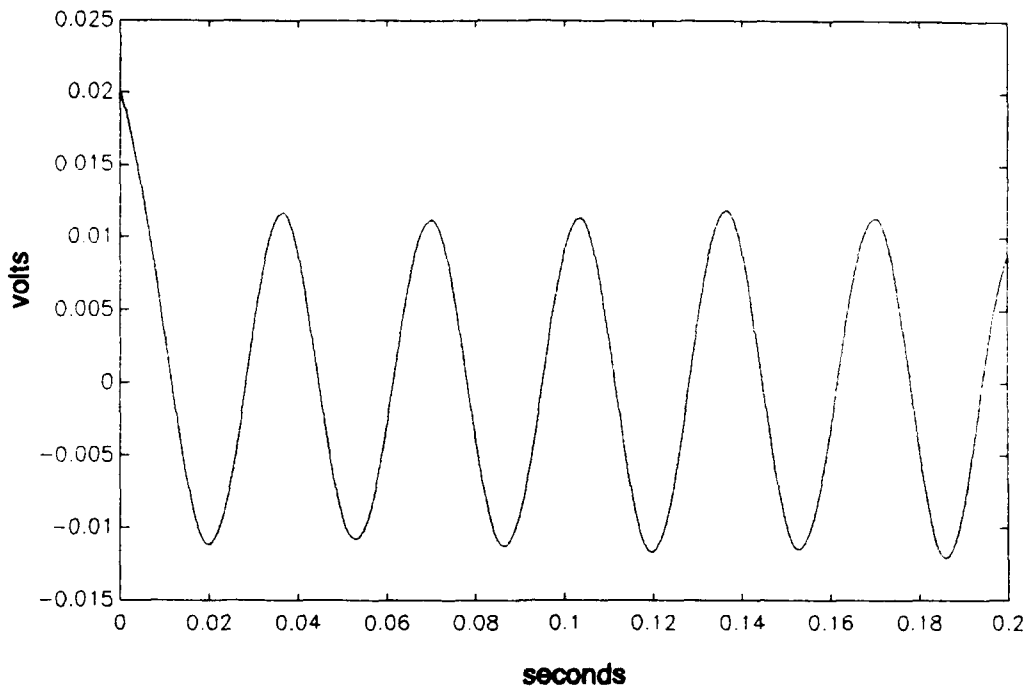


Figure 4-3. Example of Data Smoothed Incorrectly

targeting a very shiny or clean target. When a polished aluminum disk was placed in between the sensor and the beam, the signal improved significantly (down to 10mv). Once smoothed the data were stored to the hard disk and floppy. Unfortunately, the raw data was lost at this point because the smooth data was not renamed. The loss of the data was not critical to the overall purpose of the test.

A problem was noted with the SMOOTHING function. Unless the Nicolet cursor is placed in approximately the same position for each channel, the resulting smooth data will be skewed to one side, since the weighted running average is

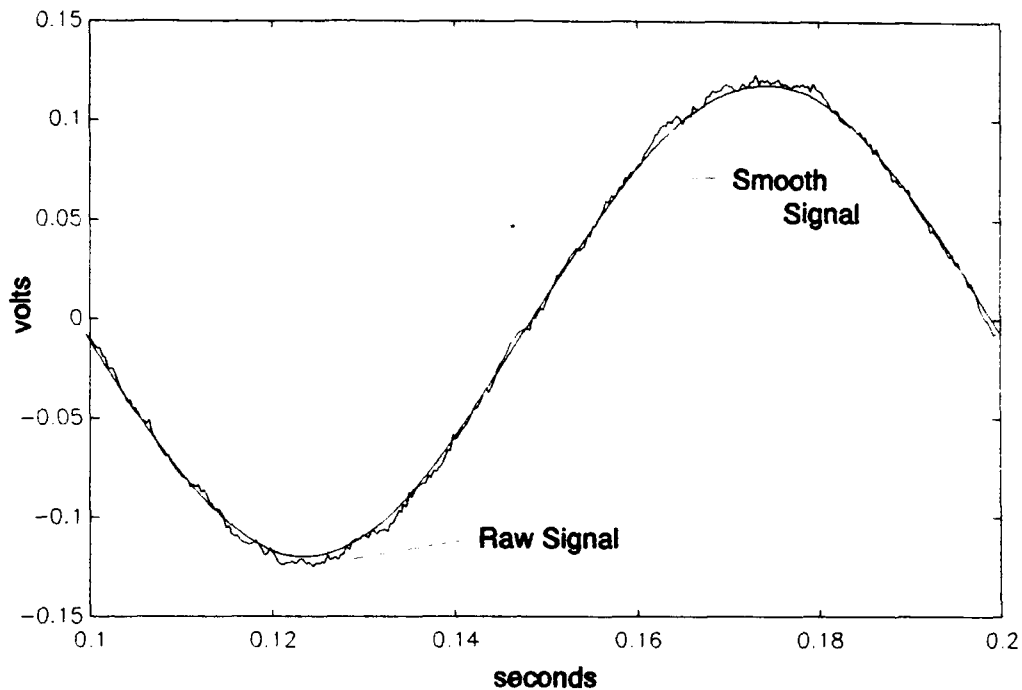


Figure 4-4. Example of Data Smoothed Correctly

performed evenly on both sides of the cursor location. An example of badly smoothed data can be seen in Figure 4-3. Furthermore, the more cycles that are present in 1 sweep, the more the SMOOTHING function will flatten the data, since the number of data points remained constant at 1000 during the test. This is what happened to the data in Figure 4-3. Too few data points were spread over too many cycles, and was interpreted as noise. Plus, the cursor was placed far to the left, so the data was unevenly smoothed as well. The lesson learned here was to always set the sweep timebase to trap the same number of cycles from frequency to frequency testing, or

to increase the number of sampled data points. Then, by placing the Nicolet cursor at the midspan zero position of the data before selecting the smooth execute command would ensure an evenly and accurate smoothing process. All final data were collected and smoothed in exactly the same way. An example of data smoothed correctly can be seen in Figure 4-4.

Once the data were acquired and successfully stored on the Nicolet, the files were then converted to ASCII and transferred to the SCGRAPH Unix system by disk. Various MATLAB script.m files were written and tested during the initial testing phase to analyze the data. In particular, AREA.m will calculate the area contained by 1 hysteresis loop using the trapezoidal rule when given 2 Nicolet channels and the frequency the data were collected. AREA.m went through several iterations, most notably AREAFIT.m. AREAFIT.m would calculate the area using polyfitted data of the upper and lower curves of the hysteresis loop and compare it to the trapezoidal rule. As the order of the polyfit was increased, the calculated area would approach the trapezoidal area, which gave confidence in the trapezoidal rule calculations. Diagnostic plots of the curves were provided for visual inspections of the hysteresis curves. Manually computing the area in the curves compared favorably with the calculated area. AREA.m also returns the peak to peak force and displacement magnitudes in volts. Refer to Appendix C for the

actual AREA.m script. Once the data were transferred to the SCGRAPH Unix system, the Script.M files were thoroughly tested. The data from the initial testing are presented in Table 4-6.

Table 4-6

Mark II Initial Testing Results

Test	Energy Dissipated (volts ²)	Peak Force (mv)	Peak Displacement (mv)
F10	0.001610	41.49	245.72
F20	0.0002823	45.35	53.40
F30	0.00006099	43.64	22.72
F40	0.000004569	38.40	11.51
G10	0.03299	295.61	190.47
G20	0.006406	204.42	60.88
G30	0.0003107	91.53	21.31
G40	0.00001202	38.82	8.61
F = No clamping force at joint			
G = Hi clamping force at joint			
# = Frequency of dynamic load			

The data in Table 4-6 seem to indicate that as the clamping pressure increases, the energy dissipation increases, which was expected. Figure 4-5 compares the hysteresis loops from the F10 and G10 tests. Note that the F10 hysteresis is much flatter, but not entirely flat. This is due to the fact that even for a no clamp condition, some energy will be dissipated since the weight of the beam is always sliding on the bottom spacer. Once the data were reduced, it was noted that controlling the tip load using the OSP-4 g-level controller was not controlling the peak force levels on the

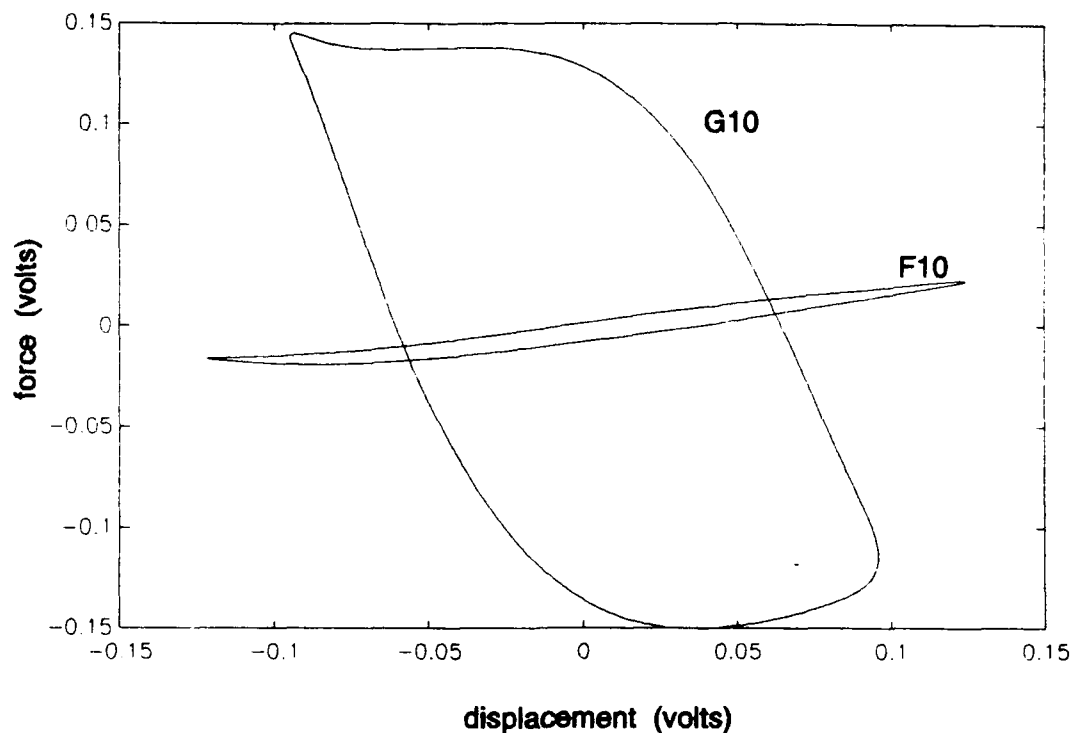


Figure 4-5. Mark II Initial Testing Hysteresis Curves F10 and G10

beam as desired. Instead as the clamping pressure was increased, the stiffness and mass of the system was, in effect, changing. In order to maintain a constant 0.2g force level, the OSP-4 was driving the shaker with a different voltage signal, thereby increasing the peak load at the end of the beam. Acceleration was remaining constant, but the effective mass of the system was changing, and force magnitudes went up. The effect of increasing clamping force is investigated in the next section. In order to control the

force levels at the end of the beam, it would be necessary to watch the force transducer signal on the oscilloscope, while manually increasing the TA30 power amplifier signal until a desired force level (in millivolts) was reached.

Several lessons were learned and procedures developed from the initial tests and are highlighted below. Refer to the next section for a detailed breakdown of the procedures used in final testing.

1. Data Smoothing procedures were developed.
2. Load Control procedures were developed.
3. The Data Logistical Trail was developed. This included everything from capturing the signals from the transducers and eventually reducing the data.
4. The MATLAB Script.M files for plotting the hysteresis loops and calculating the energy dissipated (area in the loop) were written and debugged.
5. The reflectivity and surface condition of the target affected the noise level of the Fotonic sensor, which meant the target surface on the final Mark II beam needed to be more reflective (and smoother) than on the test beam.
6. A problem with the stability of the shaker stand during initial testing was also noted (it moved under heavier dynamic loading), and was corrected by building a heavier shaker stand. Refer to Appendix A for a complete discussion on the placement and calibration of all the test equipment.
7. The last, and perhaps most important, item that was noted during initial testing pertained to the surface condition of the frictional surfaces before and after testing (see below).

No special surface preparations were performed on the frictional surfaces once they were received from the AFIT model fabrication shop. The surfaces were milled using a flycutter, and were smooth to the touch, but it was easy to see that the surfaces had been milled. The Ra readings from the Surtronic 3 averaged between 50 to 80 Ra using the microinch scale. Readings were taken only out of curiosity, since no attempt was going to be made in controlling the surface condition for the test beam. In order to test and checkout the various equipment components for the experiment, the test beam was going to be exercised at several clamping pressures and end loads at different frequencies over a period of several weeks. Not controlling the surface conditions seemed reasonable, since this would be done for the final beam, and the overall goal of the initial testing was to develop procedures and checkout the equipment. Once the test model was disassembled, it was noted that the surface conditions of the contact areas were visibly covered with rust and felt slightly gritty to the touch. The stainless steel material in the final beam would eliminate the rusting, so no further concern for the controllability of the surface conditions were made at this time.

4.2.2. Test Procedures. The final testing phase consisted of 8 different tests, which are detailed in Sections 4.2.3.1. through 4.2.3.8. The testing procedures are listed below, and are essentially the same from test to test. The testing procedures are broken into 3 general areas:

1. Pretesting Assembly and Setup
2. Testing
3. Data Reduction

4.2.2.1. Pre-Testing Assembly and Set-up.

Step 1: The Mark II baseplate is bolted to the 2-girder-plate isolation stand using 1" bolts. The levelness is checked using a level.

Step 2: An internally gauged bolt is inserted up through the baseplate and locked into place using the bolt head locking mechanism. A small T-square was used to insure the bolt was inserted and locked into position perpendicular to the baseplate bottom spacer.

Step 3: The bolt was connected to the Measurements Group 2310 Signal Conditioning Amplifier using the 4-pin connector. The gain on the amplifier was set and locked into position to match the bolt it was calibrated against. The FILTER selection was set to 10 and the EXCITATION VOLTAGE was set to 5 volts. Refer to Appendix A for details on the bolt calibration. The output of the 2310 Signal Conditioning Amplifier was fed into a Hewlett-Packard 3466A Digital

Multimeter with a FUNCTION selection of VOLTS at a range of 20.

Step 4: The frictional surfaces were wiped clean using acetone, allowed to dry, and then Ra measured using the Surtronic 3 profile analyzer. The top and bottom of the beam, and the top spacer were all measured in four locations, using the average value from 5 Ra measurements at each location. The bottom frictional surface, because of its mounted position was measured in only 3 locations. Figure 4-6 illustrates those positions. The RANGE was set to the MICROINCH scale, with the CUTOFF set at 2.5-0.1 . Refer to Appendix A for details on the operation of the Surtronic 3 and its calibration.

Step 5: The frictional surfaces are wiped clean using acetone and are allowed to dry. The beam is then mounted on top of the baseplate. Once mounted, the beam is checked for levelness using the level. The level is placed in several locations along the beam to check for levelness.

Step 6: The Fotonic sensor is secured into position and then calibrated as described in Appendix A. Once calibrated, the standoff distance is measured and the slope of the calibration curve is computed. The Fotonic sensor's DISPLACEMENT/VIBRATION switch is set to READ with a FILTER RANGE of 6 and a COARSE INTENSITY LEVEL of x.1k. The FINE INTENSITY level was taped into position during initial calibration by the AFIT

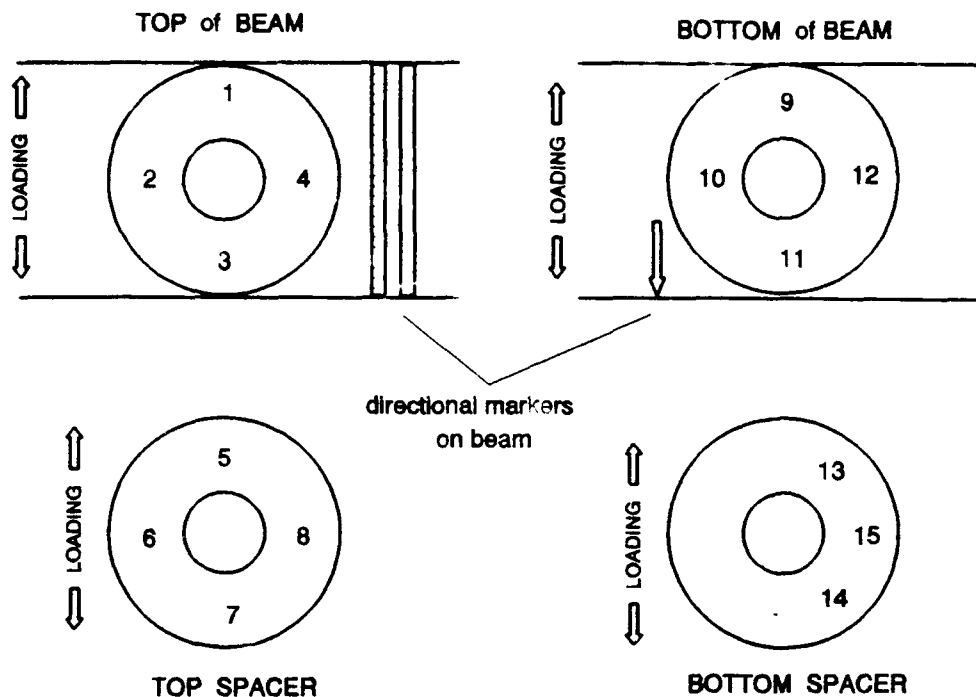


Figure 4-6. Ra Measurement Positions for Mark II

Laboratory technicians. The output of the Fotonic sensor is fed simultaneously into the Tektronix 2465B Oscilloscope (channel 2) and the Nicolet Multipro Digital Analyzer (channel 1B).

Step 7: The PCB Force Transducer is threaded onto the shaker stinger assembly, and using a 10-32 stud, is threaded onto the beam at the tip location. The shaker stinger is then bolted to the shaker face plate using 4 allen bolts. The shaker is mounted securely to a shaker stand as described in Appendix A. The beam is checked for levelness, and if not level, is disassembled and reassembled, making the necessary adjustments

to the shaker stand. The force transducer is connected to its amplifier (GAIN set to 1) with a microdot cable. The amplifier output is fed simultaneously into the Tektronix 2465B Oscilloscope (channel 1) and Nicolet Multipro Digital Analyzer (channel 1A).

Step 8: The ENDEVCO Accelerometer is mounted onto the beam opposite the force transducer using a 10-32 stud. The accelerometer is connected to the OSP-4 using a microdot cable. The accelerometer input is connected to the CHARGE-IN port on the back panel of the OSP-4. The accelerometer was calibrated with the OSP-4 as described in Appendix A.

Step 9: The Nicolet Multipro Digital Analyzer was configured for BOARD 1 with 2 CHANNELS ENABLED (1A and 1B). Channel 1A was always the force signal, and channel 1B was always the displacement signal. Each input channel was set for AC COUPLING with the FILTER selection ENABLED. The TRIGGER was set for channel 1A only. All units were set in VOLTS/SEC. The DISPLAY was set at YT for data acquisition. The CHANNEL and DISPLAY configurations are stored on the Nicolet System as TESTING.CHS and TESTING.DSS respectively. TESTING.CHS and TESTING.DSS were used throughout all testing. The number of data points collected in a sample was fixed at 1000. The timebase was adjusted as necessary to collect 3 complete cycles for each snapshot of the incoming signals. The peak-to-peak range for each channel was normally set at 300 mv.

The peak-to-peak range values, and the TRIGGER were adjusted as necessary during testing.

Step 10: Refer to the OSP-4 operation manual for switch locations. See Appendix A for calibration information. The OSP-4 front and back panels were configured as outlined in Table 4-7.

Table 4-7
OSP-4 Front and Back Panel Settings

OSP-4 Front Panel	
Dial (2.4):	1k Max Response Speed
Oscillator Mode Button (2.12):	MANUAL
Servo Mode Button (2.1):	ON
Displacement/Acceleration Control Button (2.7):	OUT
Level Multiplier Buttons (2.9):	Both OUT
Level Verniers (2.8) and Frequency (2.13):	Adjusted as required
OSP-4 Back Panel	
Toggle (2.18):	CHARGE IN
Toggle (2.20.1):	10-100 SENSITIVITY
Sensitivity Dial (2.20.2):	271.9
Switch (2.28):	EXTERNAL GROUND
Toggle (2.35):	SWEEP SPEED INTERNAL

Step 11: Warmup. The following equipment was allowed to warmup per manufacturers' specifications.

1. Fotonic Sensor (30 min)
2. OSP-4 Controller (10 min)
3. 2310 Signal Conditioning Amplifier (30 min)

In actuality, items 1, 2 and 3 were very rarely turned off during the course of the testing (2 months).

4.2.2.2. Testing. Once the Pretesting Assembly and Set-Up was completed, several tests were conducted over a period of several months. Certain steps in the pretesting phase were repeated as required and are noted with the individual test runs in the next section. Note that the numbering of the procedures continues where it left off in Section 4.2.2.1.

Step 12: Set proper TIMEBASE and CHANNEL peak levels on Nicolet.

Step 13: Recheck all bolts, attachments, and levelness.

Step 14: Recheck all transducer settings and gains.

Step 15: Retrim as necessary, the following:

(1) Fotonic sensor to read 0.00 volts using DATUM SHIFT knob

(2) Internally gauged bolt amplifier to read 0.000 volts using the AUTO BALANCE RESET toggle and TRIM dial. The bolt amplifier is reset to 0.000 volts for whatever is considered to be an unclamped position. See the test data in the next section.

Step 16: Set the desired clamping force:

(1) Place top washer into position onto of the beam.

(2) Secure top washer in place using the set screw tower assemblies. Do not completely immobilized the spacer at this point, but be sure that the set screws are in the top spacer slots, so no twisting of the spacer occurs while clamping.

(3) Place the spring and first nut onto the bolt and tighten to the desired force as seen on the

HP Multimeter (1mv/1b gain).

(4) Once the desired clamping force is reached, back down the second nut onto the first.

(5) Tighten the set screws into the top spacer securely.

(6) Record the clamping force.

Step 17: Set the OSP-4 to the desired frequency setting.

Step 18: Turn the amplifier VOLTAGE GAIN knob on the TA30 Power Amplifier until the force transduce signal, as seen on the Tektronix Oscilloscope, is at the desired peak-to-peak level.

Step 19: With the Nicolet Multipro Digital Analyzer in the REPETITIVE ONE SHOT mode, observe the signals until a desired steady state condition is reached on channel 1A, then select the ONE SHOT function, and SAVE both channels. Record the dynamic clamping force from the HP Multimeter.

Step 20: Turn the amplifier VOLTAGE GAIN knob on the TA30 Power Amplifier completely to the left (OFF). Repeat steps 18-20 until the full range of desired peak loads (F_o) for a specific clamping force has been reached.

Step 21: Loosen the set screws in the spacer, but do not completely remove them.

Step 22: With 2 wrenches, hold the top nut into place and continue to tighten the bottom nut down, until a new clamping force level is reached.

Step 23: Resecure the top nut and set screws.

Step 24: Repeat steps 18 through 23, until the full range of desired clamping forces has been reached.

Step 25: Once Step 24 is completed, release the clamping force completely by removing both nuts, the spring and the top spacer. Record the reading on the HP Multimeter. Be sure not to completely remove the set screws from the slots in the sides of the top spacer, until the spring is lifted off of the spacer. During clamping and unclamping, the force exerted by the spring on the spacer can cause it to twist and scratch up the frictional surfaces. Once unclamped, record the clamping force offset reading from the HP Multimeter.

4.2.2.3. Data Reduction. Once the testing is completed, the data reduction phase begins. Again, note that the numbering of the procedure steps continues where it left off in Section 4.2.2.2.

Step 26: SAVE the raw data into the proper directory and to floppy disk. All raw data are automatically given a Nicolet .WFT suffix and are in binary format.

Step 27: The raw data are smoothed using the Nicolet SMOOTHING function, as described in the initial test and checkout section 4.2.1. The WINDOW SIZE was always set to 99.

Step 28: The smoothed data are converted from binary to ASCII using a Nicolet provided conversion program WFT2FLT.EXE.

Step 29: Once converted into ASCII, the data are transported

(hand carried by disk) and loaded onto the SCGRAPH UNIX Operating System in order to use the MATLAB script.m files located on that system.

Step 30: Each data file is converted from DOS ASCII to UNIX ASCII using the DOS2UNIX.EXE command. First, the HEADER information in each data file must be deleted.

Step 31: Once converted, the data are loaded into MATLAB and the script files found in Appendix C are used to actually compute the area contained by the hysteresis curves.

Step 32: The data are tabulated and graphed. See the next section.

4.2.3. Test Data. Eight tests were conducted on the Mark II beam. The purpose of each test and a brief description of the types of data collected are discussed below in Sections 4.2.3.1 through 4.2.3.8. Only the Test 1 data is presented below, the rest of the test data can be found in Appendix D.

4.2.3.1. Test 1. Test 1 was the first test conducted on the Mark II beam. Refer to Section 4.2.2 for the step by step testing procedures. Table 4-8 lists the Mark II Test 1 General Parameters. Refer to Figure 4-6 for the beam positions at which the Ra measurements were made. Note that after Test 1, the frictional surfaces appeared to have oxidized due to heat generated by excessive sliding. After the test the surfaces were smoothed using several grades of emery paper and a block of wood. Subsequently, the beam was

never subjected to the magnitude of peak loads ($F_o \approx 2$ lbs) again. The Test 1 data are listed in Tables 4-9 and 4-10. Note that the AREA.m data are all in experimentally measured voltage readings from the Nicolet Digital Analyzer. All of the EXPDATA.m results are generated using the calibration constants for force and displacement, and by using the equations developed in Section 2.3.2. Refer to the AREA.m and EXPDATA.m files in Appendix C.

Table 4-8
Mark II Test 1 General Parameters

Bolt: 575B								
Frequency: 10Hz								
Sweep Time: 300 ms (1000 data points)								
Fotonic Sensor Calibration: 9.563 volts/inch								
Force Transducer Calibration: 50 mv/lb								
Approximate time beam was under cyclic loading: 15 min								

Ra measurements (microinches)								
(position)	(1)	(2)	(3)	(4)	(5)	(6)	(7)	(8)
before:	40	39	35	31	33	44	29	40
after:	42	38	37	30	29	41	27	40
(position)	(9)	(10)	(11)	(12)	(13)	(14)	(15)	
before:	41	37	44	46	xx	xx	39	
after:	46	42	50	43	xx	xx	38	

Table 4-9

Mark II Test 1 AREA.m Data (10Hz)

Clamping Force (mv)	Area $\times 10^{-3}$ (volts ²)	P-P Force (mv)	P-P Displacement (mv)
(00) 00	24.77	220.17	604.54
(29) 31	39.48	211.48	649.15
(65) 67	38.47	196.46	284.10
(116) 116	10.34	244.70	100.74

[08]

(xx) = indicated clamping force at joint before loading
xx = indicated clamping force during loading. This value is used as the actual clamping force in data reduction
[xx] = indicated clamping force when joint is unclamped

Table 4-10

Mark II Test 1 EXPDATA.m Results (10Hz)

Clamping Force (lbs)	ED $\times 10^{-2}$ (lbs-in)	Peak Force (lbs)	Peak Displacement (in)	μ
00	5.180	2.202	0.0316	.2891
31	82.57	2.115	0.0339	.2837
67	80.46	1.965	0.0149	.2624
116	21.63	2.447	0.0053	.2561

Average Peak Force (Fo) = 2.182 lbs
Average μ = 0.2728

4.2.3.2. Test 2. Test 2 was the first test after the frictional surfaces had been damaged in Test 1. The

frictional surfaces had been smoothed to a mirror finish using emery paper (grades: 240, 280, 320, 400, 600), and a block of wood. The purpose of this test was primarily to identify what magnitude of peak loads (F_o) could be applied to the beam without damaging the frictional surfaces, but still produce large enough hysteresis information for analysis.

The test was conducted in 2 parts: Test 2A and 2B. Refer to Table D-4 for the General Test Parameters in Appendix D. Test 2A and 2B data are presented in Tables D-5 through D-8. Test 2A collected energy dissipation versus clamping force data for 3 different force levels ($F_o = 0.2, 0.4, 0.8$ lbs) at 10Hz. After determining that no damage to the beam surface had occurred (visual inspection showed no signs of oxidation or scratching), Test 2B proceeded to collect data for 3 different force levels ($F_o = 0.4, 0.6, 0.8$ lbs), over a smaller range of clamping forces. The $F_o = 0.2$ lbs condition was dropped because (1) it was difficult to maintain a peak load of that magnitude, and (2) the beam was barely moving, even for the unclamped condition.

4.2.3.3. Test 3. Refer to Table D-9 for the Mark II Test 3 General Parameters. Test 3 data and results are presented in Tables D-10 and D-11 in Appendix D. The purpose of this test was to collect energy dissipation versus clamping force data for 3 different force levels ($F_o = 0.6, 0.8, 1$ lb) at 10Hz. Note that beginning with Test 3 (and ending with

Test 6), the OSP-4 g-level reading was recorded when the force and displacement signals were captured. The g-level data, using the equations found in Appendix A.1, could provide a check on whether or not the Fotonic Sensor was measuring beam displacements accurately.

4.2.3.4. Test 4. The purpose of this test was to collect energy dissipation versus clamping force data for 3 different force levels ($F_o = 0.6, 0.8, 1 \text{ lb}$) at 15Hz. Refer to Table D-12 for the Mark II Test 4 General Parameters in Appendix D. See Tables D-13 and D-14 for the Test 4 data.

4.2.3.5. Test 5. The purpose of this test was to repeat Tests 3 and 4, except only in the range of clamping forces (50-160 lbs) which appeared to produced the greatest magnitudes of energy dissipation. This was done in order to (1) test the repeatability of the experimental set-up, and (2) to collect more data points in those areas where the maximum energy dissipation seemed to be occurring. Refer to Table D-15 for the Mark II Test 5 General Parameters. The 10Hz test is presented as Test 5A data in Tables D-16 and D-17, and the 15Hz data and results are presented as Test 5B data in Tables D-18 and D-19 in Appendix D. After Test 5, it was determined that the frictional surfaces were not level (see Section 5.5.1.5. for a discussion), and the frictional surfaces were remilled.

4.2.3.6. Test 6. Test 6 was the first test after the frictional surface were re-milled. Refer to Table D-20 in Appendix D for the Mark II Test 6 General Parameters. The test is divided into two parts: Test 6A and Test 6B. See Tables D-21 through D-24 for the Test 6 data. The purpose of this test was (1) to perform a repeatability check on the hysteresis calculations, (2) to sufficiently exercise the frictional surfaces in an attempt to bring the roughness of the surfaces to a steady state condition, and (3) to get an idea on what magnitude of clamping forces and end loads (F_o) were necessary to produce a noticeable phase shift between the force and displacement signals. The purpose of the repeatability test is to verify whether or not the computed area in the selected hysteresis curves are representative of the steady state energy dissipation by the joint for a constant clamping force over a 2-3 minute interval. Because the test setup was completely disassembled, including the baseplate, the Fotonic Sensor was repositioned and recalibrated after re-assembly. Refer to Appendix A for the calibration curves and procedures.

4.2.3.7. Test 7. Test 7 attempted to force the beam at two different peak force levels ($F_o = 1$ and 1.2 lbs) over an extended period of dynamic loading. Each test consists of 3 sets of clamping force cycles. Test 7A is the $F_o = 1$ lb test, and Test 7B is the $F_o = 1.2$ lbs test. Refer

to Table D-25 for the Mark II Test 7 General Parameters. The data from the test are tabulated in Table D-26 through Table D-29 in Appendix D. A repeatability test is included with the $F_o = 1$ lb test and can be found along the test 7A data in Table D-26. The purpose of the repeatability test is to verify whether or not the computed area in the selected hysteresis curves are representative of the steady state energy dissipation by the joint for a constant clamping force over a 2-3 minute interval.

4.2.3.8. Test 8. Test 8 was the final test conducted on the Mark II beam. Refer to Table D-30 for the Mark II Test 8 General Parameters in Appendix D. The data from the test are tabulated in Tables D-31 through Table D-34. An attempt was made to force the beam at two different peak force levels ($F_o = 1$ and 1.2 lbs) over two similar periods of time. Each test consists of 7 sets of clamping force cycles. Test 8A is the $F_o = 1$ lb test, and Test 8B is the 1.2 lbs test.

CHAPTER V: Results and Discussion

5.1 Mark I

The following sections discuss the results of the Mark I testing and experimental set-up. Note that all of the Mark I testing occurred after the Mark II testing was completed. Refer to Section 4.1.1. for a discussion on the initial test and checkout of the Mark I.

5.1.1. Test Results. Fundamental to the development of the Mark I Macroslip damping model presented in Section 2.3.1. is the ability to accurately measure clamping forces and displacements. As discussed in Section 4.1.1. and Appendix A, the internally gauged bolt transducers are not capable of accurately measuring clamping forces when subjected to off-axis loading, or torsional bending, and confidence in the linearity of the Fonic sensor calibration is low. Therefore, the Mark I testing was not extensive, and no conclusive remarks about free vibration energy dissipation versus specific clamping forces can be made. However, an attempt was made to characterize the damping parameters of the Mark I by using the clamping method described in Section 4.1.1. By using quarter turns of the nut, three sets of forced vibration data were collected. Refer to Table 4-4 for the Mark I test data. As determined in Section 4.1.1., the natural frequency, ω_n , of the system is approximately 4.62

radians/second. Each successive peak, as discussed in Section 2.1.1., should be occurring every $2\pi/\omega_n$, or approximately every 1.36 seconds, which is supported by the test data. As previously discussed in Section 4.1.1. the slope of the envelope of decay of the experimental data is not linear across the whole range of data, as seen in Figure 4-2. However, the envelope of decay appears to be linear enough that some analysis of the damping characteristics can be made based on the calibration of the Fotonic sensor. Especially since a 1.5 volt reading (tip displacement \approx 2.2 inches) for the first peak matches an independently estimated tip displacement of the same magnitude using a small, rigid piece of wire attached to the weight assembly as it moved over a ruler placed under the beam. But the clamping forces were not known, and any attempt to match the theoretical model against the experimental data had to be done by guessing the clamping force. Without knowing the true clamping force or exact displacement calibration, it is difficult to accurately determine the amount of damping present. MARKPLOT.m was written to demonstrate the theoretical model and compute the envelope of decay. Refer to Appendix E for details. By choosing an average of 0.3 to represent the coefficients of friction between the spacer-beam-spacer and bolt shank-beam frictional surfaces, an initial displacement of 0.18 feet, and a clamping force of 3 lbs, MARKPLOT.m generated the

displacement versus time and slope curves shown in Figure 5-1. Note that this curve is almost identical to the experimental curve and slope shown in Figure 5-2 (note that the theoretical curve begins with an initial displacement and zero velocity, and the experimental data is acquired with an initial velocity and near zero displacement). The theoretical slope magnitude is 0.0392 feet/second, and the experimental slope magnitude (averaged between peaks 1, 2 and 3 for the 1/2 turn test data) is approximately 0.0377 feet/second. The number of displacement peaks match, and the time to decay is almost the same. But now look at the experimental displacement versus time curve in Figure 4-2. In order to produce a similar curve using the same damping model, the theoretical coefficient of friction must be decreased to 0.2 with a clamping force of 0.5 lbs. The resulting curve is shown in Figure 5-3. The experimental averaged slope is 0.0177 feet/second, and the theoretical slope is 0.0176 feet/second, and as with the previous case the curves are nearly identical. Although the magnitudes of the clamping forces seem reasonable, the coefficient of friction is not expected to change that much under these conditions. Refer to Section 5.2 for a detailed discussion on the effects of clamping force on the coefficient of friction. Therefore, without knowing the clamping forces (and with an accuracy greater than in 1 lb increments, which is the best the calibrated bolts could produce under ideal

conditions), and without knowing the coefficient of friction of the joint surfaces, then it is difficult to proceed with a valid analysis of the data.

5.1.2. Test Set-up. Several mistakes were made in the design of the Mark I. The main problem was the added friction introduced into the system by the weight of the beam on the bolt shank, which was further complicated by off-axis loading of the calibrated bolt transducers. Theoretically the friction between the beam and the bolt shank can be estimated by computing the envelope of decay for the displacement versus time curve for free vibration of just the beam on the shank. But even with no clamping force, the beam motion would reach a steady state zero condition just under 30 seconds, and would wobble slightly against the bolt shank surface for most of that time. This wobbling (which was not present whenever the joint was clamped), further complicated the problems noted in the last section with the Fotonic Sensor measurements. Not only would the Fotonic Sensor signals be reflecting back off of the target disc at large angles, but the target disc was moving vertically away from the Fotonic Sensor as the beam wobbled from side to side.

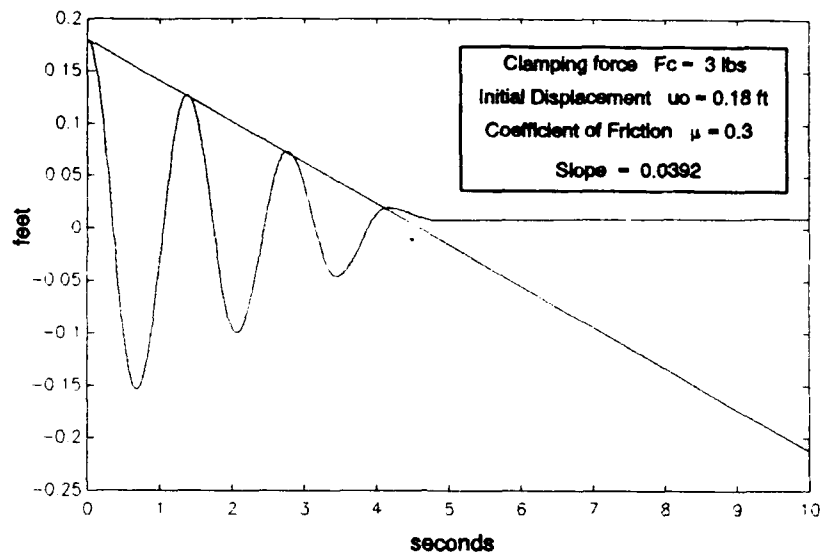


Figure 5-1. Mark I Theoretical Displacement versus Time Curve ($F_c=3$ lbs, $u_o=0.18$ ft, $\mu=0.3$, slope= 0.0392 ft/sec)

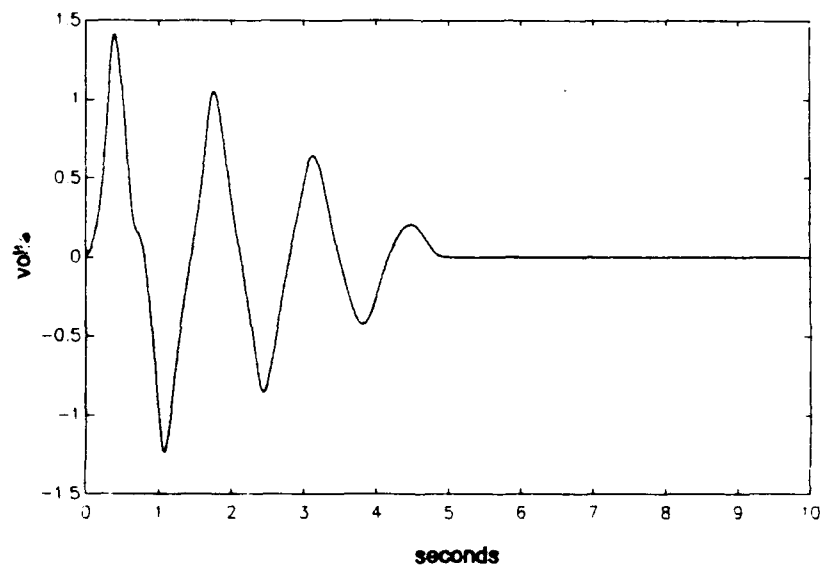


Figure 5-2. Mark I Experimental Displacement versus Time Curve (Clamping Force = $1/2$ turn)

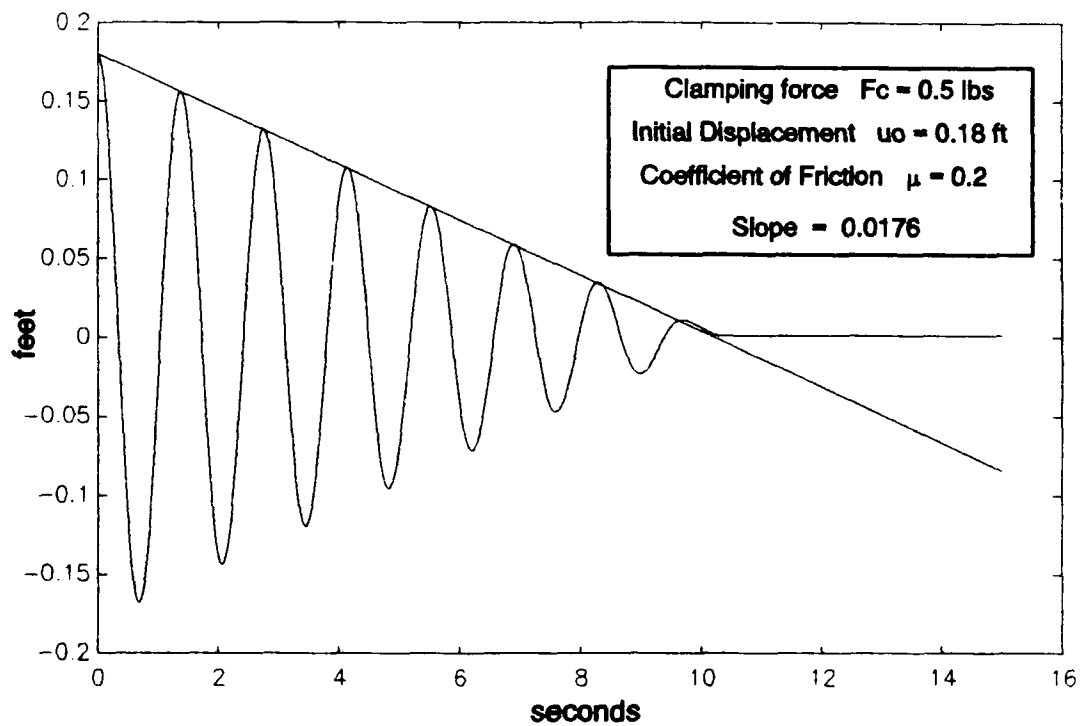


Figure 5-3. Mark I Theoretical Displacement versus Time Curve ($F_c=0.5$ lbs, $u_o=0.18$ ft, $\mu=0.2$, slope= 0.0176 ft/sec)

5.2 Mark II

The following sections discuss the results of the final 8 tests conducted with the Mark II set-up. Tests 1 through 7 are considered to be preliminary tests, with the lessons learned from each test culminating in one final test, Test 8. All the test data and results are tabulated in Appendix D. For a discussion on the final test (Test 8) results, refer to Section 5.2.2. Refer to Section 4.2.1. for a discussion on the Initial Test and Checkout of the Mark II.

5.2.1. Preliminary Mark II Tests (Tests 1 through 7).

5.2.1.1. Test 1. Originally, a goal of this thesis was to collect energy dissipation versus clamping force data for ranges of peak end loads (F_o) from 2-10lbs at clamping forces ranging from 0-200lbs for forcing frequencies from 10-40Hz. Unfortunately, the effects of temperature, or excessive heating, on the frictional surfaces was overlooked. Test 1, which ran for approximately a total of 15 minutes, produced a black layer of oxidation on the frictional surfaces, apparently from the heat generated by friction. The oxidation layer almost covered the entire frictional surfaces, and seemed heavier on the bottom surfaces. The residue did not wipe off with a dry cloth, and when touched, seemed to have changed the texture of the surfaces. However, Ra testing (see Table D-1 in Appendix D) did not indicate any significant changes in the surface roughness had occurred. On the

average, each position changed by an amount of less than $2.7 R_a$, with the greatest change occurring at position 11 (a delta of $6 R_a$).

The data collected from the test did produce the expected trend: as clamping forces increased, energy dissipation increased to a maximum, then dropped. Refer to Tables D-2 and D-3 in Appendix D. Figure 5-4 shows the results versus a theoretically computed energy dissipation versus clamping force curve. It is important to note that the theoretical model is strictly a macroslip approximation based on a computed mean coefficient of friction, μ , which is backed out of the experimental data using the theoretical model. Refer to the MATLAB script.m file EXPDATA.m in Appendix C for the μ calculation.

A flaw exists in the analysis when comparing the theoretical model versus the experimental data in that a constant coefficient of friction is assumed for all ranges of clamping forces and relative velocities between the frictional surfaces. The coefficient of friction for the macroslip model in this paper is assumed constant under all dynamic conditions, just as Lieker and Donnelly assumed in their models^{4,5}. However, the coefficient of friction is not a constant. According to Ludema, the coefficient of friction decreases approximately linearly with an increasing normal load²⁹. Groper addresses this phenomena in Reference 30. In

effect, the coefficient of friction is a very complex function of clamping force, radial position (assuming the clamping force is not uniform over the frictional surface), and surface properties (which are affected by relative surface velocities and by time, through which surface wear will occur)²⁹. For this thesis, as already discussed in Chapters 1, 2, and 3, the design of the beam-joint geometry assumes a constant, uniform clamping force and constant surface properties. Therefore, the computed coefficient of friction using the macroslip model is, at best, an approximation of the actual average dynamic coefficient of friction.

As a result, the average coefficient of friction computed from Test 1 is not disappointing, because it is within the expected values of 0.2-0.42 reported by References 28 and 31. But only 1 test was conducted under these test conditions, and only 4 data points were collected, so it is difficult to draw any conclusions based on the results obtained other than those already mentioned. However, since it was obvious that the surface properties were changing (presumably through excessive heating), it was decided to resmooth the surfaces and continue testing at lower magnitudes of peak (F_o) loading.

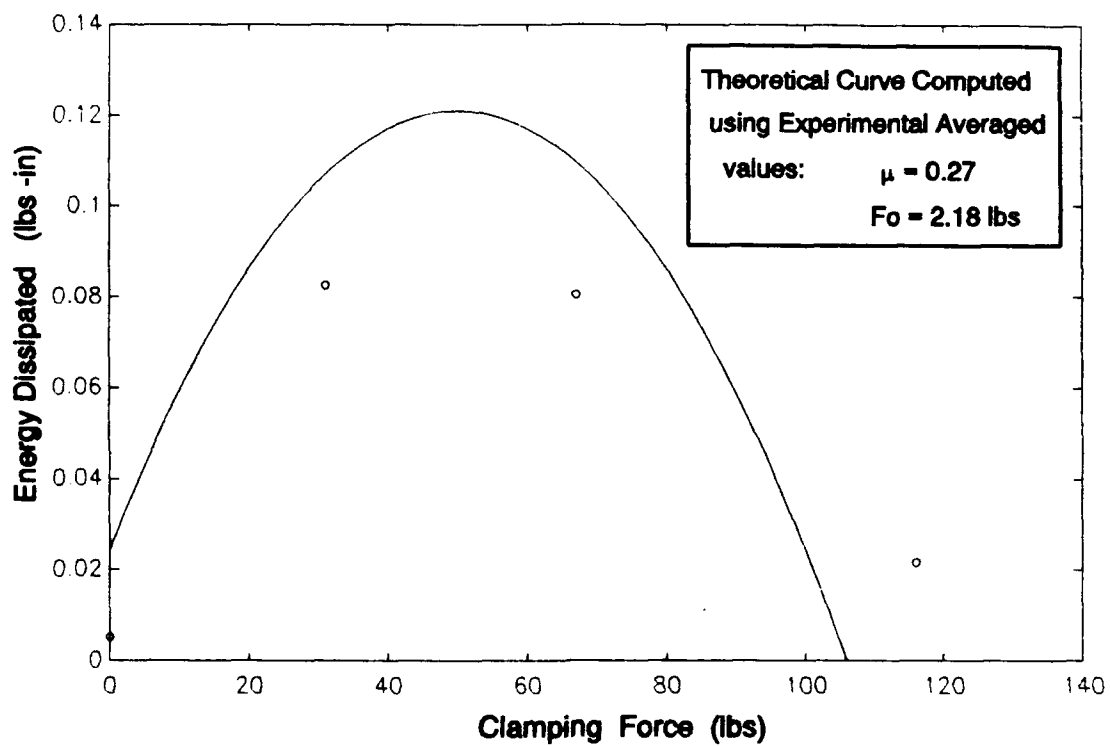


Figure 5-4. Mark II Test 1 Results versus Theoretical Energy Dissipation Curve

5.2.1.2. Test 2. Test 2 was the first test after the frictional surfaces had been damaged and resmoothed in Test 1. The purpose of Test 2 was to identify what magnitude of peak loads (F_0) could be applied to the beam without damaging the frictional surfaces, but still produce large enough hysteresis information. The test is described in Section 4.2.3.2 and the data and results are tabulated in Appendix D. Note that the theoretical model was not fully developed until after Test 5 was completed. As a result, the data collected was only reduced as far as AREA.m could take it: area in volts² which represents energy dissipation, and the peak-to-peak magnitudes of the force and displacement signals in volts (tabulated in millivolts). The data reduction performed by EXPDATA.m was done after Test 5 was completed. Test 2 proceeded very cautiously to collect data at force levels of $F_0 = 0.2, 0.4, 0.6$, and 0.8 lbs. 0.8 lbs was chosen as a maximum since it was below 0.5 times the level which changed the surfaces in Test 1. The test was conducted in 2 parts, Test 2A and 2B, and several items of interest were noted.

The area calculations between Test 2A and 2B were not exactly the same under similar clamping and dynamic loading conditions. This was not totally unexpected at this stage, since some wearing effects on the surfaces should occur over time, even for hard steel on steel.

It was difficult to consistently maintain a peak load (F_o) of 0.2 lbs, presumably because the OSP-4 was having difficulty controlling such a low load, so $F_o = 0.2$ lbs was not used for Test 2B. Furthermore, the 0.2 and 0.4 lb loads were not displacing the beam enough (≈ 8 mils maximum peak displacements) in order to consistently produce hysteresis curves much wider than the Fotonic Sensor noise levels (≈ 10 mv peak-to-peak, or ≈ 1 mil). As a result, the 0.2 and 0.4 lb loads were dropped.

Visual inspection showed no signs of oxidation or scratching on the surfaces. Ra testing did not indicate any significant changes had occurred (see Table D-4 in Appendix D). On the average, each position changed by an amount less than 1 Ra.

The data, particularly the data presented in Test 2B, does indicate the same general trend as found in the Test 1 data, with one exception. Over the entire range of data, as clamping forces were increased, the energy dissipation would increase, then peak, and then drop off. However, over the first 2 or 3 data points in each set (when the clamping force starts at zero and is increased), the energy dissipation would start out at a higher level, decrease, then increase again until a peak was reached. This was presumed to be caused by the way in which zero clamping force is defined. Zero clamping force is that condition when the top spacer is not in

place, and the internally gauged bolt 2310 amplifier is trimmed to zero. In actuality, the bottom frictional surface is "clamped" together by the weight of the beam. This trend was noted in Tests 3, 4, and 5 as well, and is accounted for by the theoretical model of THEORY.m.

5.2.1.3. Test 3. The purpose of Test 3 was to collect energy dissipation versus clamping force data for 3 different force levels ($F_o = 0.6, 0.8, 1 \text{ lb}$) at 10Hz. Based on the results of Test 2, 1 lb was selected as a peak load for 2 reasons: (1) 0.8 lb seemed to produce no noticeable changes on the frictional surfaces, (it was hoped 1 lb would do the same) and (2) a higher peak load was desired in order to get larger hysteresis curves. Also note that beginning with Test 3, the OSP-4 g level reading was recorded when the force and displacement signals were captured (refer to Tables D-9, D-10, and D-11 in Appendix D). As can be seen in the tabulated data, the computed D (peak displacement of the beam as predicted by the OSP-4) compares favorable with the measured peak displacements. The differences are assumed to be due to the fact that as the OSP-4 was trying to control the acceleration, the g-level reading would fluctuate up and down around some mean value, sometimes as much as $\pm 0.05g$. The OSP-4 had a harder time controlling the g-levels at 10Hz than at 15Hz, where smaller delta g's were noted during the control loop process. The g-level readings were discontinued after

Test 6, once the final Fotonic sensor calibration was performed.

The Test 3 results are presented graphically in Figures 5-5 through 5-7. The results are presented with a second order polynomial best fit generated by the MATLAB script file POLYWOG.m which can be found in Appendix C. A second order fit is used because the results are expected, from theory, to follow a second order curve. Note that the data points in the tabulated data where the energy dissipation is low are not shown. As mentioned previously in Section 5.2.1.2, the Fotonic Sensor signal is noisy, with noise levels approaching 10mv peak-to-peak. For this reason, when hysteresis loops were generated and areas calculated using AREA.m, the width of the hysteresis loops were monitored along the displacement axis. As a general rule, those areas, in volts², that were below a magnitude of 10^{-3} volts² were approaching signal-to-noise ratios of 2-to-1 and even 1-to-1, depending on the shape of the curve. Also discarded were those data points near the zero clamping condition, for those reasons discussed in Section 5.2.1.2.

As can be seen in Figures 5-5 through 5-7, the general trend of the results are as expected: as the clamping force was increased, the energy dissipation would reach a peak and then drop off. Figure 5-8 shows the three best fit curves for the three data sets of Test 3. As discussed in Section

5.2.1.2., the data in Test 3 was originally reduced only as far as AREA.m could take it, since EXPDATA.m was not ready until Test 5 was completed. Therefore, the discussion on the computed coefficients of friction, and comparison to the theoretical model, is deferred until Section 5.2.1.5., where the Test 5 results are presented.

5.2.1.4. Test 4. Test 4 is identical to Test 3, except the test was run at 15Hz instead of 10Hz. The Test 4 results are presented graphically in Figures 5-9 through 5-11. Refer to Tables D-12 through D-14 in Appendix D for the tabulated data and results. As with the Test 3 results, the Test 4 results presented in the tabulated data where the energy dissipation is low (less than 10^{-3} volts²) are not shown graphically. Figure 5-12 shows the three best fit curves for the 3 different data sets of Test 4. As discussed in Sections 5.2.1.2. and 5.2.1.3., the results in Test 4 were originally reduced only as far as AREA.m could take it, since EXPDATA.m was not ready until Test 5 was completed. As with the Test 3 results, the Test 4 results displayed the expected general trends for energy dissipation versus clamping forces.

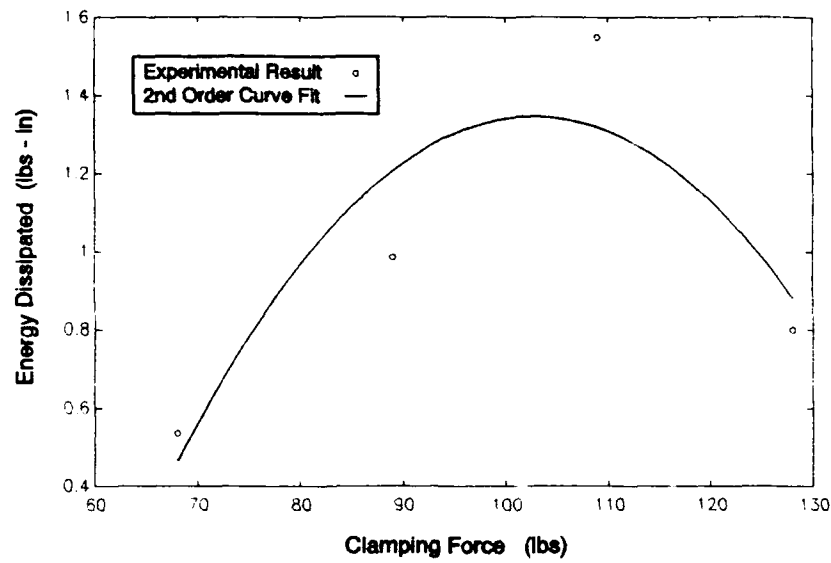


Figure 5-5. Mark II Test 3 Results for Low Fo (0.6 lb) with 2nd Order Curve Fit

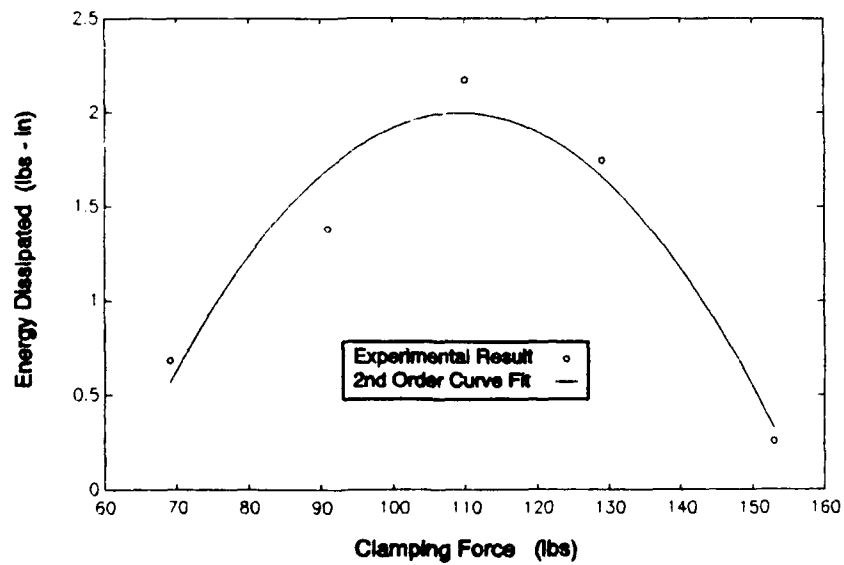


Figure 5-6. Mark II Test 3 Results for Mid Fo (0.8 lb) with 2nd Order Curve Fit

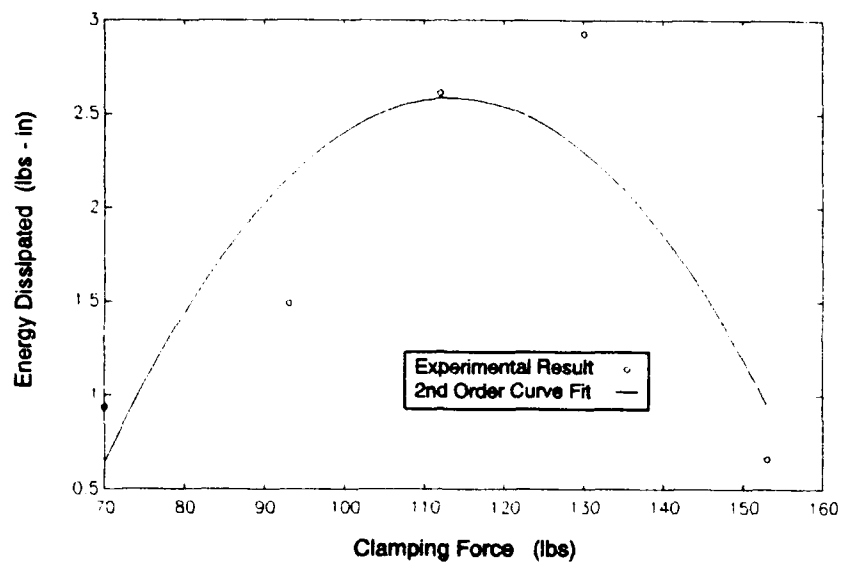


Figure 5-7. Mark II Test 3 Results for Hi Fo (1 lb) with 2nd Order Curve Fit

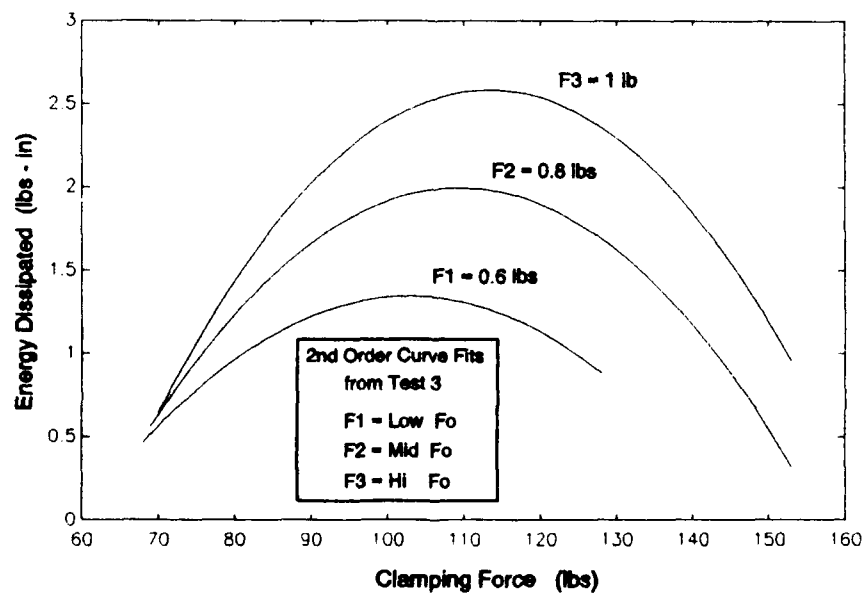


Figure 5-8. Mark II Test 3 2nd Order Curve Fits

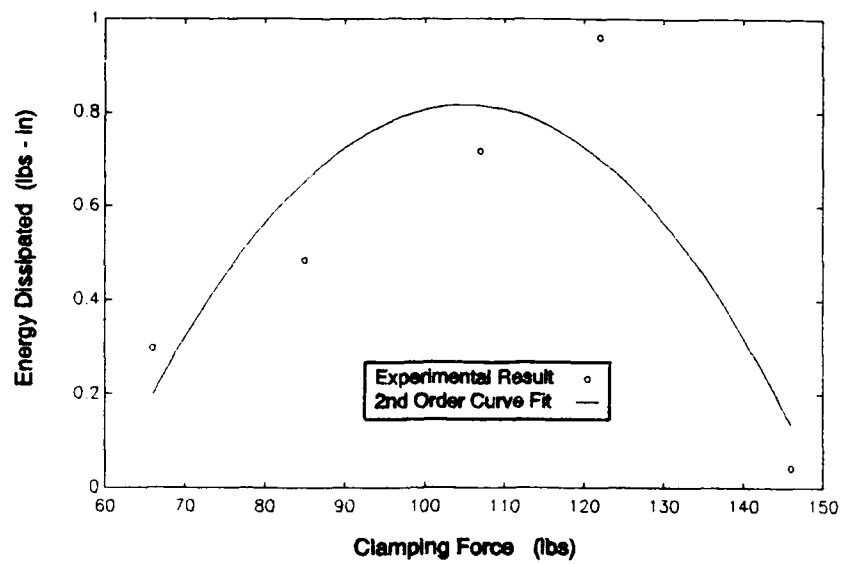


Figure 5-9. Mark II Test 4 Results for Low F_o (0.6 lbs) with 2nd Order Curve Fit

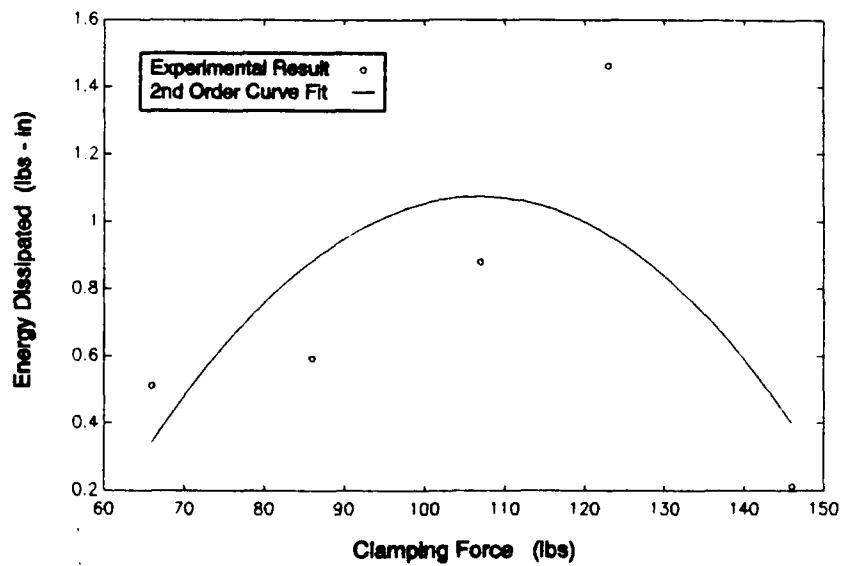


Figure 5-10. Mark II Test 4 Results for Mid F_o (0.8 lbs) with 2nd Order Curve Fit

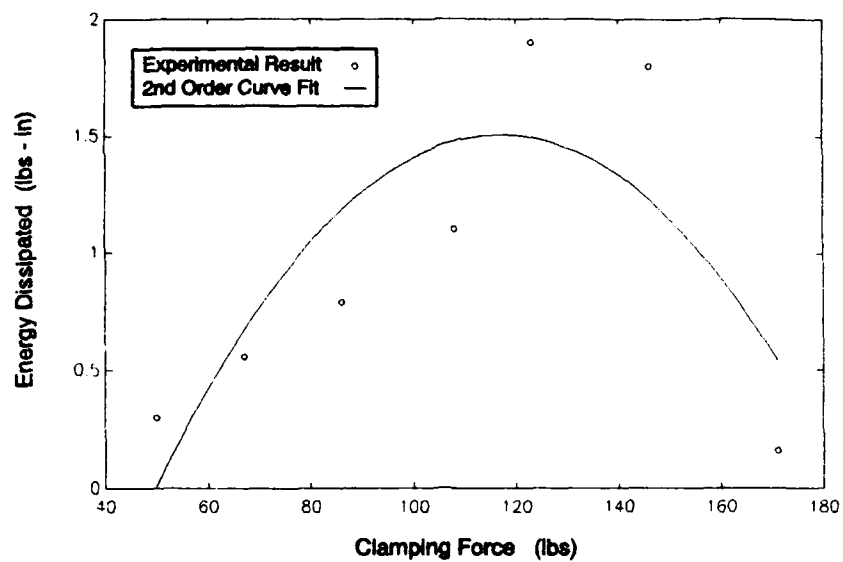


Figure 5-11. Mark II Test 4 Results for Hi Fo (1 lb) with 2nd Order Curve Fit

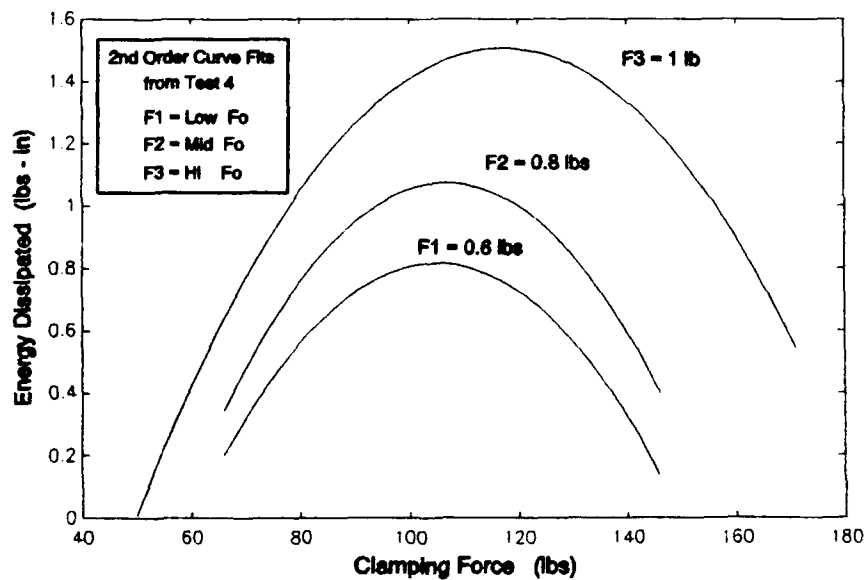


Figure 5-12. Mark II Test 4 2nd Order Curve Fits

5.2.1.5. Test 5. The purpose of this test was to basically repeat Tests 3 and 4, except only in the range of clamping forces (50-160lbs) which appeared to produce the greatest magnitudes of energy dissipation. This was done in order to (1) test the repeatability of the experiment, and (2) to collect more data points. The Test 5 results are presented graphically in Figures 5-13 through 5-20. The Test 5 data and results are listed in Appendix D in Tables D-15 through D-19. Although the general trend of the Test 5 results are good, when compared against Tests 3 and 4, the amount of scatter between the results appears to be significant. For example, Figure 5-21 illustrates a curve fit of the Test 3 data for force level 2 (0.8 lbs) when combined with the Test 5A data of the same type. Figure 5-22 shows the 2 respective curve fits based upon the separated data. Clearly, the test did not repeat itself.

A possible reason for scattering of the data can be found in the results of the Ra testing (see Table D-15 in Appendix D). Although the frictional surfaces did not oxidize (in fact, the frictional surfaces never even felt warm when touched), some light scuffing and scratching was easily visible on all the frictional surfaces and appeared to be confined within a radius of 0.6 inches from the bolt center. The bottom frictional surfaces were the worst. From Test 2 to Test 5, each position changed on the average approximately 4.5

Ra, with the exception of position 10, which changed by 97 Ra. The total (but not continuous) time the beam was under cyclic loading during tests 2 through 5 was approximately 3 hours. It seems reasonable, considering the hardness of the material and the relatively small loads applied ($F_o \leq 11b$) to the system, that it would take as long as it did for any significant changes in the surface properties to occur. The fact that the scuffing and scratching was confined to an inner radius seemed to indicate that the frictional surfaces were not entirely in contact with each other when the joint was clamped. Apparently, the re-smoothing of the frictional surfaces after Test 1, which was done by hand using emery paper wrapped around a block of wood, produced a rounding of the edges. Although not easily visible, the rounding was apparent when the frictional surfaces were remilled using a flycutter blade. The inner portions of the frictional surfaces were in fact higher than the outer edges.

The low coefficients of friction computed by EXPDATA.m are also attributed to the unevenness of the frictional surfaces. A smaller frictional contact area, under an equivalent clamping force, produces a smaller computed value for M_{gross} , which in turn leads to a smaller computed value for μ . Although the tabulated coefficients of friction in Tests 2 through 5 are an order of magnitude lower than what they should be ($\mu \leq 10^{-2}$), they are reasonable when considering

the actual frictional contact surface area is presumed to have been approximately 32% of the area used in the computation of μ . The computed coefficients of friction for Test 2 through 5 can be found in Appendix D.

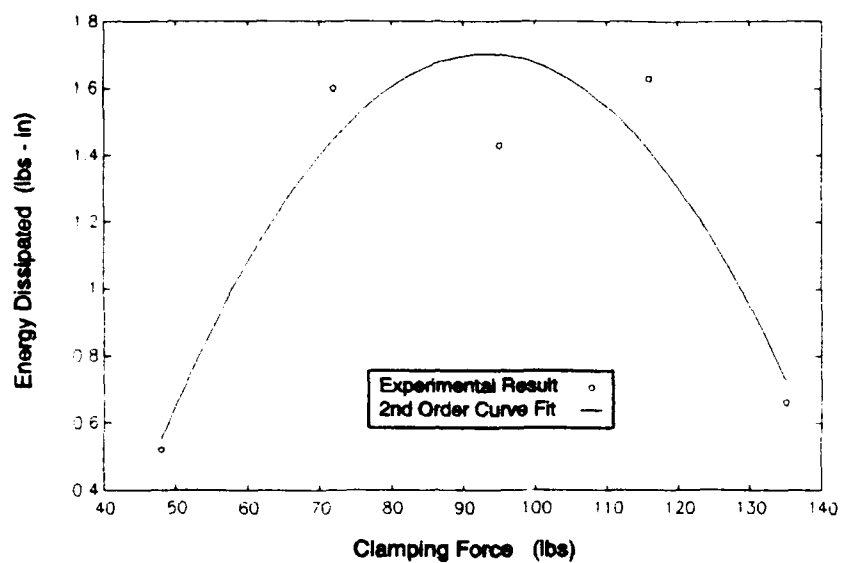


Figure 5-13. Mark II Test 5A Results for Low Fo (0.6 lbs) with 2nd Order Curve Fit

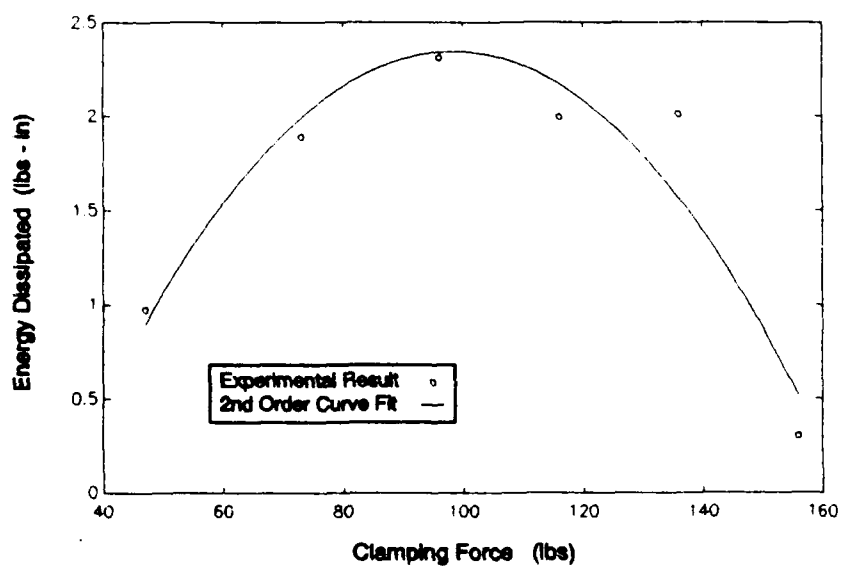


Figure 5-14. Mark II Test 5A Results for Mid Fo (0.8 lbs) with 2nd Order Curve Fit

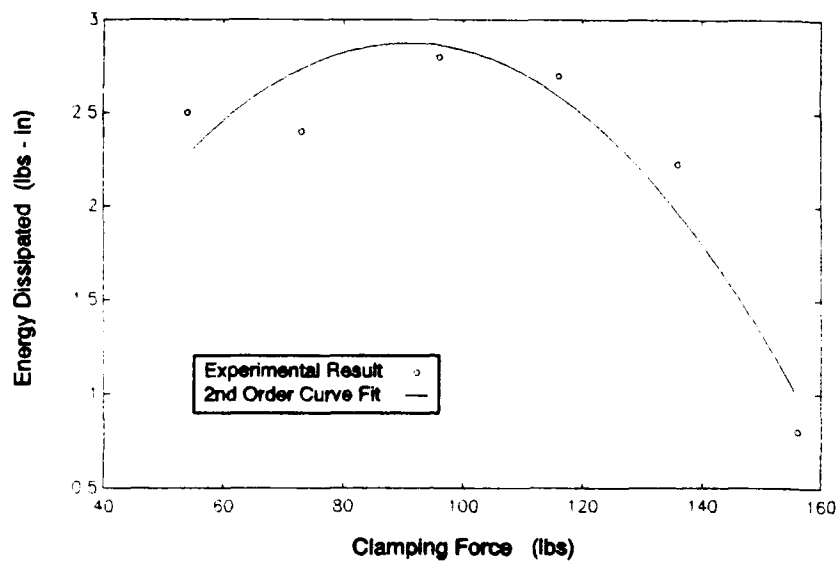


Figure 5-15. Mark II Test 5A Results for Hi Fo (1 lb) with 2nd Order Curve Fit

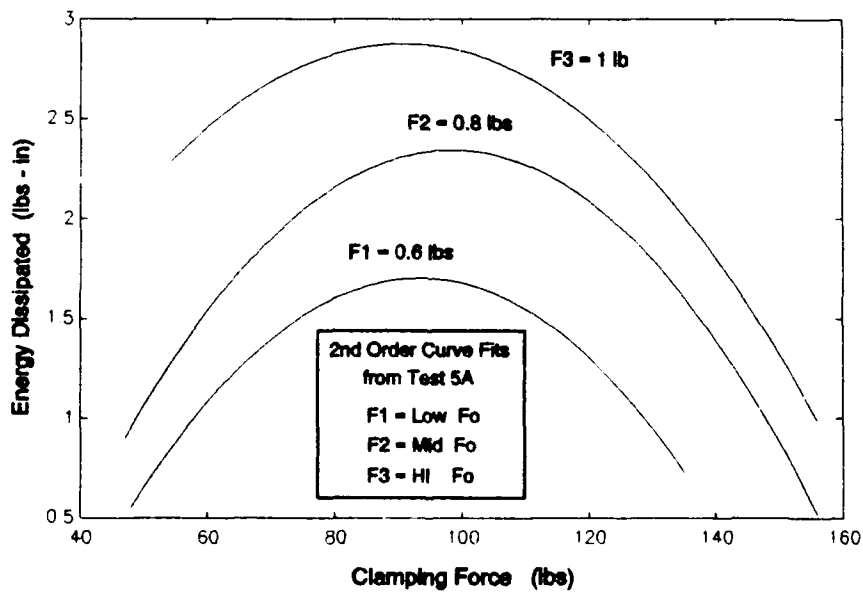


Figure 5-16. Mark II Test 5A 2nd Order Curve Fits

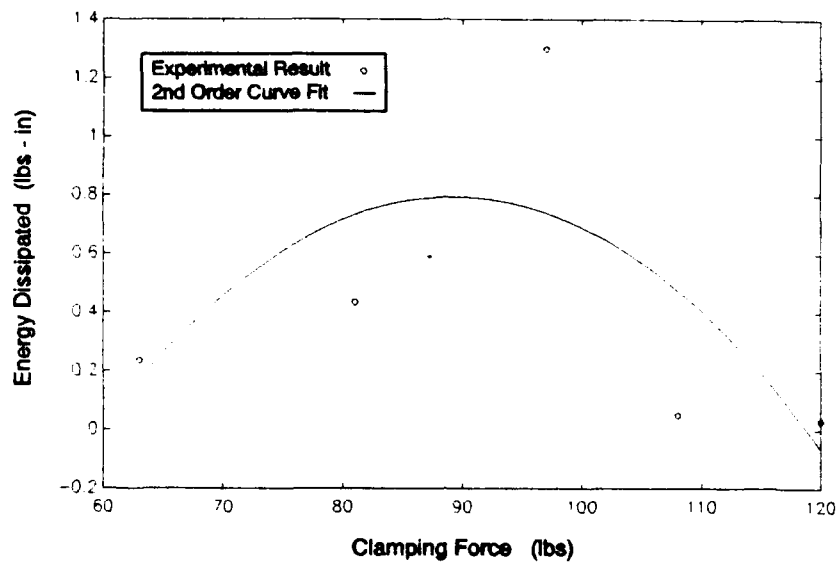


Figure 5-17. Mark II Test 5B Results for Low Fo (0.6 lbs) with 2nd Order Curve Fit

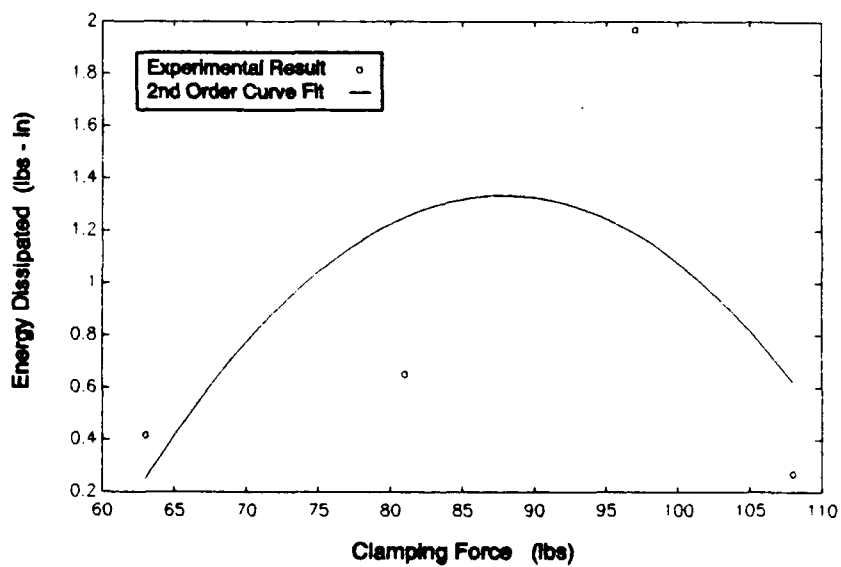


Figure 5-18. Mark II Test 5B Results for Mid Fo (0.8 lbs) with 2nd Order Curve Fit

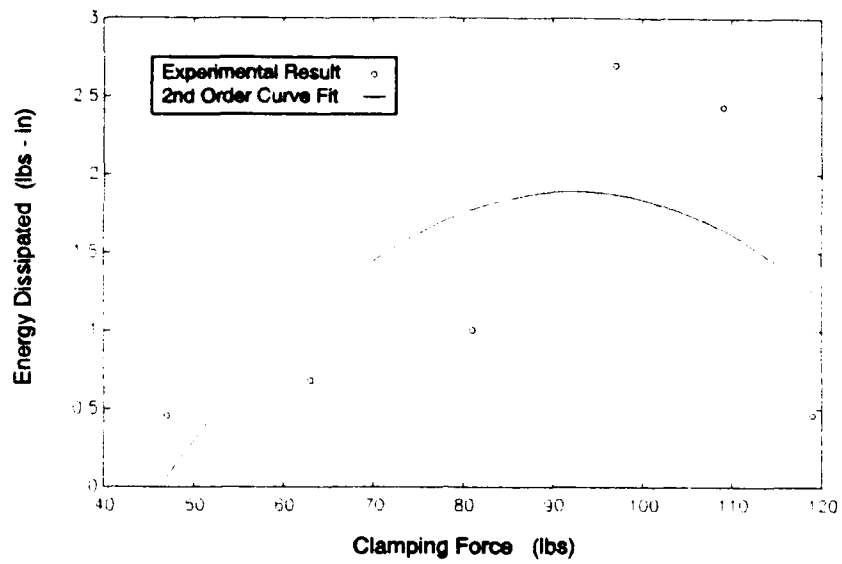


Figure 5-19. Mark II Test 5B Results for Hi Fo (1 lb) with 2nd Order Curve Fit

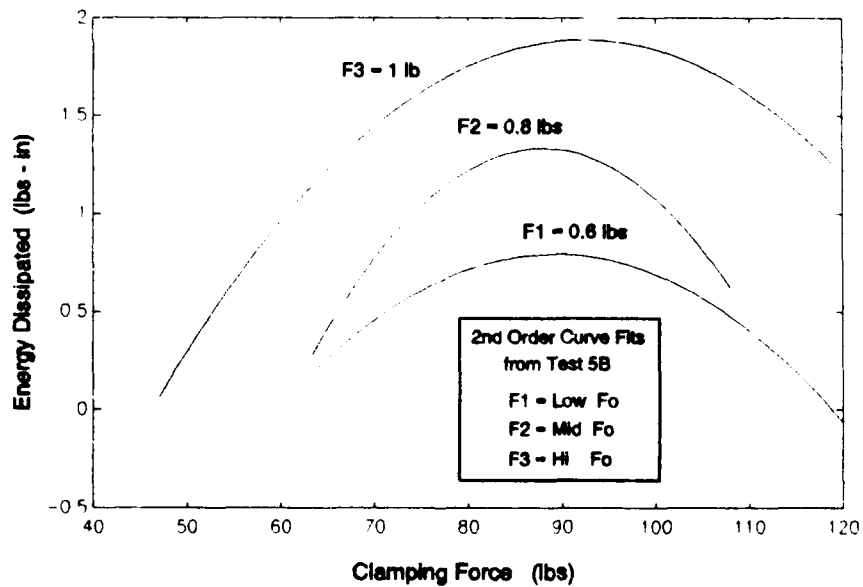


Figure 5-20. Mark II Test 5B 2nd Order Curve Fits

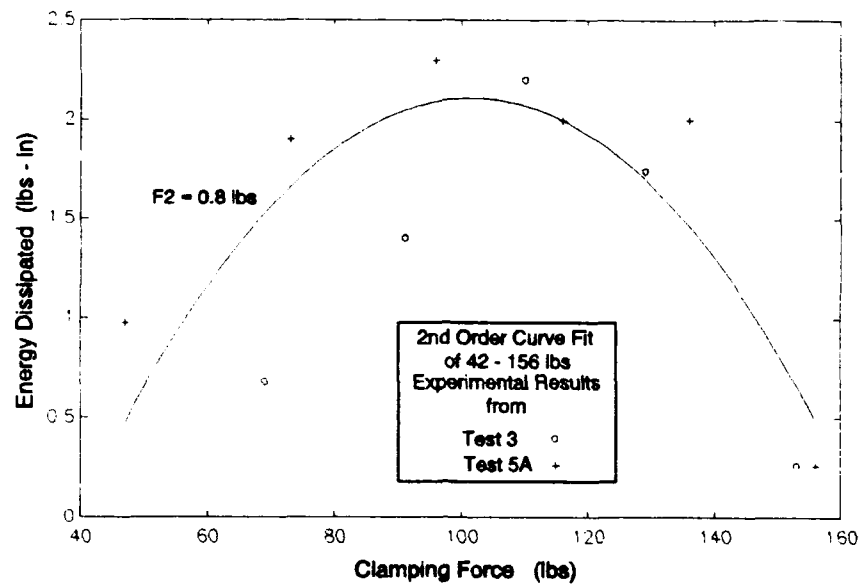


Figure 5-21. Mark II all Results from Test 3 and Test 5A for Mid Fo (0.8 lbs) with 2nd Order Curve Fit

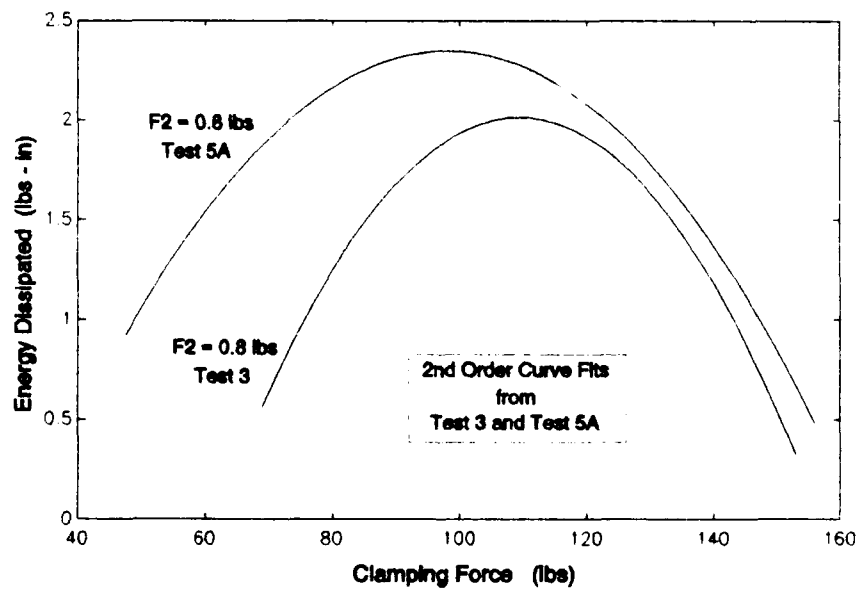


Figure 5-22. Mark II Test 3 and Test 5A for Mid Fo (0.8 lbs) 2nd Order Curve Fits

5.5.1.6. Test 6. Test 6 was the first test after the frictional surfaces were re-milled after Test 5. The purpose of Test 6 was (1) to perform a repeatability check on the hysteresis calculations, (2) to sufficiently exercise the frictional surfaces in an attempt to bring the roughness of the surfaces to a steady state condition, and (3) to get an idea on what magnitude of clamping forces and end loads (F_0) were necessary to produce a noticeable phase shift between the force and displacement signals (hysteresis loop). All of the Test 6 data and results can be found in Tables D-20 through D-24 in Appendix D.

The test is divided into two parts: Test 6A and Test 6B. During the collection of data in Test 6A it was noticed that the accelerometer was loose. The data is presented for comparison purposes to Test 6B. Note that when the accelerometer was loose the g-level derived displacements did not match the measured beam displacements as well as when the accelerometer was re-fastened. Therefore, the computed energy dissipation is suspect, and the test was repeated (Test 6B).

The repeatability checks were performed because a question was raised during the research concerning the validity of the energy dissipation calculations based on 1 hysteresis loop. Refer to the MATLAB script file AREA.m in Appendix C. Perhaps an error was made in assuming that the sampled hysteresis loop was representative of a steady state

hysteresis loop for a particular clamping force and F_o condition. However, all sampled hysteresis loops were taken from what appeared to be steady state conditions as determined by real-time monitoring of the oscilloscope and Nicolet digital analyzer. As outlined in the test procedures, once a clamping force and F_o condition were set, a certain amount of time (usually between 2-3 minutes) was permitted to elapse before any data samples were taken. The Test 6B data lists 4 sets of these repeatability checks (see Table D-23). The first three sets show hysteresis samples (15 samples total) taken after at least a 2-3 minute setting period. The computed calculations within each set are the same down to an order of magnitude of 10^{-4} volts². The fourth set of data in Test 6B shows a repeatability test taken immediately following an increase in the TA30 Power Amplifier Gain. The 5 samples were taken within a 0-1.5 minute interval following the increase in gain. Note that the force and displacement data are fluctuating, but the energy dissipation data appears to begin settling at the end of the sampling interval. The results of the repeatability tests are that a sampled hysteresis loop taken from a steady state condition after approximately 2-3 minutes of settling time, appears to be representative of an average hysteresis loop.

Test 6 was also intended to bring the roughness of the surfaces to a steady state condition. As mentioned

previously, Tests 2 through 5 exercised the frictional surfaces for approximately 3 hours over the course of several days. Test 6 exercised the joint for approximately 7 hours, almost all of it continuously. When the testing was completed, the frictional surfaces did not feel warm to the touch. The average change in R_a for each position was less than 2 R_a , with almost all of that occurring at position 9, which recorded a change of 10 R_a (see Table D-20). Subsequent testing (Tests 7 and 8) of the beam produced average changes of less than 1 R_a , with the largest magnitude of 4 R_a occurring at position (1) during Test 7 (see Tables D-25 and D-30). No visual changes were noted in the frictional surfaces, with the exception of 2 small holes (less than 1/32 inches across) which appeared on the bottom frictional surfaces located at the outer radius. One hole was on the bottom spacer, and one hole was on the bottom surface of the beam. When the beam is fitted onto the bottom spacer, the holes lay on top of each other. It is suspected that a burr was left on one of the surfaces during the milling process, and under cyclic loading, created those holes. However, the holes are small and are located right at the edge, and are considered negligible in the computations performed by EXPDATA.m. As a result, the cycling of the joint in Test 6 was considered to have been sufficient to have created a steady state condition to the frictional surfaces.

The last goal of Test 6 was to identify what magnitude of clamping forces and F_o loadings were necessary to generate sufficiently large hysteresis loops. Sufficiently large hysteresis loops are those with a width along the displacement axis greater than or equal to 20 mv. Because the re-milling of the frictional surfaces succeeded in bringing all the frictional surfaces into contact with each other, the immediate result was that the joint reached a fully clamped condition at a much lower clamping force than during Tests 2, 3, 4 and 5. This meant that the clamping force range over which the joint was going to dissipate energy had been reduced. This created a problem because it is difficult to adjust the clamping force in increments less than 10 lbs. It was apparent that the energy dissipation level had already peaked and gone down once a 40-50 lb clamping force had been reached. This meant that only 3 to 4 data points at best could be sampled in the clamping force range of interest. Of course, this assumes a maximum F_o less than the one used in Test 1. Increasing F_o would increase the effective clamping force range, but the surface properties would be in danger of changing through excessive heating. Recall that the Test 1 frictional surfaces had been milled as well. It is assumed that the Test 1 and Test 6 frictional surfaces were both level, and therefore, both fully in contact during clamping. An assumption was made that the level of loading which

affected the surfaces in Test 1 would affect the surfaces in Test 6 in the same way. However, since the effective range of the energy dissipation was low, a small chance was taken by loading the beam at $F_o = 1.2$ lbs in order to increase the energy dissipation range. Part of the 7 hour loading time of the joint during Test 6 included 2.5 hours of continuous loading at $F_o=1.2$ lbs, with no adverse effects as previously discussed in this section.

5.2.1.7. Test 7. Test 7 forced the joint at two different peak force levels ($F_o = 1$ and 1.2 lbs) over an extended period of dynamic loading. See Tables D-25 through D-29 in Appendix D for the data and results for Test 7. Based on the results from Test 6, further testing at frequencies higher than 10 Hz were discontinued. Assuming the F_o magnitudes stayed the same, higher frequencies would only move the beam faster over smaller peak-to-peak distances. Both conditions are undesirable, since higher relative velocities would generate higher temperatures, and smaller peak-to-peak distances would begin to rapidly decrease the signal to noise ratio of the Fotonic sensor. The purpose of the test was the same as all the others (collect energy dissipation data), but also to determine whether or not temperature was having some effect on the energy dissipation levels. It was hoped, that by running the test over an extended period of time and collecting data at timed intervals over two tests (Test 7A and

7B), the data would show more signs of repeatability. A problem with this approach, is that the loading must stop for the clamping pressure to be brought back down to zero (re-trimmed). If the frictional surface is heating up slightly over an extended period of time, then it can only be assumed that once stopped the joint is dissipating what little heat has built up very rapidly. During Test 7, the approximate duration of cyclic loading was 4.5 hours. Again, immediately following the test, the frictional surfaces did not feel warm to the touch.

Figures 5-23 and 5-24 show the results against the theoretical energy dissipated versus clamping force curve. THEORY.m generated the theoretical curve using the average experimental F_o , and the average coefficient of friction calculated by EXPDATA.m. Note that the data are significantly scattered about the theoretical curve. As mentioned in the Test 6 discussion, it was difficult to obtain more than 3 data points within the desired range of clamping forces. Almost all the data sets start at the highest recorded level of energy dissipation (near the clamping force ≈ 10 lbs mark), then begin to drop. Also note that the computed coefficients of friction are scattered, but the average values are within 10% of the average value of μ computed in Test 1. The wide range of μ 's computed by the theoretical model is presumed to be a result of the assumptions made when developing the model

(constant, dynamic μ for macroslip conditions), and are discussed in Section 5.2.1.1.

Nothing absolutely conclusive can be made from comparing the experimental data against the theoretical curve, other than the data are scattered, and there is not enough of them to make justifiable speculations. However, the average values of the computed coefficients of friction are closer to the expected values than in any other previous test with the exception of Test 1. Therefore, one final test (Test 8) was performed.

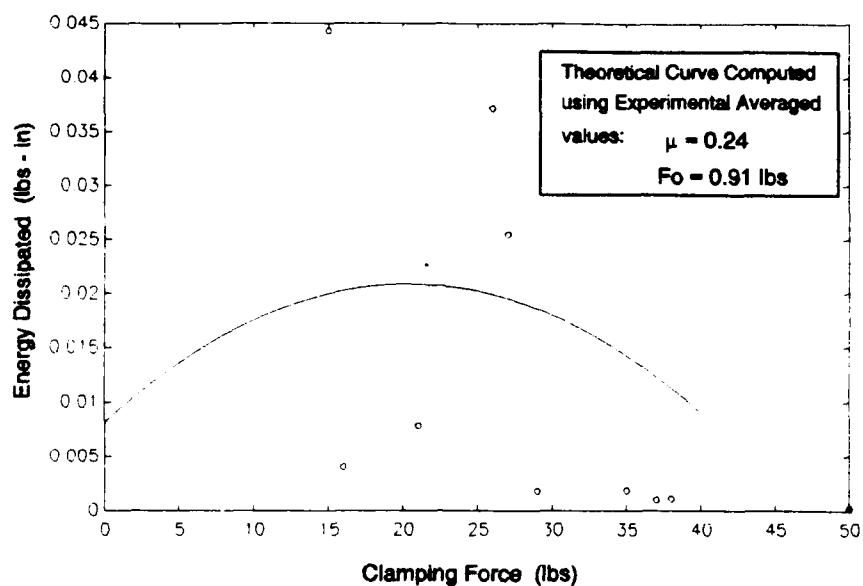


Figure 5-23. Mark II Test 7A Results plotted against Theoretical Energy Dissipation Curve

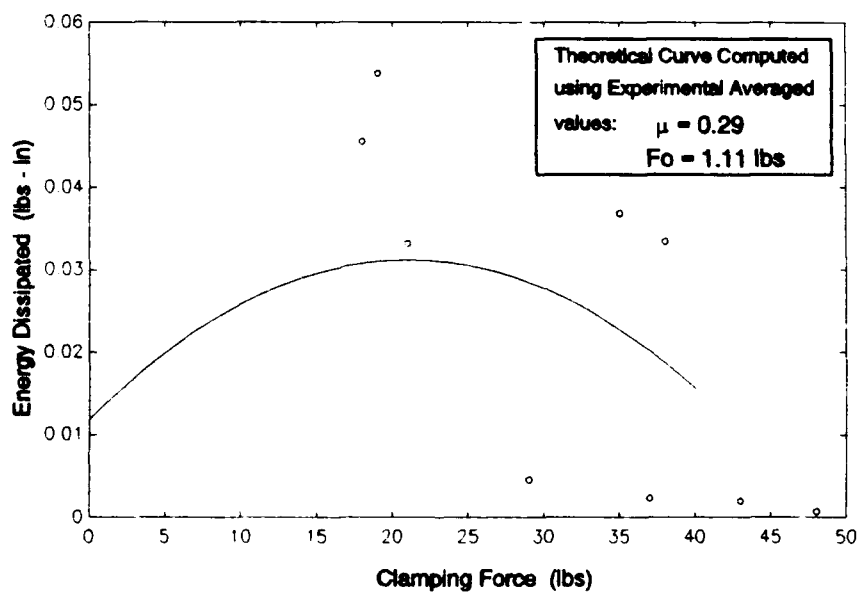


Figure 5-24. Mark II Test 7B Results plotted against Theoretical Energy Dissipation Curve

5.2.2. Final Mark II Test (Test 8). Test 8 was the final test on the Mark II. All of the Test 8 data and results can be found in Tables D-30 through D-34 in Appendix D. Essentially, Test 7 was repeated, except the number of data sets collected was more than doubled, and the duration of the cyclic loading on the joint spanned approximately 10 hours. Also note, that for this test, the second locking nut was not used. Instead, a lock washer was used between the spring and the first nut. The lock washer seemed to hold a constant clamping force as well as the locking nut, and provided a smoother transition between clamping forces. Refer to the next Section 5.2.3. for more details on the usage of the lock washer versus locking nut. Based on the Ra readings before and after the test, no changes in the frictional surface roughness occurred. The average change in each position was less than 2 Ra. Refer to Table D-30 for the Test 8 Ra measurements. Again, as with Test 7, no detectable heating of the surfaces occurred, as measured by touching the surfaces after the tests were completed.

The results are graphically presented in Figures 5-25 and 5-26, along with the theoretical energy dissipated versus clamping force curves. For Test 8A and 8B, the experimentally computed average coefficients of friction including all of the data are 0.38 and 0.40, respectively. The average coefficients of friction computed by EXPDATA.m are within the

expected 0.2-0.42 range reported by References 28 and 31. See Tables D-32 and D-34 for a listing of all the computed coefficients of friction. Note that the averaged μ 's include some negative and near zero ($\mu \leq .01$) values (see Tables D-32 and D-34). Obviously, a negative coefficient of friction can not exist, although EXPDATA.m computed 3 of them from the data. As discussed in Section 5.2.1.1., the macroslip model is attempting to compute an assumed constant coefficient of friction based on the experimental data provided without considering the effects of microslip, varying clamping forces, and non-uniform pressure distributions. Therefore, the negative coefficients are included in the average when computing the mean values of μ . Even so, the average values for μ are within the expected range.

But now look at Figures 5-27 and 5-28, where the results from Test 8A and 8B are plotted against theoretical curves using a computed average μ excluding the negative and near zero ($\mu \leq .01$) values tabulated in Tables D-32 and D-34. The average values of μ for Test 8A and Test 8B are now 0.43 and 0.45 respectively, which are within 10% of the reported value of $\mu = 0.42$ found in Reference 28. Figures 5-27 and 5-28 show less scattering of the results against the theoretical curve than in Figures 5-25 and 5-26. Note that the energy dissipation results corresponding to the negative and near zero μ values are not plotted in Figures 5-27 and 5-28.

As with Test 7, nothing absolutely conclusive can be made about the results when comparing the experimental results against the theoretical curve, other than the results are scattered and the repeatability of the experiment is not good. However, two general trends are noted. The first is that the theoretical model is predicting a maximum energy dissipation occurring around the 10-15 lb mark, which the experimental results tend to support. Although the energy dissipation magnitudes vary sometimes by as much as a factor 2, the expected trend of energy dissipation reaching a peak and then dropping is evident. Secondly, the theoretical model is predicting a fully clamped condition above 30-35 lbs, which the results strongly support.

The positive results of Test 8 are encouraging because the general trend of the results support the fundamental concepts of the theory: as clamping force is increased, energy dissipation should reach a peak, and then drop. However, the negative results of Test 8 are disturbing, namely the non-repeatability of the data. That problem is addressed further in the next section.

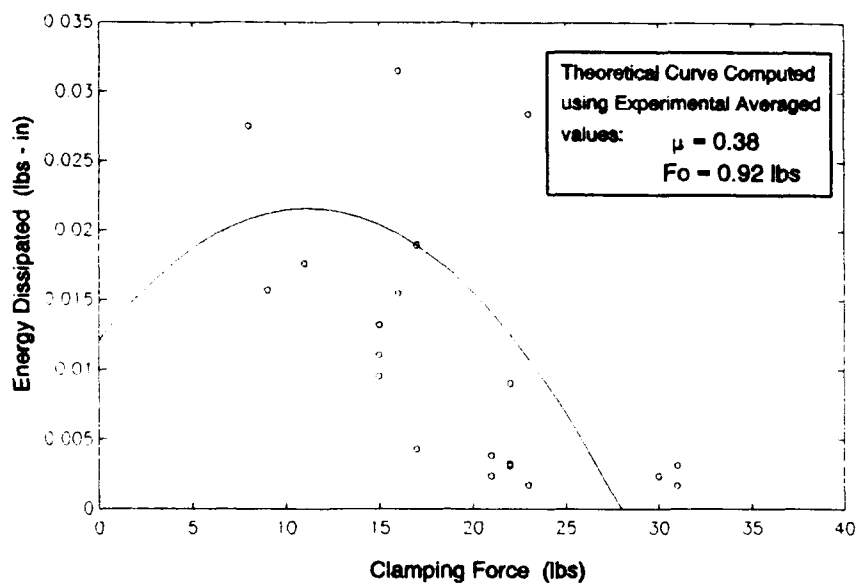


Figure 5-25. Mark II Test 8A Results plotted against Theoretical Energy Dissipation Curve ($\mu=0.38$)

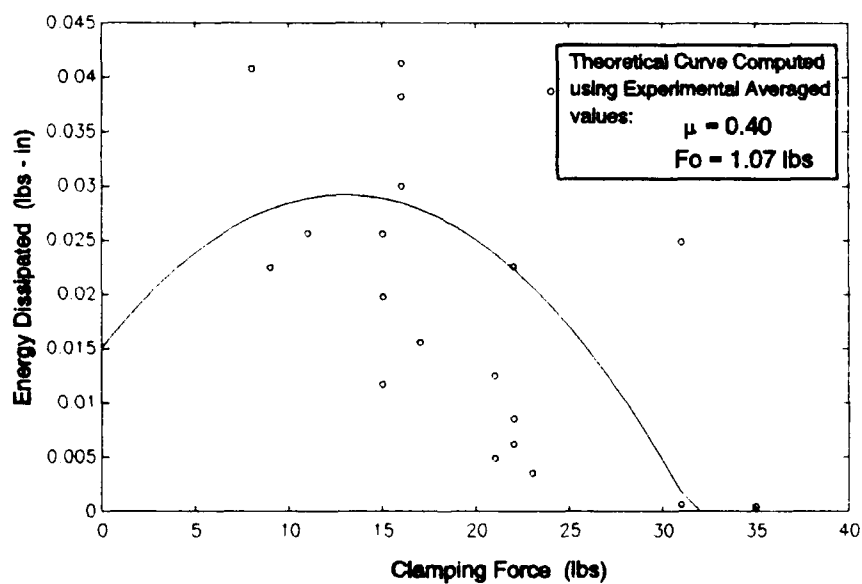


Figure 5-26. Mark II Test 8B Results plotted against Theoretical Energy Dissipation Curve ($\mu=0.40$)

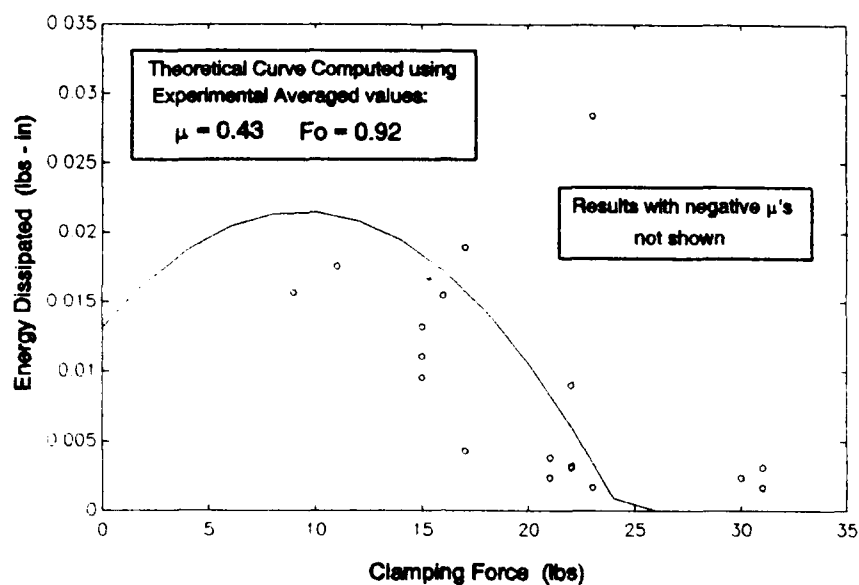


Figure 5-27. Mark II Test 8A Results plotted against Theoretical Energy Dissipation Curve ($\mu=0.43$)

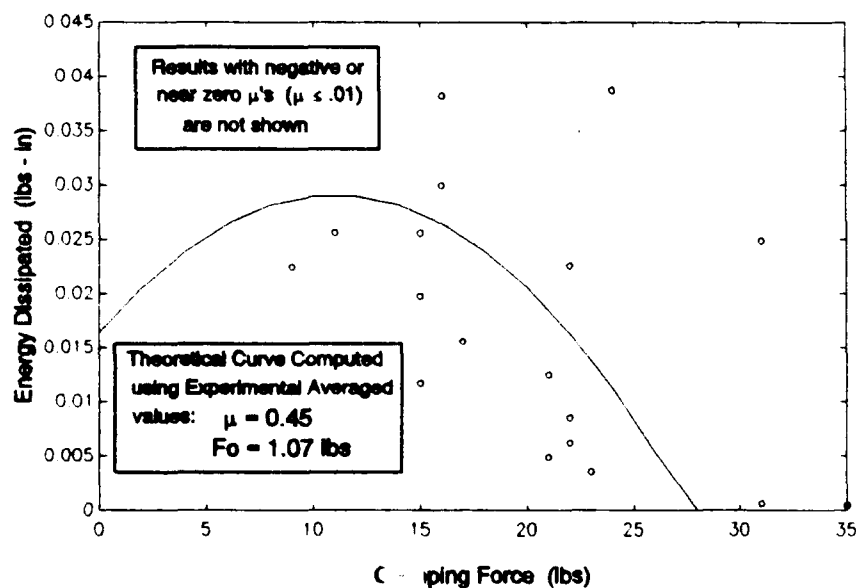


Figure 5-28. Mark II Test 8B Results plotted against Theoretical Energy Dissipation Curve ($\mu=0.45$)

5.2.3. Mark II Test Set-Up. As discussed in the previous sections, the repeatability of the experiment is not good. This section looks at possible reasons for that non-repeatability, especially in the area of the test equipment and set-up.

The ability of the calibrated bolt to produce repeatability clamping forces under the dynamic conditions of this experiment are debatable because of the problems with the off-axis loading and the back slope hysteresis (see Appendix A.9). The bolt is subjected to some torsional loading as the beam is cycled. Note that all of the tabulated data in the AREA.m Tables in Appendix D list the preload clamping force along with the clamping force under dynamic conditions. The dynamic clamping force was used when reducing the data. Although the dynamic clamping forces stayed constant during the loading, sometimes the dynamic clamping forces were lower than the preload clamping force. Once the clamping force dropped, a hysteresis was present (refer to Appendix A.9). The final released value of the bolt almost always showed a positive hysteresis, sometimes as high as 9 lbs. During the testing, whenever a drop in the clamping force was noted, the clamping force was released and retrimmed. However, the second locking nut is suspected of introducing greater error than the off-axis loading or hysteresis. By locking the second nut down, it was noted occasionally that the clamping

force would jump by 5-10 lbs, depending on how hard it was backed down onto the first nut. This apparent increase in clamping force is not considered to have actually been transmitted to the joint. The lock washer used in Test 8 never displayed that characteristic. In Test 8, the joint consistently reached a fully clamped condition near the same clamping force, further justifying the use of the lock washer over the second locking nut.

A second problem has to do with the operating limits of the equipment. Originally, the testing was designed to occur at peak end loads of F_o much larger than 1 lb, and over a larger range of clamping forces. The problems noted with Test 1 (excessive heating) changed that, and as a result, the range over which data could be collected was brought closer to the lower operating limits of the equipment, especially the Fotonic sensor's noise levels and the OSP-4, which is frequency limited to a lower bound of 5 Hz.

A third problem has to do with the nature of rotational versus translational friction analysis. Any unevenness in the frictional surfaces, and especially any unlevelness in the beam joint geometry itself, would be amplified as erroneous data on the order of magnitude equivalent to F_o times the moment arm. Although the levelness of the baseplate, joint, and beam was constantly monitored between loading, the accuracy of levelness was limited by the accuracy imparted by

a hand held level. An example can be found by examining the energy dissipation calculations from Tests 2-5 near the zero clamping condition (refer to Appendix D). A reason for the fluctuating energy dissipation near the zero clamped condition could be because the beam was possibly wobbling over the frictional surface when the top spacer was not clamped down. It is possible that the higher dissipation levels at the zero clamped condition were from the beam rubbing against the bolt shank. This phenomena was not noticed in Tests 6-8, where the joint was never cycled without the top spacer locked into place over the beam.

A fourth problem with the experiment is the lack of control over the adhesiveness of the surface properties. In particular, the effects that temperature and humidity may have had on them. The Surtronic 3 profile analyzer monitored the physical characteristics of the frictional surfaces, but could not monitor any other properties of the surface. Ludema discusses the debate on whether friction is due primarily to adhesion or the interlocking of the surface asperities²⁹. Ludema states that a modern view of friction is primarily due to adhesion, but an adhesion that is limited by the oxides and absorbed gases found on all surfaces during sliding which are destroyed by peeling when the load is removed²⁹. Ludema also reports that there is usually little effect on the coefficient of friction of metals until the temperature becomes high

enough to increase the oxidation rate, which usually decreases μ^{29} . This could explain the difference in the computed average μ 's between Test 1 (≈ 0.27) and Test 8 (≈ 0.43). Recall that oxidation occurred in Test 1. Ludema lists a dynamic, dry μ for hard steel on hard steel of 0.42^{29} . The adhesiveness theory could also explain why the average energy dissipation between Tests 6, 7, and 8 are different. During the course of each test, the frictional surfaces were never separated, but between testing, the joint was completely disassembled for Ra testing. Note that the data tend to be more repeatable during the course of a test than between tests. It could also be possible that the location of the experimental set-up (next to the loading dock bay in room 150) provided an unsuitable environment for the test. Opening and closing of the loading dock door would produce noticeable changes in the local environment (especially humidity).

The last possible cause of nonrepeatability, and perhaps the one with the greatest impact, has to do with the inability to actually reproduce peak force loads, or F_o , from test to test. Recall from the discussion about the initial testing in Section 4.2.1. that the OSP-4 controls acceleration loading at the beam tip, but not actual F_o levels, because the effective mass of the system was changing as the clamping force was increased. Therefore, the F_o levels had to be controlled by manually adjusting the gain control on the TA30 voltage

amplifier. As an example, refer to the Test 8A results in Table D-32 in Appendix D. Note that the average peak force is 0.9213 lbs, but the low and high peak values are 0.7285 lbs and 1.008 lbs respectively. Now look at the Test 8A results plotted against the theoretical curves using $F_o = 0.72$ lbs and $F_o = 1.1$ lbs in Figure 5-29. Note that all almost all the data points are bounded by the upper and lower theoretical curves. It appears that the inability to consistently reproduce F_o levels is a principal cause for the nonrepeatability of the data. Part of the problem is that the F_o levels are so low in magnitude, and difficult to manually reproduce between tests, using the TA30 power amplifier. It is possible that a larger range of F_o magnitudes would produce a greater separation between F_o data sets. Unfortunately, temperature effects precluded that for this experimental set-up.

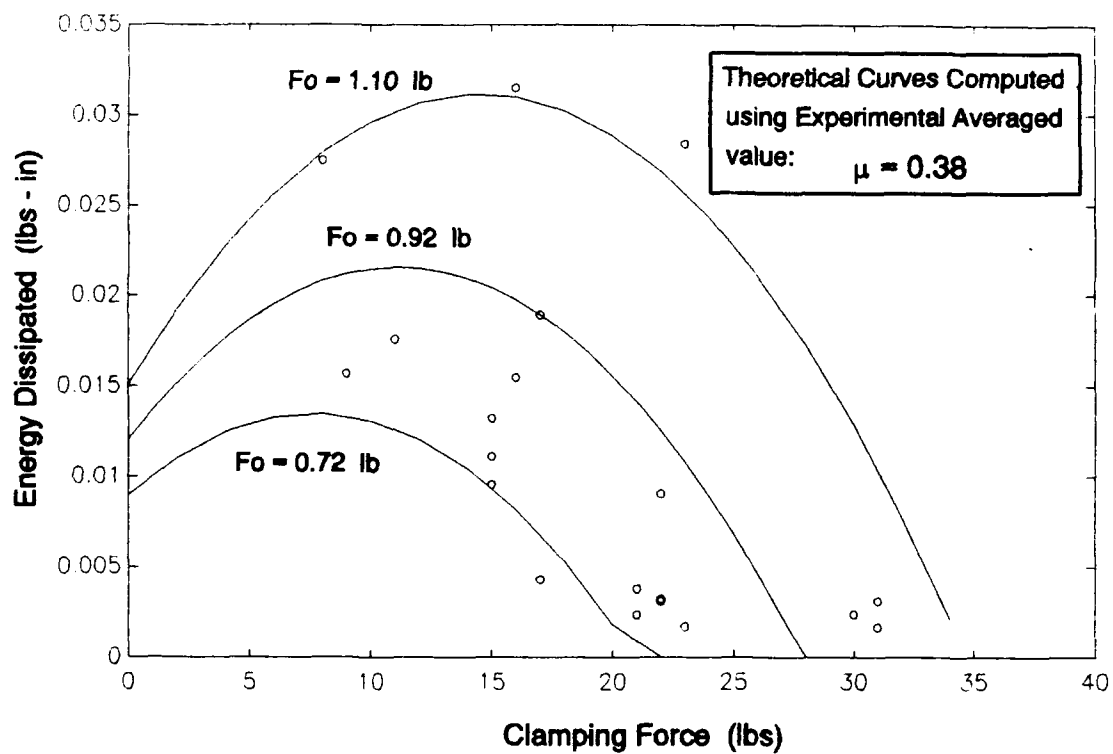


Figure 5-29. Mark II Test 8A Results plotted against Upper and Lower Theoretical Energy Dissipation Curves

VI. Conclusions and Recommendations

Two experimental models of a pin-type joint were built and tested for the purpose of collecting and analyzing Coulomb friction damping data due to rotational slip. One model (Mark I) was a free vibration model, and the other (Mark II) was a forced vibration model. The data were compared against two theoretical macroslip models.

6.1 Conclusions

The Mark I experimental set-up was ideally suited for free vibration testing, but experimentally isolating the energy dissipation to the joint surfaces was not accomplished due to the weight of the beam on the bolt shank. Furthermore, the inability to accurately measure the clamping force at the joint prevented detailed analysis of the data. However, the free vibration macroslip model does appear to be capable of predicting energy dissipation versus clamping force characteristics provided the clamping force and coefficient of friction are known.

The Mark II theoretical forced vibration model does appear to be capable of matching the experimentally obtained energy dissipation versus clamping force curves given an approximate $\pm 20\%$ change in the peak magnitude of the forcing function. There were several problems with the Mark II

experimental set-up, most notably the inability to obtain repeatable clamping force readings and to apply forcing functions of the same magnitude, and the failure to independently measure the coefficient of friction. It is difficult to conclude which problem had a greater impact on the scatter of the experimental data. It is known however that the effects of temperature on the frictional surfaces must be addressed, and the failure to do so early in the research helped to create the problems noted above, partly because the dynamic operating ranges of the clamping forces and beam loadings were expected to be conducted at much higher levels.

6.2 Recommendations

No recommendations are made concerning the theoretical macroslip models, since the models appear to behave according to the expected theoretical results as outlined in this thesis. Instead, recommendations are made in the area of collecting sound experimental data from which to judge the validity of the theoretical models. Recommendations for further study with the Mark I and Mark II experimental set-ups are listed below.

Recommendations for further study with the Mark I and Mark II experimental set-ups are:

1) Design a method to reduce the frictional contact of the beam on the bolt shank, such as a ball bearing sleeve insert that fits inside the bolt hole in the beam and over the bolt shank.

2) Redesign the set screw tower assembly to allow for a smoother process (reduce the number of steps involved) when adjusting the clamping force, such as a spacer attached inbetween two rods which would permit the spacer to slide up and down onto the beam.

3) Select a shaker-amplifier-controller set-up which would permit more precise applications of forcing functions at lower frequencies and peak force magnitudes.

4) Select a different means of measuring clamping force (i.e. one that is not so susceptible to torsional bending or off-axis loading), such as the Bolt Force Sensor Hollow-Compression Strain Gauge Load Cell⁴⁰, and one that is capable of measuring clamping forces accurately over a much lower range.

5) Placing the entire experimental set-up, especially the Mark II, onto a level vibration isolation stand, to ensure the levelness of the set-up.

6) Select a true non-contact angle measuring transducer or select a smaller (less bulkier) linear non-contact transducer which would permit displacement readings over a larger range of displacements.

7) Reduce the size of the frictional surfaces in contact (while still maintaining the rigid beam assumption) at the joint in order to increase the range of clamping forces from which an optimum energy dissipated-clamping force pair can be found for a given forcing function peak magnitude.

8) Try to locate the experiment in a more controlled atmospheric environment.

9) Develop a means to monitor the frictional surface temperatures during testing.

10) Develop a method by which the coefficient of friction of the frictional surfaces can be independently measured under a rotational slip condition.

Appendix A: Test Equipment Specifications

A.1 Model 5PM Shaker

A Unholtz-Dickie Corporation Model 5PM shaker was used to supply sinusoidal loads during testing. The system specifications are listed in Table A-1. The system performance is based on the operation of the 5PM shaker with the Unholtz-Dickie Model TA30 power amplifier. Based on the discussion and background found in the introduction concerning large space structures, low vibratory motion is of primary interest. As a result, most testing will be conducted between 10 and 40 Hz. The lower limit is far enough away from the lower operating limit of the shaker (2 Hz), and is limited to a maximum acceleration of 2.5g's which is acceptable. The upper limit of 40 Hz was picked for 2 reasons. The first reason was simply to define some bounded region for testing. The second reason was to stay well below 120 Hz in order to avoid any possible electrical noise signals. A 3 inch long, .25 inch diameter steel rod was fabricated to be used as the shaker stinger. Refer to the Model 5PM shaker operating and maintenance manual for a complete list of all the system specifications and operating instructions³³.

The shaker was originally bolted to a small plywood base which sat on top of a cinder block, with a small foam pad between the plywood and the cinder block. It was thought that

this arrangement would be sufficient during all phases of testing, since the shaker was heavy (85lbs) compared to the expected magnitude of the peak end loads of under 10lbs. However, it was noted during initial testing that the shaker stand would vibrate at higher clamping pressures, even for small loading. A tool-die cart was modified and bolted to the floor near the test setup to serve as a shaker stand, but once the shaker was mounted, the entire assembly could be seen to shake under dynamic testing. A final shaker mount was built using a 100lb, 1 inch thick steel plate which was bolted to the bottom of the shaker. The shaker and plate were then bolted on top of 2 steel rails, each weighing approximately 45 lbs. The steel rails were bolted to the floor. To further increase the mass of the system, a 50lb weight was placed on top of the rails, just behind the shaker. An accelerometer was attached to the shaker mount and connected to the Nicolet Digital Analyzer. For high clamping pressures (near fully clamped), and for peak loads at 1g levels for frequencies ranging from 5-500Hz, no noticeable changes were seen in the acceleration signal. FFTs (Fast Fourier Transforms) of the acceleration signal using the Nicolet FFT function showed no resonant peaks below 2000Hz. Since all testing would be conducted below 40Hz, the test stand was considered to be sufficiently rigid.

Table A-1
Model 5PM Shaker Specifications³³

Force Output Rating	50 lbs, peak Sine
Shaker Stroke	0.5 inches
Free Table Axial Resonant Frequency	7300 Hz, Nom
Armature Assembly Effective Weight	0.71 lbs, Nom
Maximum Free Table Acceleration	63 g
Shaker Table Suspension Stiffness	60 lbs/in, Nom
Total Weight with Trunnion Base	85 lbs

The following are the conversion formulas for vibration measurements³³:

$$\begin{aligned}
 g \text{ (pk)} &= .0511 f^2 D(\text{in pk-pk}) \\
 D \text{ (in pk-pk)} &= (19.56/f^2) g \text{ (pk)} \\
 V \text{ (in pk/sec)} &= (61.45/f) g \text{ (pk)} \\
 D \text{ (in pk-pk)} &= (0.3183/f) V(\text{in pk-pk})
 \end{aligned}$$

where f = frequency (Hz or cycles per sec)
 g = acceleration due to gravity (386 in/sec²)
 V = velocity (in/sec)
 D = displacement (in pk-pk or double amplitude)

A.2 Model TA30 Power Amplifier

The Unholtz-Dickie Corporation Model TA30 Solid State Power Amplifier is designed to drive the Model 5PM shaker to full performance from 2Hz to 10,000Hz. The specifications of the Model TA30 can be found in Table A-2. Refer to the Model TA30 Power Amplifier instruction manual for a complete list of all the system specifications and operating instructions³³.

Table A-2

Model TA30 Power Amplifier Specifications³³

Power Output	250 VA, 20 to 10,000 Hz with shaker load
Frequency Range	2 to 20,000 Hz
Frequency Response	± 3 dB, 20 to 20,000 Hz
Input Impedance	7,000 ohms minimum
Input Voltage	1 V rms for full output (10 V rms available)
Harmonic Distortion	0.5% max, 5 to 10,000 Hz
Hum and Noise	75 Db below full output
Cooling	Air (internal fan)
Power Requirements	860 VA at full output; 105-125 V 60 Hz 210-250 V 50 Hz
Weight	59 lbs

A.3 Oscillator-Servo-Programmer (OSP-4)

The Unholtz-Dickie Oscillator-Servo-Programmer (OSP-4) Sine Vibration Controller provides for the signal generation and control during the sinusoidal vibration testing. The OSP-4 is designed to work with the Model 5PM shaker and Model TA30 Power Amplifier. The oscillator originates the signal voltage which is fed to the Servo-Programmer and Power Amplifier, which in turn drives the shaker. See Figure 1-4 for a simplified schematic. The oscillator can be used manually or automatically to sweep at any frequency from 5 to 5000 Hz. The Servo-Programmer will maintain constant set values of

displacement or acceleration during frequency sweeping. The Servo-Programmer automatically adjusts the magnitude of the oscillator output voltage fed to the power amplifier to account for variations in system frequency response due to resonant characteristics of the items mounted on the shaker table and the inherent shaker system response itself. All that is required for constant displacement or acceleration control is a signal from any piezoelectric accelerometer. In order to make the built-in vibration meter in the Servo-Programmer read correctly with any accelerometer, it is necessary to calibrate the sensitivity dial on the rear panel of the OSP-4 to the sensitivity of the accelerometer being used. This step was accomplished when the accelerometer was calibrated. Refer to Section A.4. Table A-3 lists some of the specifications for the OSP-4. Refer to the OSP 4 operating and maintenance manual for a complete list of all the system specifications and operating instructions³³.

Oscillator-Servo-Programmer (OSP-4) Specifications³³

A.4 Accelerometer

A-6

1001.1 mv/g @ 100 Hz. The test accelerometer was placed on top of the standard accelerometer, and with an HP 3466A Digital Multimeter, the gain on the OSP-4 was set to 10mV and locked into place. The gain setting on the rear panel gain sensitivity dial on the OSP-4 was set and locked into place at 271.9. In order to verify the readings of the HP 3466A Digital Multimeter, it was calibrated against the FLUKE 5100B calibrator. ENDEVCO accelerometer model 2235C has a calibrated frequency response from 4 to 5000 Hz. See Table A-4 for the specifications on the accelerometer.

Table A-4

ENDEVCO Accelerometer Model 2235C Specifications³⁴

Charge Sensitivity	31.0 Pc/g
Frequency Response	4-5000 Hz
Maximum Transverse Sensitivity	2.5%
Transducer Capacitance	807 pf

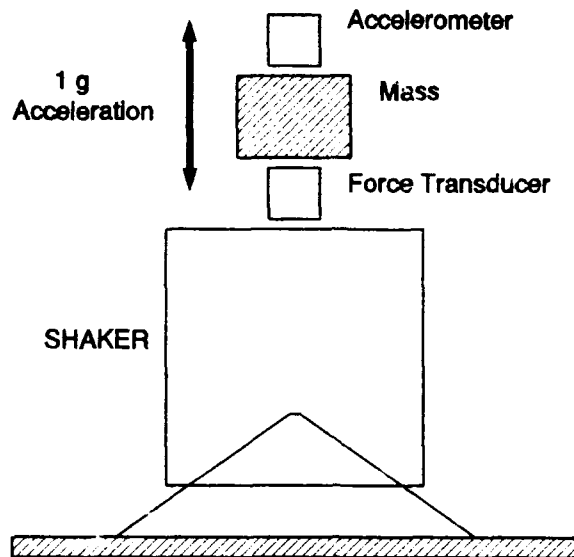


Figure A-1. Schematic of Force Transducer Calibration Set-up

A.5 Force Transducer

A PCB Piezotronics Quartz Force Transducer Model No. 208A02 was used to measure the force on the beam. The 208A02 was connected to the beam with a threaded 10-32 stud on one side and connected to the shaker via the stinger on the other side. The 208A02 is rated at $\pm 100\text{lb}$. A PCB Piezotronics Power Unit Model 480C06 was used to power the force transducer, debias the output signal, and amplify the signal. The output of the power unit is fed simultaneously into a Tektronix 2465B oscilloscope and the Nicolet Multipro Digital Analyzer. The oscilloscope was used for diagnostic monitoring

during testing; the digital analyzer was used to actually trap the force versus time data from the force transducer. See Table A-6 for specifications on the force transducer and power unit. The force transducer was calibrated by placing it onto the shaker as shown in Figure A-1. A known mass was placed on top of the force transducer by means of a threaded 10-32 stud. The ENDEVCO accelerometer 2235C was fixed into placed on top of the mass in the same manner. The OSP-4 was set to oscillate a 20Hz with a 1g level peak load. The Nicolet was set for a timebase of 200ms sweep, and 5 different sweeps were collected. Each sweep was smoothed using the Nicolet SMOOTHING function and the peak values were picked off using the Nicolet PEAK function. The combined weight of the accelerometer, known mass, and both 10-32 studs was then divided into the peak values to obtain a mv/lb calibration constant. The data from the 5 sweeps are listed in Table A-5.

Table A-5
Force Transducer Calibration Data

SWEEP	\pm Peak Value (mv)	\pm Calibration Constant (mv/lb)
1	35.16 -35.92	49.5 50.7
2	35.17 -35.68	49.5 50.2
3	35.07 -35.75	49.4 50.3
4	35.20 -35.88	49.6 50.5
5	35.01 -35.80	49.3 50.4
Combined weight of accelerometer, two 10-32 studs, and mass was 322.2 grams or 0.7103lbs		AVG: 49.94 mv/lb

Table A-6

PCB Model No. 208A02 Force Transducer
and PCB Model No. 480C06 Power Unit Specifications³⁵

PCB Model No. 208A02 Force Transducer	
Range, Tension, Compression	50 Mv/lb
Maximum Compression	5,000 lb
Resonant Frequency (no load)	70,000 Hz
Low Frequency (-5%)	0.0003 Hz
Shock (no load)/Vibration	10,000/2,000 g
PCB Model No. 480C06 Power Amplifier Unit	
Transducer Excitation	+18 VDC
Excitation Current (constant)	2 ma
Voltage Gain (selectable)	1, 10, 100
Frequency Response (all gains)	.15 - 100,000 Hz
Output Signal	±5 Volts
Noise (pk-pk Output)	
x1	0.2 mv
x10	2.0 mv
x100	20.0 mv

A.6 Fotonic Sensor

The MTI 1000 Fotonic Sensor is a fiber optic measurement system which performs non-contact displacement/vibration and surface condition measurements. The MTI 1000 imposes no load on the target under measurement and remains unaffected by magnetic and electrical fields. For this thesis, an MTI 1000 Fotonic Sensor Instrument Model KD-320 (serial no. 3801 0845) with a probe/plug-in module 125R was available. The probe/plug-in Module specifications are listed in Table A-7.

Table A-7

Fotonic Sensor Probe/Plug-in Module Specifications³⁶

Probe Number	125R
Probe Length	36 inches
Frequency Response	70 kHz
Output Signal Ripple (mv pk-pk)	20 mv
Without the Optical Extender: (from manual)	
Resolution (% of Range)	
Dynamic	0.2
Static	0.05
Front Slope Characteristics	
Sensitivity	0.6 micro inches
Linear Range	4 mils
Standoff	2.5 mils
Back Slope Characteristics	
Sensitivity	18 micro inches
Linear Range	70 mils
Standoff	55 mils
With the Optical Extender: (calibrated in laboratory)	
Indicated Linear Range	~ 100 mils
& Standoff	~ 370-500 mils
Noise Levels	10 mv pk-pk
Calibration Constants	See Appendix D

In order to avoid sensitivity loss and increase the stand-off distance, a KD-LS-1 optical extender accessory was used. Since the target reflectance influences the displacement readings, one edge of the Mark II beam was polished to a

mirror finish using 5 different grades of emery paper (240, 280, 320, 400, 600 grade). A 1 inch diameter polished aluminum disc was fabricated and used as the reflectance target for the Mark I beam. The target disc was attached near the top of the Mark I beam using superglue. The Fotonic Sensor was calibrated per the instructions in the KD-320/340 Fotonic Sensor operation instruction manual³⁶. Calibration went as follows:

- (1) The beam was mounted into place and leveled.
- (2) The sensor probe was mounted along side of the beam using a specially fabricated probe mount built by the AFIT Model Shop. The probe mount securely fixes the probe into the desired location, and is separated from the Beam-Joint assembly.
- (3) With the beam unclamped, the end of the beam was displaced using a table mounted micrometer. The Nicolet Digital Analyzer was used to measure the corresponding millivolt change. A displacement versus millivolt calibration curve was generated for TIP DISPLACEMENTS. Whenever the Fotonic sensor was moved, or the surface condition of the beam changed, the sensor was recalibrated.

The operating manual did not contain the operating specifications for the optical extender, but an in-house calibration following the calibration procedures, indicated that the Fotonic sensor with the optical sensor had a linear range of approximately 100 mils with a standoff distance of .37 inches (370 mils). With this information as a starting point, the sensor was then mounted approximately 3.5 inches from the center of the bolt center, with a standoff distance from the beam of approximately .4 inches. For a full 0.5 inch

displacement of the beam tip (shaker limitation), the sensor would see a maximum displacement of less than 100 mils. By calibrating the sensor against tip displacements, any measured sensor reading would be the distance travelled by the force measured at the tip. Since the sensor was recalibrated several times, the actual standoff distance varied. Furthermore, since the beam edge, once polished, was more reflective and smoother (as determined by the profile analyzer) than the in-house calibration target, the actual standoff distances fell between .4 to .5 inches. Once a linear range was found, the actual standoff distances were measured using a Scherr Tumico Dial Caliper. See Figures A-2 for an example calibration curve, and refer to the KD-320/340 Fotonic Sensor operating instruction manual for complete details on the calibration procedures. Calibration curve data is also listed along with the test data in Chapter 4.

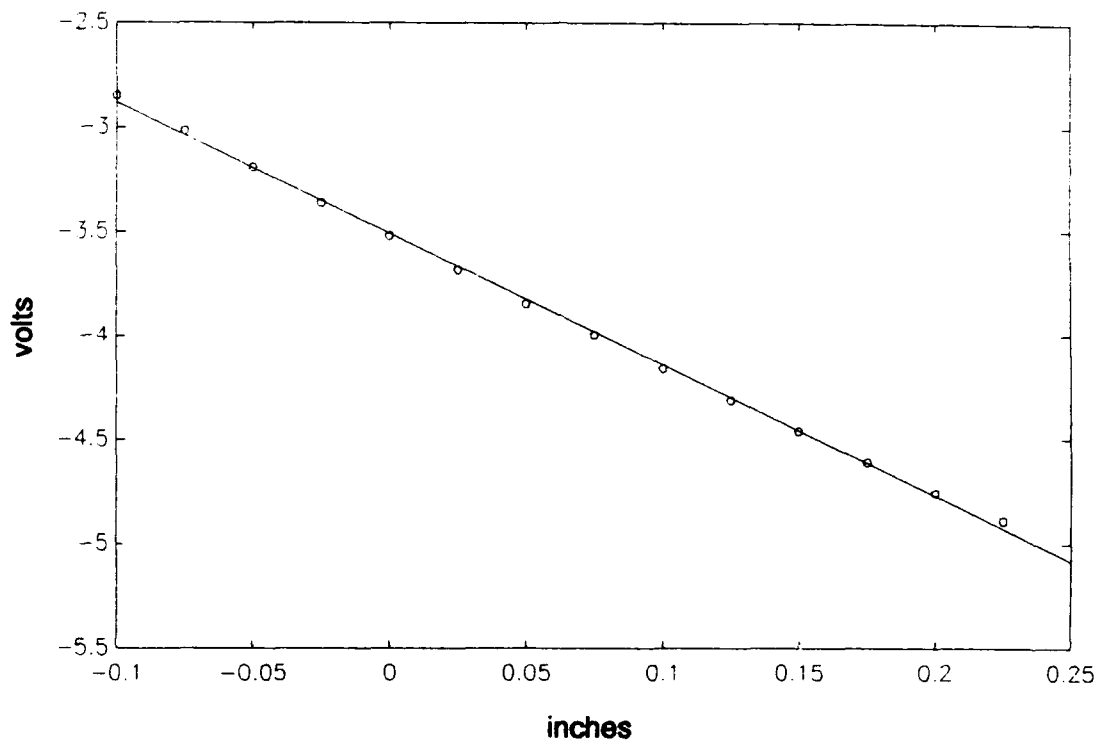


Figure A-2. Fotonic Sensor Calibration Curve for Mark II
Tests 6,7, and 8

A.7 Digital Analyzer

A Nicolet Multipro Digital Analyzer was used for data acquisition during testing. A MultiPro Digitizer 120 Board was used to trap the analog signal inputs from the force transducer and the Fotonic sensor. Each 120 Board can process 4 channels with a 12 bit (0.025%) resolution at a 1Ms/s digitizing rate. Refer to the Nicolet Multipro Data Acquisition Systems Operation Manual for complete specifications and operating procedures³⁷. The Nicolet was used to digitize analog signals of force and displacement for a given interval. The data were processed by the SMOOTHING function on the Nicolet system. The SMOOTHING function reduces the high frequency noise on a captured waveform, by calculating a weighted running average of the data points in a selected waveform section. Refer to Chapter 4 Test Procedures and Data for the specific input, timebase, and triggering parameters that were used during testing.

A.8 Surtronic 3 Profile Analyzer

In an attempt to monitor the surface finish of the beam and spacer frictional surfaces, measurements of the frictional surfaces' roughness were made periodically. See Chapter 4 Test Procedures and Data for the specific tests that were conducted. The Rank Taylor Hobson Limited Surtronic 3 provides a numerical assessment of the roughness (but not the

waviness or curvature) of a surface by what is known as the Ra (Roughness average) method. The Ra height of the roughness irregularities on a surface is defined as the average value of the departures from its center line, throughout a prescribed sampling length. Ra is normally obtained with a profile analyzer or similar instrument that moves a stylus across the surface of the test material. The stylus displacements are sensed electrically and are integrated over the traverse length to yield Ra. The average roughness is measured in micrometers (microns) or microinches. Figure A-3 shows a typical surface roughness trace. The Surtronic 3 can accurately measure surface irregularities as small as 2-8 micro inches (.05-.2 microns) high which is considered to be a superfinished surface. The Surtronic 3 was tested against the supplied Reference Specimen Type 112 1107. The Reference Specimen has a roughness standard of 239 micro inches (6.07 micro meters). The Surtronic 3 consistently read 243-244 when tested on the Specimen, which is within the 4% range specified in the operating instructions manual. The Surtronic 3 was also tested on a gauge block at the AFIT Model Shop. A gauge block is considered to be superfinished. The gauge block test consistently produced readings of 5 and 6, which was within the 2-8 microinch range specified in the operating instructions manual. The gauge block test, in conjunction with the reference test, were consistent enough to validate

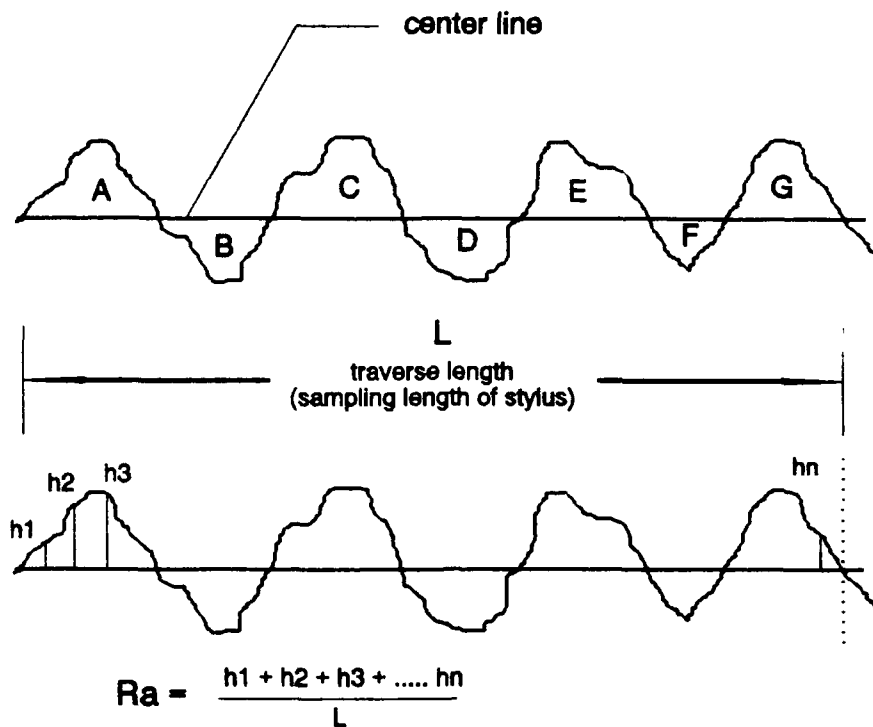


Figure A-3. Definition of Ra^{38}

the usefulness of the Surtronic 3 in measuring surface roughness. See Table A-8 for some of the specifications on the Surtronic 3. Refer to the Surtronic 3 operating instructions manual for all of the specifications³⁸. An excellent reference for a more thorough discussion on surface roughness and profile analyzers can be found in Reference 26.

Table A-8
Surtronic 3 Specifications³⁸

Overall Accuracy of Ra Measurement	$\pm 2\%$ of reading ± 1 unit in least significant decade
Accuracy of Reference Specimen	Within 4% of marked value
Pick up type	Variable Reluctance Diamond (radius 200 microinches)

A.9 Internally Gauged Bolt Transducers

In order to determine the optimum clamping pressure for energy dissipation, it is necessary to know the clamping pressure at the joint. Originally, a torque wrench was considered as a means of measuring the clamping pressure of the bolt. However, once the bolt is tighten down and subjected to dynamic loads, the clamping pressure is likely to change²⁵. During the literature search, a dissertation was found in which an internally mounted strain gauge transducer was used to measure the clamping pressure of a bolted assembly²⁷. This arrangement would permit real time monitoring of the clamping pressure and allow accurate clamping pressure versus energy dissipation (hysterisis loop) tabulations.

To predict what range of clamping pressures were required in order to fully clamp the joint, the following calculations were made based on the results derived from Chapter 2. Recall that Equation (2-28) gives the moment at which gross slip will

occur in terms of the axial clamping pressure P as

$$M_{gross} = \frac{2}{3} \pi \mu P R^3 \quad (A-1)$$

But this assumes the joint surface has a full radial surface defined from a zero radius to outer radius R . The joint in this thesis has a hole in the middle, so Equation (A-1) becomes

$$M_{gross} = \frac{2}{3} \pi \mu P (R^3 - R_{hole}^3) \quad (A-2)$$

Also note that there are 2 frictional surfaces, and that the clamping pressure P can be represented by F_c divided by the area A of the surface. Substituting into (A-2) gives

$$M_{gross} = \frac{4}{3} \pi \mu \left(\frac{F_c}{A} \right) (R^3 - R_{hole}^3) \quad (A-3)$$

where A is equal to

$$A = \pi (R^2 - R_{hole}^2) \quad (A-4)$$

Furthermore, the induced maximum moment on the joint is the magnitude of the shaker applied load F_0 times the length from the center of the bolt to the shaker attachment point L . Therefore (A-4) becomes

$$(F_0) (L) = \frac{4}{3} \pi \mu \left(\frac{F_c}{A} \right) (R^3 - R_{hole}^3) \quad (A-5)$$

Solving for the clamping force F_c yields,

$$F_c = \frac{3}{4} \frac{(R^2 - R_{hole}^2) L F_0}{\mu (R^3 - R_{hole}^3)} \quad (A-6)$$

Assuming:

L = 20" (max distance from bolt center to shaker)
R = 0.75" (radius of 1.5 inch dia spacer)
 $R_{hole} = 0.25"$ (radius of 0.5 inch dia bolt hole)

Then F_c can be found in terms of the coefficient of friction and the shaker end load as:

$$F_c = 18.462 \left(\frac{F_0}{\mu} \right) \text{ lbs} \quad (A-7)$$

Table A-9 lists, for comparison, the axial clamping forces required for the corresponding applied end load assuming a coefficient of friction of 0.3.

Table A-9

Axial Clamping Forces versus Applied End Loads
for fully Clamped Joint (Coefficient of Friction = 0.3)

Applied End Load F_0 (in lbs)	Axial Clamping Force F_c (in lbs)
50	3076
25	1538
10	615
5	307

Based on the results in Table A-9, combined with the intention of applying end loads in magnitude of 10 lbs or less, an internally gauged bolt linear over a range of 0-1000 lbs was

originally desired. But, realizing that the coefficient of friction for steel can vary widely from a lower range of .2 to an upper bound of .4 or higher, an internally gauged bolt was requested calibrated over a 0-4000 lb range²⁸. A lower coefficient of friction will increase the required clamping force of the joint to prevent slip as seen by Equation (A-7). This is not considered a problem however, since the applied load of the shaker can be accurately reduced and controlled in order to compensate for lower coefficients of friction.

Four internally gauged 0.5 inch bolts were purchased from Carron & Company³⁹. All the bolts are 4.5 inches long. Two bolts have a 1.5 inch shank and two bolts have a 1.75 inch shank. The different shank lengths were requested in order to accommodate the varying baseplate-spacer-beam thicknesses between the Mark I and Mark II designs. All four bolts have miniature modular transducer (MMT) inserts mounted in the bolt shanks. The specification of the bolts are listed in Table A-10.

Table A-10
Internally Gauged Bolt Specifications³⁹

Serial Number	572 B	573 B	574 B	575 B
Unthreaded Shank Length	1.5"	1.5"	1.75"	1.75"
Gain Setting	864.5	837.5	902.1	914.1
All Bolts (1/2 x 20):				
Material	Grade 18-8 Stainless Steel			
Rated Capacity (Tension)	4000 lbs			
Signal Sensor	4 arm bonded strain gauge bridge			
Bridge Resistance	120 Ohms			
Max Bridge Excitation	5 Volts			
Nonlinearity	Less than 1.5% (Full Strength)			
Connector	Standard Western Regional wiring with 4 pin miniature connector			

All 4 bolts were factory calibrated using a 10 point computer calibration procedure. The calibration was reaccomplished upon receipt of the bolts for 2 reasons: (1) to become familiar with the sensitivity of the transducers, and (2) to calibrate the bolts with the power amplifier to be used during actual testing. Clamps were made for the bolts in order to calibrate the bolts using the Material Test System (MTS) 110 kips machine and the 458-20 micro-console. Each bolt was fitted into the clamps and placed in the MTS. Great care was taken to level the clamps before testing began in order to ensure that the load line was parallel with the bolt shank. This was necessary in order to eliminate any bending (off-axis

loading) forces on the bolt. Levelling was accomplished using the MTS levels. The 4-pin connector was attached to the bolt and then connected to a measurements group 2310 signal amplifier. A 5 volt excitation was selected with a gain setting factor x100. An HP 3466A Digital Multimeter was used to monitor the output of the power amplifier. With no load on the bolt, the power amplifier was auto "zeroed" and trimmed in order to get a 0.000 volt reading on the multimeter. The MTS load was increased slowly from a zero load valve in lbs up to 3000 lbs, and brought back down to zero. The gain sensitivity dial on the power amplifier was adjusted to read 1 millivolt for every 1 pound of applied load. Several things were noted:

(1) The bolts were very sensitive to off axis loading. Calibration would vary as much as ten percent for small off axis loadings (less than 1/8 inch).

(2) A hysteresis loop was present. Going from zero to 3000 lbs and back down would show a loading of up to 30 lbs when none existed going up from zero.

(3) The calibration data showed a 1mV to 1lb correlation until approximately 1500 lbs. From 1500 lbs to 2500 lbs, the nonlinearity stayed well below the 1.5% specification. Above 2500 lbs and especially over 3000 lbs, the nonlinearity approached and even exceeded the 1.5% specification. In particular, bolt 573B displayed poor linearity above 2000 lbs (as much as 2 to 3%)

(4) The final power amplifier gain settings were repeatable for each bolt within the specifications discussed above. Once a gain setting was found, it could be cleared and redialed, producing the same results.

After speaking with a Carron & Company test engineer, it was found that the off-axis loading phenomena and hysteresis are normal occurrences. It was also discovered that these bolts will yield just above 5,000 lbs, so the increasing nonlinearity above 3,000 lbs is expected, but should still remain within 1.5% up to 4000 lbs. To receive good calibrated readings, loading should start at zero and go up. Once a load is brought down, it should be brought all the way down to zero and the power amplifier should be re-trimmed before applying any more loading. It is felt that the problem due to off-axis loading will not present itself as a problem, since the design of the beam-joint mechanism is fabricated in such a manner as to minimize off-axis loading. The top and bottom spacers will be fixed into place and will be perfectly aligned about the bolt's load axis. Furthermore, the combined thickness of the two spacers, the beam, and the baseplate is almost 2 inches, and should be sufficient enough to keep the bolt properly aligned. The gain settings for each bolt can be found in Table A-10.

Appendix B: Simple Spring-Mass FRICTION.m Script File

The following is the MATLAB FRICTION.m script file for the friction model described in Section 2.1.1. Following the file are some plots from the program.

```
function [x,xdot]=friction(m,k,mu,xo,t)
% FRICTION [x,xdot]=friction(m,k,mu,xo,t) returns:
%   x      displacement vector
%   xdot    velocity vector
% for the single DOF system with friction damping:
%
%   
$$m \ddot{x} + k x = +/- F_s$$

%
% where:
%   m      mass
%   k      spring constant
%   mu     coeff of friction
%   xo     initial displacement from x=0
%   t      time vector
%   Fs     friction force
%
%   NOTE:  use SI units (kg,m,sec)
%          input t vector must be (n x 1)
%          initial velocity is assumed zero
w=sqrt(k/m); % w=natural frequency
g=9.81;      % g=gravitational force in SI
to=0;        % time zero
[r,c]=size(t); % r=size of time vector t rows
%   if the initial displacement times k is not greater than
%   the friction force, then x=xo and xdot=zero for all t
%
if abs( (xo*k) / (mu*m*g) ) <= 1
    for i=1:r;
        x(i,1)=xo;
        xdot(i,1)=0;
    end,return
end
%
for i=1:r;
%   If xo>0, then xdot is neg and Fs is positive
%   If xo<0, then xdot is pos and Fs is negative
%   a and b are sign change variables
    if xo>0
        a=1;
        b=-1;
    else
        a=-1;
        b=1;
    end
end
```

```

        end
%      NOTE:  term with initial velocity value is omitted
%             since xdot(0) is always zero
%
x(i)=a*mu*m*g*(1/k-1/k*cos(w*(t(i)-to)))+xo*cos(w*(t(i)-to));
xdot(i)=a*mu*m*g*(w/k*sin(w*(t(i)-to)))-xo*w*sin(w*(t(i)-to));
%
%  Once xdot changes sign, then the sign of x and xdot
%  equations are changed, and xo is set equal to the last
%  calculated x and to is set equal to the last t used
%
        if sign( xdot(i,1)) ~= b
            xo = x(i,1);
            to = t(i,1);
%
%  at anytime after the motion stops, a check is made to see
%  if the friction force is greater than the k times
%  displacement force
%
            if abs( (xo*k)/(mu*m*g) ) <=1
                for j=i:r;
                    x(j,1)=xo;
                    xdot(j,1)=0;
                end,return
            end
%
        end
%
end
plot(t,x);xlabel ('seconds');ylabel('meters');grid;x;xdot;

```

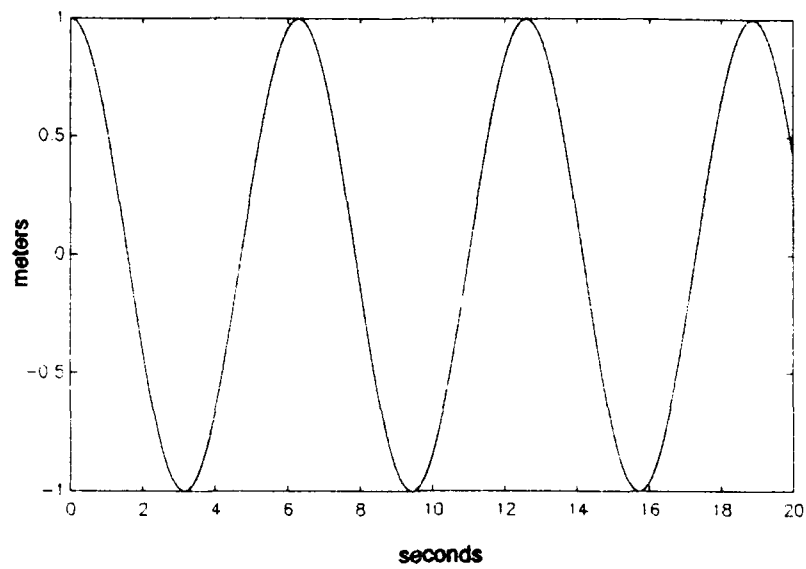


Figure B-1. MATLAB Friction.m Plot ($m=1$ kg, $k=1$ N/m, $\mu=0.0$, $x_0=1$ m)

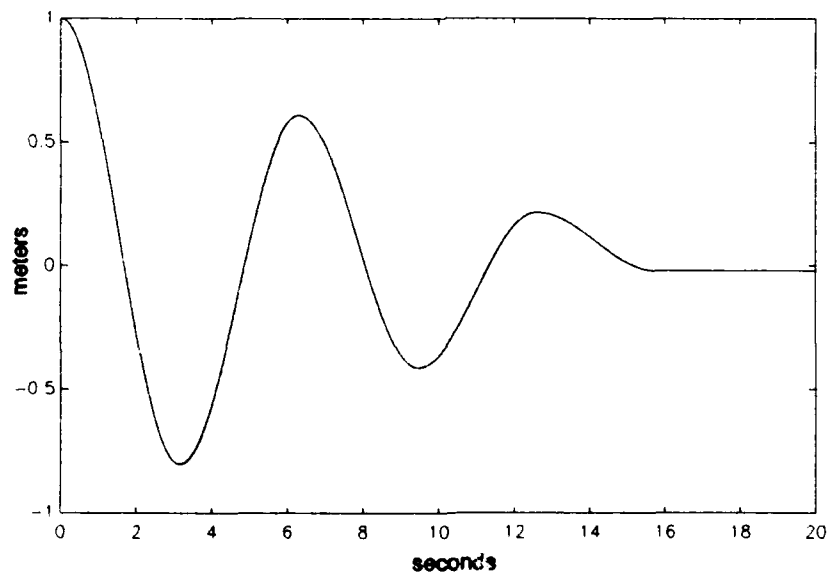


Figure B-2. MATLAB Friction.m Plot ($m=1$ kg, $k=1$ N/m, $\mu=0.01$, $x_0=1$ m)

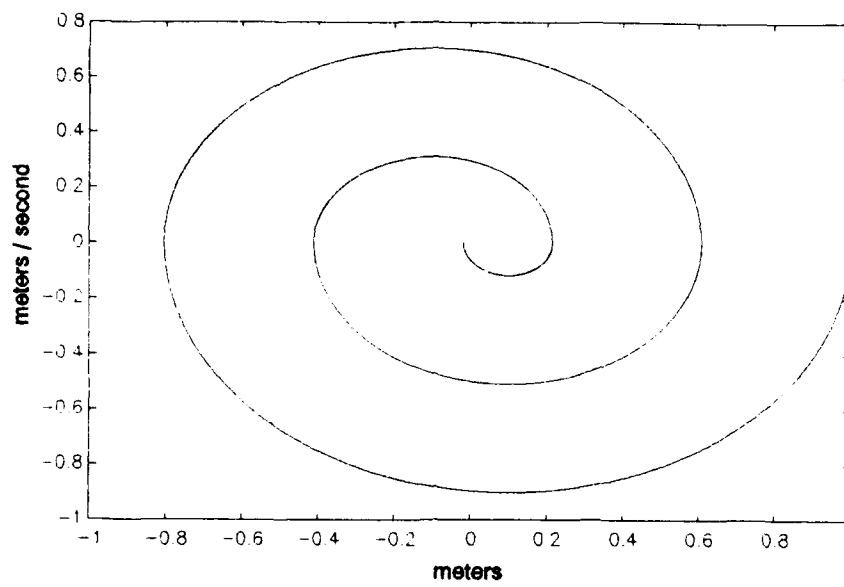


Figure B-3. MATLAB Friction.m Plot ($m=1$ kg, $k=1$ N/m, $\mu=0.01$, $x_0=1$ m)

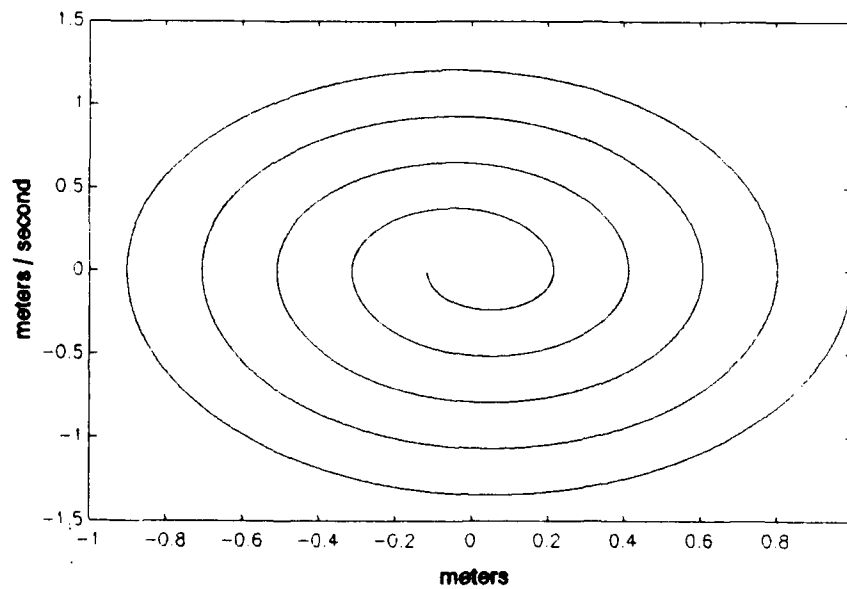


Figure B-4. MATLAB Friction.m Plot ($m=1$ kg, $k=2$ N/m, $\mu=0.01$, $x_0=1$ m)

Appendix C: MATLAB Script.m Files

The following MATLAB Script.m files were written and used as necessary throughout this thesis:

1. AREA.m/AREACALC.m/AREAFIT.m: AREA.m calculates the area in a hysteresis loop using the trapezoidal rule. A diagnostic plot of the hysteresis loop is provided. AREACALC.m omits the plot. AREAFIT.m is an early version of AREA.m which compared polyfitted versus trapezoidal area calculations. Only the AREA.m code is listed below.
2. CHPLOT.m/CHNOPLOT.m: Channel plot program. Plots data channels from Nicolet. CHNOPLOT is a no plot version of CHPLOT. Only CHPLOT.m is listed below.
3. EXPDATA.m: Computes from experimental data (provided by AREA.m) the coefficient of friction (μ), peak force (F_o) in lbs, peak displacement in inches, and the energy dissipated in lbs-inches.
4. HLOOP2.m/HNOPLOT.m: Hysteresis plot program. HNOPLOT is a no plot version. Only HLOOP2.m is listed below.
5. MOMENT.m/MTHEORY.m/MTHEORY1.m: MOMENT.m computes theoretical steady state displacement, velocity, and force signals for Mark II beam under dynamic loading, and plots all 3 signals. MTHEORY.m and MTHEORY1.m are the same as MOMENT.m except no plot is provided, and MTHEORY1.m does not consider the weight of the beam on the bottom frictional surface. Only MTHEORY.m is listed below.
6. POLYWOG.m: Polyfit routine for computing and plotting experimental data (energy dissipated, clamping force) against a 2nd order best fit curve.
7. THEORY.m/THEORY1.m: Computes and plots energy dissipated versus clamping force curves. THEORY1.m does not consider the weight of the beam on the bottom frictional surface. Only THEORY.m is listed below.
8. MARK1.m/MARKPLOT.m/MARK1MU: MARK1 and MARKPLOT compute theoretical displacements, velocities, and slopes for Mark I beam under free vibration conditions. MARK1MU computes μ and slope from experimental data. Only MARKPLOT is listed below.

AREA.m

```
function [TRAPAREA,ppf,ppd]=area(ch1a,ch1b,cycle)
%
% [TRAPAREA,ppf,ppd]=AREA(ch1a,ch1b,cycle) computes the
%           area of a
%           force vs displacement hysteresis loop
%           ch1a = 2 column data matrix (   force   , time)
%           ch1b = 2 column data matrix (displacement, time)
%           cycle = cycle in Hz at which data was sampled
%
%           NOTE: at least 2 cycles of data are required to insure
%                   one complete hysteresis loop is trapped and
%                   analyzed.
%           AREA returns:
%           TRAPAREA = area in loop from trapazoidal rule
%           DIAGNOSTIC PLOT = hysteresis loop; trapazoidal increments
%           ppf = peak to peak force           magnitude
%           ppd = peak to peak displacement magnitude
%           NOTE: If no plot is desired, use AREACALC.m
(x,y,t)=hplot(ch1a,ch1b,cycle);[xrow,scol]=size(x);
% shift plot over to first quadrant
[minx,minxpos]=min(x);[miny,minypos]=min(y);
x=x+abs(minx);y=y+abs(miny);
%
%           plot(y,x);hold;
% find the min and max values of force
[minx,minxpos]=min(x);
[maxx,maxxpos]=max(x);
% if minxpos is not at the beginning of the data, put it there
if minxpos~=1;
    if abs(xrow-minxpos)>0;
        for i=0:abs(xrow-minxpos);
            xq(i+1,1)=x(minxpos+i,1);
            yq(i+1,1)=y(minxpos+i,1);
        end;
    else;
        xq(1,1) = x(minxpos,1);
        yq(1,1) = y(minxpos,1);
    end;
    for i=1:minxpos-1;
        xq(abs(xrow-minxpos+1)+i,1)=x(i,1);
        yq(abs(xrow-minxpos+1)+i,1)=y(i,1);
    end;
else;
    xq=x;yq=y;
end;
x=xq; y=yq;
% these lines are diagnostic checks
[maxy,maxypos]=max(y);
```

```

                                [minx,minxpos]=min(x);
                                [maxx,maxxpos]=max(x);
                                size(x);

%
                                ppf=maxx;
                                ppd=maxy;

% isolate 2 lines of data (top and bottom)
                                for i=0:maxxpos-1;
                                    firstx(1+i,1)=x(minxpos+i,1);
                                    firsty(1+i,1)=y(minxpos+i,1);
                                end;
[xrow,xcol]=size(x);
                                for i=0:xrow-maxxpos;
                                    secondx(1+i,1)=x(maxxpos+i,1);
                                    secondy(1+i,1)=y(maxxpos+i,1);
                                end;

%% trapezoidal calculation
                                x1=firstx;y1=firsty;x2=secondx;y2=secondy;integral=0;integra2=0;
                                for i=1:maxxpos-i;
                                    var1=abs( x1(i+1,1)-x1(i,1) );
                                    var2=abs( y1(i+1,1)-y1(i,1) );
                                    if y2(i+1,1) > y2(i,1);
                                        int=abs(y2(i,1))*var1+0.5*var1*var2;
                                    else;
                                        int=abs(y2(i+1,1))*var1+0.5*var1*var2;
                                    end;
                                    integral=integral+int;
                                end;
                                for i=1:xrow-maxxpos-1;
                                    var1=abs( x2(i+1,1)-x2(i,1) );
                                    var2=abs( y2(i+1,1)-y2(i,1) );
                                    if y2(i+1,1) > y2(i,1);
                                        int=abs(y2(i,1))*var1+0.5*var1*var2;
                                    else;
                                        int=abs(y2(i+1,1))*var1+0.5*var1*var2;
                                    end;
                                    integra2=integra2+int;
                                end;

                                TRAPAREA=abs(integra2-integral);
                                plot(y,x);hold;xlabel('displacement (volts)');ylabel('force (volts)');
                                title('diagnostic plot for integration calculation');
                                for i=1:xrow-maxxpos;
                                    testx=[x2(i,1),x2(i,1)];testy=[ 0 ,y2(i,1)];
                                    plot(testy,testx);testx=0;testy=0;
                                end;
                                for i=1:maxxpos;
                                    testx=[x1(i,1),x1(i,1)];testy=[ 0 ,y1(i,1)];
                                    plot(testy,testx);testx=0;testy=0;
                                end;hold;TRAPAREA;ppf;ppd;

```

CHPLOT.m

```
function [col1,col2]=chplot(channel)
% CHPLOT will plot columns 1 and 2 from a Nicolet Channel data file
%   column 1:  force, displacement, acceleration...
%   column 2:  time
%   be sure data file only has 2 columns (data,time)
%   [col1,col2]=CHPLOT(channel)
[r,c]=size(channel);
for i=1:r;
    x(i)=channel(i,1);
    y(i)=channel(i,1);
end;
x=x';t=t';plot(t,x);xlabel('seconds');ylabel('volts');col1=x;col2=t;
```

EXPDATA.m

```
function[ED,peakf,peakd,mu,D]=expdata(area,ppf,ppd,cycle,Fc,glevel,cal);
%   function [ED,peakf,peakd,my,D]=expdata(area,ppf,ppd,cycle,Fc,glevel)
%   returns:
%       ED = energy dissipated (in lbs-in)
%       peakf = peak magnitude force (lbs)
%       peakd = peak magnitude displacement (in)
%       mu = calculated coefficient of friction
%       D = computed peak displacement from g level (in)
%   for:   area = area calculated from AREA.m
%           (energy dissipated in volts ^2)
%       ppf = peak-peak force (mv)
%       ppd = peak-peak dis (mv)
%       cycle = frequency cycle data was trapped (Hz)
%       Fc = clamping force (lbs)
%       glevel = observed acceleration g reading from OSP-4
%       cal = Fotonic sensor calibration in (volts/inch)
%
peakf=(ppf /2) / 50; % lbs
peakd=( (ppd/2) / cal ) / 1000 ; % inches
peakdf=peakd/12 ; % feet

I=(1/12) * ( (2/12)^2 + (40/12^2 ) * (11.25/32.2); % slugs-ft^2
Mgross=(19.5/12)*(-(peakdf*I*(2*pi*cycle)^2)/(19.5/12)^2+peakf); %lbs-ft
xr=((1^3-.25^3)/(1^2-.25^2)) / 12; % feet
mu=(Mgross*3/4) / ((Fc+(.5)*(11))*xr); % unitless
D= .5 * (19.56/cycle^2*glevel); % peak d in inches
ED=area*(1000/50)/cal; % ED in lbs-in
ED;peakf;peakd;my;D;
```

HLOOP2.m

```
function [x,y,t]=hloop2(chla,chlb,cycle)
% HLOOP2 [x,y,t]=HLOOP2(chla,chlb,cycle) plots a
% force vs displacement hysteresis curve
%
% chla = 2 column data file (force, time)
% chlb = 2 column data file (disp, time)
% cycle = cycle freq in Hz
%
% [x,y,t]=[force vector,displacement vector,time vector]
% NOTE: be sure input data files contain at least 1
% or more cycles
%
[x1,t1]=chnoplot(chla); [y1,t1]=chnoplot(chlb);
%
[r,c]=size(t1); freq=1/cycle;
%
timept=abs(t1(1,1)-t1(2,1)); % time interval between data
%
%sweepptm is time it takes to collect all data points
% (normally 1000 pts)
sweepptm=r*timept;
%
noc=sweepptm/freq; % number of cycles contained in sweep
%
% ppc is number of data points in 1 cycle (points per cycle)
%
ppc=fix(freq/timept);
%
for i=1:ppc;
    x2(i,1)=x1(i,1);
end;
%
% identifies the first min peak value of chla
%
[w,z]=min(x2); x2size=size(x2);
%
% strip off the data from 1 cycle starting with the min peak
% value from the first cycle in chla
%
for i=1:ppc;
    x(i,1)=x1(z+i,1);
    y(i,1)=y1(z+i,1);
    t(i,1)=t1(z+i,1);
end;
x; y; t; plot(y,x); xlabel('displacement'); ylabel('force');
```

MTHEORY.m

```
function [force,x,xdot,t,D]=mtheory(Fo,Fc,my,cycle)
% MTHEORY
% [force,x,dot,t,D]=mtheory(Fo,Fc,my,cycle)
% Fo = applied sinusoidal load magnitude (lbs)
% Fc = clamping force (lbs)
% mu = coefficient of static friction
%
% force = force vector of shaker (lbs)
% x = displacement vector (in)
% xdot = velocity vector (in/s)
% D = PEAK displacement (in)
%
% NOTE: No plot is provided. See MOMENT.m for plot
w=2*pi*cycle; % rad/sec
xr=(1^3-.25^3)/(1^2-.25^2) / 12; % feet
timestep= (1/cycle)/100; % seconds
t=(0:timestep:(1/cycle)*4)'; % seconds
[row,col]=size(t);
Mgross=2*( (2/3)*mu(Fc+(.5)*11)*xr ); %lbs-ft
I=(1/12)*( (2/12)^2 + (40/12)^2 )*(11/32.2); % slugs-ft^2
n=0;
% begin calculation
%
D=(Fo-Mgross/(19.5/12))*((19.5/12)^2/(w^2*I); % feet
if D<=0;x=0*t;xdot=0*t;force=-Fo*sin(w*t);n=1;end;
if n == 0;
x=D*sin(w*t); % feet
xdot=D*w*cos(w*t); % feet/sec
force=-D*I*w^2/(19.5/12)^2*sin(w*(t)); % lbs

for i=1:row;

if xdot(i) > 0;
force(i)=force(i)+Mgross/(19.5/12);

elseif xdot(i) < 0;
force(i)=force(i)-Mgross/(19.5/12);
else;
force(i)=force(i);
end;
end;
else;end;
x=x*12;xdot*12;D=D*12; % feet to inches conversion
%plot(t,x,xdot,t,force);
%xlabel('time');
force; x; t; xdot; D;
```

POLYWOG.m

```
function [x,y]=polywog(clampv,dampv);
%   [x,y]=polywog(clampv,dampv) returns
%
%   x=clamping force vector
%   y=2nd order polyfit curve of energy dissipated
%
%   if given:      clampv=experimental clamping force vector
%                  dampv =experimental energy dissipated vector
%   plot is provided
x=(min(clampv):1:max(clampv))';
v=polyfit(clampv,dampv,2);
y=polyval(v,x);
plot(x,y,clampv,dampv,'o');
xlabel('Clamping Force (lbs)');ylabel('Energy Dissipated');
x;y;
```

THEORY.m

```
function [ED,Fc]=theory(Fo,my,cycle)
%
%   [Ed,Fc]=theory(Fo,my,cycle) returns
%       ED      = energy dissipaton vector (lbs-in)
%       Fc      = clamping pressure vector (lbs)
%
%   When given:
%       Fo      = max magnitude of forcing function (lbs)
%       mu      = coefficient of friction
%       cycle   = frequency of displacement in Hz
%
%   A plot of clamping force vs energy dissipated is displayed
%   Script files called: MTHEORY.m and AREACALC.m
Fc=(0:1:40)';
[row,col]=size(Fc);
for i=1:row;

    [f,x,xdot,t,D]=mtheory(Fo,Fc(i),mu,cycle);
%       NOTE: channel 1a is dispalcement and time, unlike with
%             experimental data (where it's channel 1b). This
%             has to do with the way in which AREACALC performs
%             its area under the curve calculation.
    [ED,(i),ppf,ppd]=areacalc([x t],[f t],cycle);
end;
plot(Fc,ED);xlabel('clamping force (lbs)');ylabel('Energy Dissipated');
Fc;ED;
```


MARKPLOT.m

```

function [u,udot,slope]=markplot(mu,uo,Fc,t);
%
%      [u,udot,slope] = mark1(mu,uo,Fc,t)
%
%      mu      =      coefficient of friction
%      uo      =      initial displacement in feet
%      Fc      =      clamping force in lbs
%      t      =      time vector in seconds (1 by n)
%      note: uo is limited to 3 inches max for linear analysis
%      u,udot = displacement (ft) and velocity (ft/sec)
%      slope = envelope of decay (ft/sec)
W=26                                     % lbs
xcm=16.57/12;                           % feet
Io=1.6834;                              % slugs-ft^2
xr=((1^3-.25^3)/(1^2-.25^2))/12;        % feet
L=21.5/12;                              % feet
to=0;                                    % seconds
wn=sqrt(W*(xcm)/Io);                    % wn in rad/sec
Mgross=4/3*mu*Fc*xr;                    % lbs-feet
g=32.174;                               % ft/sec^2
Mshank=W*mu*.25/12;                     % lbs-feet
[r,c]=size(t);
Mt=Mgross + Mshank;                     % lbs-feet
cl=Mt*L/(Io*wn^2);                      % feet
slope=2*(Mt*L)/(Io*wn*pi);              % feet/sec
y=-slope*t+uo;
if sign(uo) < 0; uo=-uo;y=-slope*t+uo;uo=-uo;end;
if abs(wn^2*uo) <= abs(Mt/Io);
    for i=1:r;
        u(i)=uo;udot(i)=0;
    end;return;
end;
for i=1:r;
    if uo>0; a=1;b=-1;
    else; a=-1;b=1;
    end;
    u(i)=a*cl*(1-cos(wn*(t(i)-to))) + uo*cos(wn*(t(i)-to));
    udot(i)=a*cl*(wn*sin(wn*(t(i)-to)))-uo*wn*sin(wn*(t(i)-to));
    if sign(udot(i)) ~=b;
        uo=u(i);to=t(i);
        if abs(wn^2*uo) <= abs(Mt/Io);
            for j=1:r;
                u(j)=uo;udot(j)=0;
            end;return;
        end;
    end;
end;
end;plot(t,u,t,y);xlabel('seconds');ylabel('feet');u;udot;slope;

```

Appendix D: Mark II Test Data

Table D-1

Mark II Test 1 General Parameters

Bolt: 575B
Frequency: 10Hz
Sweep Time: 300 ms (1000 data points)
Fotonic Sensor Calibration: 9.563 volts/inch
Force Transducer Calibration: 50 mv/lb
Approximate time beam was under cyclic loading: 15 min

Ra measurements (microinches)								
(position)	(1)	(2)	(3)	(4)	(5)	(6)	(7)	(8)
before:	40	39	35	31	33	44	29	40
after:	42	38	37	30	29	41	27	40
(position)	(9)	(10)	(11)	(12)	(13)	(14)	(15)	
before:	41	37	44	46	xx	xx	39	
after:	46	42	50	43	xx	xx	38	

Table D-2

Mark II Test 1 AREA.m Data (10Hz)

Clamping Force (mv)	Area $\times 10^{-3}$ (volts ²)	P-P Force (mv)	P-P Displacement (mv)
(00) 00	24.77	220.17	604.54
(29) 31	39.48	211.48	649.15
(65) 67	38.47	196.46	284.10
(116) 116	10.34	244.70	100.74

[08]

(xx) = indicated clamping force at joint before loading
 xx = indicated clamping force during loading. This value is used as the actual clamping force in data reduction.
 [xx] = indicated clamping force when joint is unclamped

Table D-3

Mark II Test 1 EXPDATA.m Results (10Hz)

Clamping Force (lbs)	ED $\times 10^{-2}$ (lbs-in)	Peak Force (lbs)	Peak Displacement (in)	μ
00	5.180	2.202	.0316	.2891
31	82.57	2.115	.0339	.2837
67	80.46	1.965	.0149	.2624
116	21.63	2.447	.0053	.2561
Average Peak Force (Fo) = 2.182 lbs				
Average μ = .2728				

Table D-4

Mark II Test 2 General Parameters

Bolt: 575B
 Frequency: 10Hz
 Sweep Time: 300 ms (1000 data points)
 Fotonic Sensor Calibration: 8.759 volts/inch
 Force Transducer Calibration: 50 mv/lb
 Approximate time beam was under cyclic loading: .75 hrs

Ra measurements (microinches)								
(position)	(1)	(2)	(3)	(4)	(5)	(6)	(7)	(8)
before:	12	10	15	11	09	14	09	10
after:	11	09	15	12	08	13	08	09
(position)	(9)	(10)	(11)	(12)	(13)	(14)	(15)	
before:	11	07	12	09	xx	xx	14	
after:	12	08	13	09	xx	xx	14	

Table D-5

Mark II Test 2A AREA.m Data (10Hz)

Clamping Force (mv)	Area $\times 10^{-3}$ (volts ²)	P-P Force (mv)	P-P Displacement (mv)
(00) 00	.4502	17.63	41.25
(18) 18	.0141	18.26	6.33
(53) 54	.0039	15.92	4.19
(80) 81	.0034	18.88	2.77
(100) 100	.0015	19.56	3.00
(115) 115	.0015	20.67	2.47
(00) 00	1.123	41.52	107.66
(18) 18	.4541	43.05	25.25
(53) 54	.1393	45.17	17.27
(80) 81	.0296	44.23	7.26
(100) 100	.0231	46.13	7.55
(115) 115	.0095	45.59	6.20
(00) 00	1.907	89.96	202.18
(18) 19	1.147	87.02	283.66
(53) 54	5.817	89.74	92.16
(80) 82	.4836	95.97	23.65
(100) 100	.2809	88.60	18.56
(115) 115	.2111	94.19	15.31

[04]

(xx) = indicated clamping force at joint before loading
 xx = indicated clamping force during loading. This
 value is used as the actual clamping force in
 data reduction
 [xx] = indicated clamping force when joint is unclamped

Table D-6

Mark II Test 2A EXPDATA.m Results (10Hz)

Clamping Force (lbs)	ED $\times 10^{-2}$ (lbs-in)	Peak Force (lbs)	Peak Displacement (in)	μ
00	.1028	.1763	.0024	.2055
18	.0032	.1826	.0004	.0996
54	.0009	.1592	.0002	.0350
81	.0008	.1888	.0002	.0294
100	.0003	.1956	.0001	.0249
115	.0003	.2067	.0001	.0232
00	.2564	.4152	.0062	.4226
18	.1037	.4305	.0014	.2206
54	.0318	.4517	.0010	.0964
81	.0068	.4423	.0004	.0685
100	.0053	.4613	.0004	.0586
115	.0022	.4559	.0003	.0510
00	.4354	.8996	.0115	1.097
19	.2619	.8702	.0162	.1228
54	1.328	.8974	.0053	.1603
82	.1104	.9597	.0014	.1441
100	.0006	.8860	.0011	.1113
115	.0005	.9419	.0009	.1048

Table D-7

Mark II Test 2B AREA.m Data (10Hz)

Clamping Force (mv)	Area $\times 10^{-3}$ (volts ²)	P-P Force (mv)	P-P Displacement (mv)
(00) 00	.0317	40.47	67.21
(06) 07	.0883	38.03	63.68
(18) 19	.9925	45.77	113.72
(34) 35	.2302	39.37	100.64
(65) 67	1.658	42.32	141.22
(80) 80	1.521	39.97	130.72
(94) 94	.1334	42.12	34.08
(00) 00	.0937	58.85	98.78
(06) 07	.1259	58.68	98.02
(18) 20	.7082	69.62	168.47
(34) 36	.3594	61.36	149.12
(50) 51	1.446	59.77	179.57
(65) 67	2.943	65.44	199.54
(80) 81	3.198	56.51	205.4
(94) 93	.5278	62.36	61.52
(00) 00	.2726	84.60	145.09
(06) 07	.1619	83.14	139.07
(18) 20	.8953	91.27	215.39
(34) 36	.5074	86.33	202.01
(50) 51	1.973	84.19	230.55
(65) 67	4.552	93.55	266.23
(80) 81	4.018	75.66	262.19
(94) 92	1.802	81.62	113.14

[04]

(xx) = indicated clamping force at joint before loading
 xx = indicated clamping force during loading. This
 value is used as the actual clamping force in
 data reduction
 [xx] = indicated clamping force when joint is unclamped

Table D-3

Mark II Test 2B EXPDATA.m Results (10Hz)

Clamping Force (lbs)	ED $\times 10^{-2}$ (lbs-in)	Peak Force (lbs)	Peak Displacement (in)	μ
00	.0072	.4047	.0038	.6323
07	.0202	.3803	.0036	.2601
19	.2266	.4577	.0065	.1111
35	.0526	.3937	.0058	.0556
67	.3786	.4232	.0081	.0187
80	.3473	.3997	.0075	.0160
94	.0305	.4212	.0020	.0480
00	.0214	.5885	.0056	.9134
07	.0288	.5868	.0056	.4020
20	.1617	.6962	.0096	.1680
36	.0821	.6136	.0085	.0905
51	.3302	.5977	.0103	.0452
67	.6720	.6544	.0114	.0373
81	.7302	.5651	.0117	.0147
93	.1205	.6236	.0035	.0681
00	.0623	.8460	.0083	1.295
07	.0370	.8314	.0079	.5690
20	.2044	.9127	.0123	.2272
36	.1159	.8633	.0115	.1334
51	.4505	.8419	.0132	.0765
67	1.039	.9355	.0152	.0618
82	.9775	.7566	.0150	.0245
92	.4115	.8162	.0065	.0793

Table D-9

Mark II Test 3 General Parameters

Bolt: 575B
 Frequency: 10Hz
 Sweep Time: 300 ms (1000 data points)
 Fotonic Sensor Calibration: 8.759 volts/inch
 Force Transducer Calibration: 50 mv/lb
 Approximate time beam was under cyclic loading: .75 hrs

Ra measurements (microinches)

(position)	(1)	(2)	(3)	(4)	(5)	(6)	(7)	(8)
before:	11	09	15	12	08	13	08	09
after:	12	11	16	13	08	15	10	13
(position)	(9)	(10)	(11)	(12)	(13)	(14)	(15)	
before:	12	08	13	09	xx	xx	14	
after:	13	10	14	11	19	16	15	

Table D-10
Mark II Test 3 AREA.m Data (10Hz)

Clamping Force (mv)	Area $\times 10^{-3}$ (volts ²)	P-P Force (mv)	P-P Displacement (mv)	g reading from OSP-4
(00) 00	.1111	61.84	88.83	.064
(08) 08	1.153	65.68	125.65	.080
(12) 13	.7926	55.15	124.71	.085
(31) 32	.8756	46.06	147.11	.097
(46) 47	.6211	48.40	134.01	.084
(65) 68	2.344	45.37	153.93	.099
(85) 89	4.316	45.97	202.11	.119
(105) 109	6.789	54.78	199.61	.125
(128) 128	3.505	57.03	90.81	.067
(152) 152	.4962	68.57	23.85	.025
(174) 174	.0970	64.01	10.43	.020
(00) 00	.2113	80.27	116.69	.083
(08) 08	1.374	77.01	143.33	.092
(12) 13	1.262	78.00	171.55	.114
(31) 32	.8348	56.45	165.73	.108
(46) 48	.9721	64.06	165.67	.102
(65) 69	2.983	73.36	200.73	.126
(85) 91	6.057	69.28	244.26	.149
(105) 110	9.497	71.13	251.64	.156
(128) 129	7.639	75.0	151.40	.100
(152) 153	1.119	89.52	37.32	.030
(174) 174	.2709	85.28	15.88	.020
(00) 00	.3471	96.71	142.77	.102
(08) 08	1.626	99.52	182.68	.118
(12) 14	1.548	91.52	203.87	.133
(31) 33	1.886	98.64	224.71	.138
(46) 50	2.222	98.07	212.46	.130
(65) 70	4.102	98.21	253.38	.154
(85) 93	6.530	87.87	256.21	.163
(105) 112	11.44	86.16	286.89	.180
(128) 130	12.84	90.50	227.59	.144
(152) 153	2.903	109.59	63.09	.046
(174) 174	.5087	101.36	21.09	.023

[09]

(xx) = indicated clamping force at joint before loading
xx = indicated clamping force during loading. This
value was used as the actual clamping force in
data reduction
[xx] = indicated clamping force when joint is unclamped

Table D-11

Mark II Test 3 EXPDATA.m Results (10Hz)

Clamping Force (lbs)	ED x10 ⁻² (lbs-in)	Peak Force (lbs)	Peak Displacement (in)	D (in)	μ
00	.0254	.6184	.0051	.0063	1.047
08	.2633	.6584	.0072	.0078	.3786
13	.1810	.5514	.0071	.0083	.1987
32	.1999	.4606	.0084	.0095	.0451
47	.1418	.4840	.0076	.0082	.0464
68	.5352	.4537	.0088	.0097	.0187
89	.9855	.4597	.0115	.0116	-.0010
109	1.550	.5478	.0114	.0122	.0106
128	.8003	.5703	.0052	.0066	.0376
152	.1133	.6857	.0014	.0024	.0558
174	.0221	.6401	.0006	.0020	.0478
00	.0482	.8027	.0067	.0081	1.351
08	.3137	.7701	.0082	.0090	.4535
13	.2882	.7800	.0098	.0111	.2894
32	.1906	.5645	.0095	.0106	.0677
48	.2220	.6406	.0095	.0100	.0673
69	.6811	.7336	.0115	.0123	.0506
91	1.383	.6928	.0139	.0146	.0187
110	2.169	.7113	.0144	.0153	.0158
129	1.744	.7507	.0086	.0098	.0416
153	.2555	.8932	.0021	.0029	.0709
174	.0619	.8528	.0009	.0020	.0630
00	.0793	.9671	.0081	.0100	1.615
08	.3713	.9952	.0104	.0115	.5921
14	.3535	.9152	.0116	.0130	.3178
33	.4306	.9864	.0128	.0135	.1694
50	.5074	.9807	.0121	.0127	.1231
70	.9366	.9821	.0145	.0151	.0734
93	1.491	.8787	.0146	.0159	.0407
112	2.612	.8616	.0164	.0176	.0237
130	2.932	.9050	.0130	.0141	.0391
153	.6629	1.096	.0036	.0045	.0835
174	.1162	1.014	.0012	.0022	.0745

Table D-12

Mark II Test 4 General Parameters

Bolt: 575B
 Frequency: 15Hz
 Sweep Time: 200 ms (1000 data points)
 Fotonic Sensor Calibration: 8.759 volts/inch
 Force Transducer Calibration: 50 mv/lb
 Approximate time beam was under cyclic loading: .75 hrs

Ra measurements (microinches)								
(position)	(1)	(2)	(3)	(4)	(5)	(6)	(7)	(8)
before:	12	11	16	13	08	15	10	10
after:	13	11	20	12	09	14	10	11
(position)	(9)	(10)	(11)	(12)	(13)	(14)	(15)	
before:	13	10	14	11	19	16	15	
after:	17	31	18	10	23	18	15	

Table D-13

Mark II Test 4 AREA.m Data (15Hz)

Clamping Force (mv)	Area $\times 10^{-3}$ (volts ²)	P-P Force (mv)	P-P Displacement (mv)	g reading from OSP-4
(00) 00	.0490	55.73	52.69	.076
(08) 09	.0063	54.64	82.16	.097
(23) 23	.1045	60.44	74.69	.102
(50) 49	.5054	54.90	89.74	.121
(69) 66	1.304	49.78	106.82	.152
(82) 85	2.121	46.17	131.76	.176
(105) 107	3.142	62.06	156.68	.212
(121) 122	4.209	54.73	159.21	.224
(147) 146	.1939	60.32	21.00	.038
(171) 171	.1096	59.02	13.30	.028
(196) 196	.0883	56.57	10.64	.026
(00) 00	.0889	79.17	74.78	.109
(09) 09	.3356	75.80	104.58	.130
(23) 23	.1429	78.01	94.41	.127
(50) 50	.8724	80.70	115.15	.157
(69) 66	2.260	78.36	143.86	.198
(82) 86	2.590	71.34	150.16	.204
(105) 107	3.852	77.77	171.27	.235
(121) 123	6.411	78.80	195.26	.273
(147) 146	.9275	85.25	36.99	.057
(171) 171	.3936	90.29	21.42	.042
(196) 196	.3316	83.58	20.22	.036
(00) 00	.1080	91.15	86.24	.126
(23) 23	.2446	105.41	121.98	.166
(50) 50	1.319	103.58	141.32	.194
(69) 67	2.435	92.78	159.39	.219
(82) 86	3.445	94.96	173.85	.238
(105) 108	4.663	91.67	186.59	.258
(121) 123	8.178	98.18	216.63	.299
(147) 146	7.848	88.46	129.54	.183
(171) 171	.6902	107.91	28.40	.051
(196) 196	.6430	98.78	26.53	.043

[10]

(xx) = indicated clamping force at joint before loading
 xx = indicated clamping force during loading. This
 value is used as the actual clamping force in
 data reduction
 [xx] = indicated clamping force when joint is unclamped

Table D-14

Mark II Test 4 EXPDATA.m Results (15Hz)

Clamping Force (lbs)	ED $\times 10^{-2}$ (lbs-in)	Peak Force (lbs)	Peak Displacement (in)	D (in)	μ
00	.0112	.5573	.0030	.0033	.7189
09	.0014	.5464	.0047	.0042	.1153
23	.0239	.6044	.0043	.0044	.1060
49	.1154	.5490	.0051	.0053	.0213
66	.2978	.4978	.0061	.0066	-.0010
85	.4843	.4617	.0075	.0077	-.0342
107	.7174	.6206	.0089	.0092	-.0238
122	.9611	.5473	.0091	.0097	-.0305
146	.0443	.6032	.0012	.0017	.0454
171	.0250	.5902	.0008	.0012	.0411
196	.0202	.5657	.0006	.0011	.0353
00	.0203	.7917	.0043	.0047	1.022
09	.0766	.7580	.0060	.0057	.2068
23	.0326	.7801	.0054	.0055	.1418
50	.1992	.8070	.0066	.0068	.0526
66	.5160	.7836	.0082	.0086	.0072
86	.5914	.7143	.0086	.0089	-.0099
107	.8796	.7777	.0098	.0102	-.0138
123	1.464	.7880	.0111	.0119	-.0244
146	.2118	.8525	.0021	.0025	.0607
171	.0899	.9029	.0012	.0018	.0625
196	.0757	.8358	.0012	.0016	.0505
00	.0247	.9115	.0049	.0055	1.175
23	.0559	1.054	.0070	.0072	.2058
50	.3012	1.036	.0081	.0084	.0759
67	.5560	.9278	.0091	.0095	.0193
86	.7866	.9496	.0099	.0103	.0072
108	1.065	.9167	.0107	.0112	-.0063
123	1.867	.9818	.0124	.0130	-.0154
146	1.792	.8846	.0074	.0080	.0195
171	.1576	1.079	.0016	.0022	.0735
196	.1468	.9878	.0015	.0019	.0588

Table D-15

Mark II Test 5 General Parameters

Bolt: 575B
 Frequency: 10Hz and 15Hz
 Sweep Time: 300 ms and 200 ms (1000 data points)
 Fotonic Sensor Calibration: 8.759 volts/inch
 Force Transducer Calibration: 50 mv/lb
 Approximate time beam was under cyclic loading: .75 hrs

Ra measurements (microinches)								
(position)	(1)	(2)	(3)	(4)	(5)	(6)	(7)	(8)
before:	13	11	20	12	09	14	10	11
after:	19	11	25	10	11	13	12	13
(position)	(9)	(10)	(11)	(12)	(13)	(14)	(15)	
before:	17	31	18	10	23	18	15	
after:	23	104	26	10	33	19	15	

Table D-16

Mark II Test 5A AREA.m Data (10Hz)

Clamping Force (mv)	Area $\times 10^{-3}$ (volts ²)	P-P Force (mv)	P-P Displacement (mv)	g reading from OSP-4
(48) 48	2.259	46.85	145.79	.091
(66) 72	6.909	60.24	202.90	.122
(90) 95	6.280	58.41	181.86	.109
(113) 116	7.130	61.31	190.61	.115
(134) 135	2.678	56.71	75.13	.055
(156) 156	.2312	62.82	20.65	.024
(48) 47	4.264	77.12	197.13	.121
(66) 73	8.265	70.01	225.57	.135
(90) 96	10.11	85.90	230.63	.138
(113) 116	8.743	72.47	214.76	.129
(134) 136	8.788	87.87	145.08	.095
(156) 156	1.144	84.57	39.87	.035
(48) 54	10.95	101.20	297.98	.162
(66) 73	10.37	83.83	257.54	.154
(90) 96	12.34	100.06	256.39	.154
(113) 116	11.81	95.21	258.56	.152
(134) 136	9.762	93.48	151.68	.100
(156) 156	3.500	101.43	70.10	.051

[07]

(xx) = indicated clamping force at joint before loading
 xx = indicated clamping force during loading. This
 value was used as the actual clamping force in
 data reduction
 [xx] = indicated clamping force when joint is unclamped

Table D-17

Mark II Test 5A EXPDATA.m Results (10Hz)

Clamping Force (lbs)	ED $\times 10^{-2}$ (lbs-in)	Peak Force (lbs)	Peak Displacement (in)	D (in)	μ
48	.5158	.4658	.0083	.0089	.0337
72	1.578	.6024	.0116	.0119	.0242
95	1.434	.5841	.0104	.0107	.0228
116	1.628	.6131	.0109	.0112	.0199
135	.6615	.5671	.0043	.0054	.0390
156	.0528	.6282	.0012	.0023	.0501
47	.9736	.7712	.0113	.0118	.0840
73	1.887	.7001	.0129	.0132	.0319
96	2.309	.8590	.0132	.0135	.0449
116	1.996	.7247	.0123	.0126	.0263
136	2.007	.8787	.0083	.0093	.0536
156	.2612	.8457	.0023	.0034	.0650
54	2.500	1.012	.0170	.0158	.0760
73	2.368	.8383	.0147	.0151	.0433
96	2.818	1.001	.0146	.0151	.0562
116	2.697	.9521	.0148	.0149	.0408
136	2.229	.9348	.0087	.0098	.0576
156	.7992	1.015	.0040	.0050	.0736

Table D-18

Mark II Test 5B AREA.m Data (15Hz)

Clamping Force (mv)	Area $\times 10^{-3}$ (volts ²)	P-P Force (mv)	P-P Displacement (mv)	g reading from OSP-4
(46) 47	.8260	61.10	110.64	.149
(64) 63	1.036	54.18	107.88	.147
(86) 81	1.904	61.09	126.34	.177
(99) 97	5.677	59.86	134.10	.182
(108) 108	.2149	57.37	27.81	.041
(120) 120	.1412	54.67	23.62	.036
(134) 134	.0875	59.18	15.71	.036
(156) 156	.0482	56.20	12.18	.024
(166) 166	.0063	63.09	11.58	.024
(46) 47	1.469	83.56	140.27	.193
(64) 63	1.820	76.82	133.54	.184
(86) 81	2.848	78.25	143.81	.204
(99) 97	8.614	79.64	166.01	.228
(108) 108	1.174	78.57	48.34	.067
(120) 120	.7051	76.26	40.85	.058
(134) 135	.2068	80.46	22.58	.038
(156) 156	.1436	75.08	17.80	.031
(166) 166	.1097	77.15	14.87	.029
(46) 47	1.981	104.74	162.67	.224
(64) 63	2.993	100.40	160.27	.220
(86) 81	4.397	102.07	172.29	.245
(99) 97	11.93	101.56	197.84	.270
(108) 109	10.63	96.54	152.48	.198
(120) 119	2.007	94.60	58.71	.081
(134) 134	.3999	101.91	30.96	.048
(156) 156	.3462	96.93	25.31	.040
(166) 166	.2432	98.36	20.49	.035

[06]

(xx) = indicated clamping force at joint before loading
 xx = indicated clamping force during loading. This
 value was used as the actual clamping force in
 data reduction
 [xx] = indicated clamping force when joint is unclamped

Table D-19

Mark II Test 5B EXPDATA.m Results (15Hz)

Clamping Force (lbs)	ED $\times 10^{-2}$ (lbs-in)	Peak Force (lbs)	Peak Displacement (in)	D (in)	μ
47	.1886	.6110	.0063	.0065	.0098
63	.2366	.5418	.0062	.0064	-.0037
81	.4348	.6109	.0072	.0077	-.0072
97	1.296	.5986	.0077	.0079	-.0132
108	.0491	.5737	.0016	.0018	.0527
120	.0322	.5467	.0013	.0016	.0471
134	.0200	.5918	.0009	.0016	.0509
156	.0110	.5620	.0007	.0010	.0430
166	.0014	.6309	.0007	.0010	.0464
47	.3354	.8356	.0080	.0084	.0286
63	.4156	.7682	.0076	.0080	.0153
81	.6503	.7825	.0082	.0089	.0058
97	1.967	.7964	.0095	.0099	-.0088
108	.2681	.7857	.0028	.0029	.0656
120	.1610	.7626	.0023	.0025	.0611
135	.0472	.8046	.0013	.0017	.0681
156	.0328	.7508	.0010	.0013	.0568
166	.0250	.7715	.0008	.0013	.0564
47	.4523	1.048	.0093	.0097	.0539
63	.6834	1.004	.0091	.0096	.0350
81	1.004	1.021	.0098	.0106	.0204
97	2.724	1.016	.0113	.0117	-.0015
109	2.427	.9654	.0087	.0086	.0212
119	.4583	.9460	.0034	.0035	.0717
134	.0913	1.019	.0018	.0021	.0857
156	.0791	.9693	.0014	.0017	.0723
166	.0555	.9836	.0012	.0015	.0712

Table D-20

Mark II Test 6 General Parameters

Bolt: 575B								
Frequency: 10Hz								
Sweep Time: 300 ms (1000 data points)								
Fotonic Sensor Calibration: 6.7913 volts/inch								
Force Transducer Calibration: 50 mv/lb								
Approximate time beam was under cyclic loading: 7 hrs								
Approximate clamping force between sets: 40-60 lbs								

Ra measurements (microinches)								
(position)	(1)	(2)	(3)	(4)	(5)	(6)	(7)	(8)
before:	27	17	38	13	20	31	20	31
after:	26	20	41	14	19	31	20	31
(position)	(9)	(10)	(11)	(12)	(13)	(14)	(15)	
before:	50	22	55	22	28	28	25	
after:	40	23	54	23	29	26	25	

Table D-21

Mark II Test 6A AREA.m Data (10Hz)

Clamping Force (mv)	Area x10 ⁻³ (volts ²)	P-P Force (mv)	P-P Displacement (mv)	g reading from OSP-4	Run Time Between Sets
(59) 60	1.629	51.81	44.94	.050	(5 min)
	1.512	49.18	44.46	.049	
	1.432	47.93	43.61	.048	
	1.385	47.55	42.67	.048	
	1.363	47.16	42.42	.048	
					10 min
(59) 60	1.428	47.83	43.46	.048	(3 min)
	1.416	48.40	43.00	.045	
	1.367	48.92	41.90	.044	
	1.312	48.94	40.99	.045	
	1.295	49.04	40.77	.043	

[02]

(xx) = indicated clamping force at joint before loading
 xx = indicated clamping force during loading. This
 value was used as the actual clamping force in
 data reduction
 [xx] = indicated clamping force when joint is unclamped

Table D-22

Mark II Test 6A EXPDATA.m Results (10Hz)

Clamping Force (lbs)	ED $\times 10^{-2}$ (lbs-in)	Peak Force (lbs)	Peak Displacement (in)	D (in)	μ
(59) 60	.4797	.5181	.0033	.0049	.0817
	.4453	.4918	.0033	.0048	.0765
	.4217	.4793	.0032	.0047	.0743
	.4079	.4755	.0031	.0047	.0741
	.4014	.4716	.0031	.0047	.0735
(59) 60	.4205	.4783	.0032	.0047	.0742
	.4170	.4840	.0032	.0044	.0757
	.4026	.4892	.0031	.0043	.0775
	.3864	.4894	.0030	.0044	.0781
	.3814	.4904	.0030	.0042	.0785

Table D-23

Mark II Test 6B AREA.m Data (10Hz)

Clamping Force (mv)	Area $\times 10^{-3}$ (volts ²)	P-P Force (mv)	P-P Displacement (mv)	g level from OSP-4	Run Time Between Sets
(50) 51	4.177	81.94	74.64	.059	(2 min)
	4.183	82.88	73.37	.059	
	4.181	83.16	72.84	.059	
	4.186	83.84	72.16	.056	
	4.196	84.85	71.38	.055	
					10 min
(50) 51	4.074	82.66	70.77	.057	(2min)
	4.054	82.39	70.46	.056	
	4.057	81.94	71.03	.056	
	4.058	81.67	71.11	.057	
	4.026	81.10	71.17	.056	
					10 min
(50) 51	4.093	78.24	76.20	.062	(3 min)
	4.070	77.85	76.41	.063	
	4.077	77.76	76.72	.062	
	4.089	77.73	76.98	.065	
	4.083	77.81	76.88	.066	
					10 min
(50) 51	5.172	87.13	84.23	.060	(Fo gained up)
	4.847	88.67	81.24	.068	
	4.682	91.53	78.59	.063	
	4.522	95.93	74.82	.059	
	4.505	98.71	73.16	.060	
Note 1	-	-	-		3 hrs
Note 2	-	-	-		2.5 hrs
<hr/>					
(xx)	= indicated clamping force at joint before loading				
xx	= indicated clamping force during loading. This value was used as the actual clamping force in data reduction				
[xx]	= indicated clamping force when joint is unclamped				
Note 1:	Joint is reclamped to 40lbs, Fo=40mv for 3 hrs Stopped, surfaces felt cold and looked unchanged				
Note 2:	Joint is reclamped to 40lbs, Fo=60mv for 2.5 hrs Stopped, surfaces felt cold and looked unchanged Ra tested				

Table D-24

Mark II Test 6B EXPDATA.m Results (10Hz)

Clamping Force (lbs)	ED x10 ⁻² (lbs-in)	Peak Force (lbs)	Peak Displacement (in)	D (in)	μ
51	1.230	.8194	.0055	.0058	.1473
	1.232	.8288	.0054	.0058	.1505
	1.231	.8316	.0054	.0058	.1516
	1.233	.8384	.0053	.0055	.1538
	1.236	.8484	.0053	.0054	.1568
51	1.120	.8266	.0053	.0056	.1519
	1.194	.8239	.0052	.0055	.1514
	1.195	.8194	.0052	.0055	.1499
	1.195	.8167	.0051	.0056	.1492
	1.186	.8110	.0053	.0055	.1477
51	1.205	.7824	.0056	.0061	.1370
	1.199	.7785	.0056	.0062	.1359
	1.201	.7776	.0056	.0061	.1354
	1.204	.7773	.0057	.0063	.1352
	1.202	.7781	.0057	.0064	.1354
51	1.523	.8713	.0062	.0059	.1530
	1.427	.8867	.0060	.0066	.1590
	1.379	.9153	.0058	.0062	.1680
	1.332	.9593	.0055	.0058	.1816
	1.327	.9871	.0054	.0059	.1897

Table D-25

Mark II Test 7 General Parameters

Bolt: 575B
 Frequency: 10Hz
 Sweep Time: 300 ms (1000 data points)
 Fotonic Sensor Calibration: 6.7913 volts/inch
 Force Transducer Calibration: 50 mv/lb
 Approximate time beam was under cyclic loading: 4.5 hrs
 Approximate clamping force between sets: 20 lbs

Ra measurements (microinches)								
(position)	(1)	(2)	(3)	(4)	(5)	(6)	(7)	(8)
before:	26	20	41	14	19	31	20	31
after:	22	20	38	14	19	30	20	31
(position)	(9)	(10)	(11)	(12)	(13)	(14)	(15)	
before:	40	23	54	23	29	26	25	
after:	39	23	54	25	30	26	25	

Table D-26

Mark II Test 7A AREA.m Data (10Hz)

Clamping Force (mv)	Area x10 ⁻³ (volts ²)	P-P Force (mv)	P-P Displacement (mv)	Run Time Between Sets
(20) 21	2.475	99.42	44.71	1 hour
(28) 29	.5637	95.39	20.59	
(37) 37	.3177	97.14	17.44	
[03]				
(15) 16	1.258	88.27	207.76	3 hours
(26) 27	8.016	81.81	133.91	
(38) 38	.3373	100.95	11.04	
[04]				
(14) 15	13.94	96.03	208.97	10 min
(25) 26	11.68	82.29	206.50	
(35) 35	.5814	98.59	13.92	
[02]				
(50) 50	.0474	83.05	8.35	
(50) 50	.0489	82.70	8.17	
(50) 50	.0436	82.63	8.22	
[01]				
<hr/>				
(xx)	=	indicated clamping force at joint before loading		
xx	=	indicated clamping force during loading. This value was used as the actual clamping force in data reduction		
[xx]	=	indicated clamping force when joint is unclamped		

Table D-27

Mark II Test 7A EXPDATA.m Results (10Hz)

Clamping Force (lbs)	ED $\times 10^{-2}$ (lbs-in)	Peak Force (lbs)	Peak Displacement (in)	Friction Coefficient μ
21	.7811	.9942	.0036	.4471
29	.1792	.9539	.0016	.3584
37	.1010	.9714	.0014	.3000
16	.4200	.8827	.0165	.1396
27	2.548	.8181	.0106	.1663
38	.1073	1.010	.0009	.3119
15	4.432	.9603	.0166	.1965
26	3.713	.8229	.0164	.0707
35	.1848	.9859	.0011	.3237
50	.0151	.8305	.0007	.2017
50	.0155	.8270	.0007	.2010
50	.0139	.8263	.0007	.2007
Mean Values: Peak Force (Fo) = .9069 lbs				
μ = .2431				

Table D-28

Mark II Test 7B AREA.m Data (10Hz)

Clamping Force (mv)	Area $\times 10^{-3}$ (volts ²)	P-P Force (mv)	P-P Displacement (mv)	Run Time Between Sets
(20) 21	10.44	133.45	112.90	
(29) 29	1.435	115.14	32.02	
(36) 37	.7266	113.89	23.49	
[04]				1 hour
(19) 19	16.92	97.22	263.65	
(38) 38	10.52	102.49	133.20	
(48) 48	.2206	112.2	8.55	
[09]				3 hours
(17) 18	14.33	108.70	187.85	
(34) 35	11.59	101.62	157.96	
(43) 43	.6196	112.71	11.69	
[05]				
(xx) = indicated clamping force at joint before loading xx = indicated clamping force during loading. This value was used as the actual clamping force in data reduction [xx] = indicated clamping force when joint is unclamped				

Table D-29

Mark II Test 7B EXPDATA.m Results (10Hz)

Clamping Force (lbs)	ED $\times 10^{-2}$ (lbs-in)	Peak Force (lbs)	Peak Displacement (in)	Friction Coefficient μ
21	3.319	1.335	.0090	.5107
29	.4562	1.152	.0026	.4233
37	.2310	1.139	.0019	.3485
19	5.379	.9722	.0210	.0714
38	3.344	1.025	.0106	.1912
48	.0701	1.122	.0007	.2850
18	4.556	1.087	.0149	.2867
35	3.685	1.016	.0126	.1750
43	.1970	1.127	.0009	.3129
Mean Values: Peak Force (Fo) = 1.1082 lbs				
$\mu = .2895$				

Table D-30

Mark II Test 8 General Parameters

Bolt: 575B
 Frequency: 10Hz
 Sweep Time: 300 ms
 Fotonic Sensor Calibration: 6.7913 volts/inch
 Force Transducer Calibration: 50 mv/lb
 Approximate time beam was under cyclic loading: 10 hrs
 Approximate clamping force between sets: 20 lbs

Ra measurements (microinches)

(position)	(1)	(2)	(3)	(4)	(5)	(6)	(7)	(8)
before:	22	20	38	14	19	30	20	31
after:	19	17	37	15	20	29	21	31
(position)	(9)	(10)	(11)	(12)	(13)	(14)	(15)	
before:	39	23	54	25	30	26	25	
after:	38	22	55	28	31	28	25	

Table D-31
Mark II Test 8A AREA.m Data (10Hz)

Clamping Force (mv)	Area x10 ⁻³ (volts ²)	P-P Force (mv)	P-P Displacement (mv)	Run Time Between Sets
(15) 16	9.906	79.40	270.06	1 hour
(21) 23	8.936	94.16	162.63	
(30) 31	.5225	95.92	12.18	
[01]				
(14) 16	4.864	90.09	78.35	3 hours
(20) 22	1.010	94.05	23.00	
(31) 31	.9797	94.54	7.95	
[06]				
(13) 15	4.156	93.96	61.60	30 min
(20) 21	.7432	100.55	17.17	
(35) 35	***	***	***	
[04]				
(14) 15	3.001	100.75	44.16	Beam Stopped 1 hour
(20) 22	.9783	100.51	18.74	
(30) 30	.7425	95.23	6.03	
[00]				
(10) 9	4.931	72.85	122.41	1 hour
(15) 15	3.483	87.93	55.97	
(21) 21	1.197	95.05	18.55	
[00]				
(10) 8	8.649	76.38	259.72	3 hours
(16) 17	5.948	97.92	84.86	
(21) 22	2.839	96.30	38.62	
[05]				
(10) 11	5.524	81.38	89.58	
(17) 17	1.351	100.54	21.24	
(22) 23	.5293	95.09	11.89	
[04]				
(xx) = indicated clamping force at joint before loading				
xx = indicated clamping force during loading. This value was used as the actual clamping force in data reduction				
[xx] = indicated clamping force when joint is unclamped				
*** = data lost during processing				

Table D-32

Mark II Test 8A EXPDATA.m Results (10Hz)

Clamping Force (lbs)	ED $\times 10^{-2}$ (lbs-in)	Peak Force (lbs)	Peak Displacement (in)	Friction Coefficient μ
16	3.149	.7940	.0215	-.0474
23	2.841	.9416	.0129	.2050
31	.1661	.9592	.0010	.3511
16	1.546	.9009	.0062	.4206
22	.3211	.9405	.0018	.4390
31	.3115	.9454	.0006	.3510
15	1.321	.9396	.0049	.5040
21	.2363	1.006	.0014	.4995
35	***	***	***	***
15	.9540	1.008	.0035	.5882
22	.3110	1.005	.0015	.4786
30	.2364	.9523	.0005	.3660
9	1.568	.7285	.0097	.3222
15	1.107	.8793	.0044	.4753
21	.3805	.9505	.0015	.4683
8	2.750	.7638	.0206	-.0724
17	1.891	.9792	.0067	.4375
22	.9025	.9630	.0031	.4249
11	1.756	.8138	.0071	.4441
17	.4295	1.005	.0017	.5802
23	.1623	.9509	.0009	.4461

Mean Values: Peak Force (F_o) = 0.9213 lbs
 μ (all values) = 0.3841
(excluding the negative μ 's)
= 0.4334

Table D-33
Mark II Test 8B AREA.m Data (10Hz)

Clamping Force (mv)	Area x10 ⁻³ (volts ²)	P-P Force (mv)	P-P Displacement (mv)	Run Time Between Sets
(15) 16	12.98	91.25	296.76	1 hour
(21) 24	12.18	97.12	211.91	
(30) 31	7.820	125.56	84.43	
[01]				
(14) 16	9.420	94.33	152.97	3 hours
(20) 22	2.687	111.98	41.64	
(31) 31	.1951	112.34	10.21	
[06]				
(13) 15	8.040	107.14	109.07	30 min
(20) 21	1.535	113.99	26.01	
(35) 35	.1378	110.10	7.88	
[04]				
(14) 15	3.685	111.21	51.11	Beam Stopped 1 hour
(20) 22	1.950	115.25	28.44	
(30) 30	***	***	***	
[00]				
(10) 9	7.060	85.05	154.20	1 hour
(15) 15	6.204	100.34	97.62	
(21) 21	3.932	115.04	45.28	
[00]				
(10) 8	12.82	97.23	300.28	3 hours
(16) 16	16.74	115.32	199.76	
(21) 22	7.101	116.76	81.81	
[05]				
(10) 11	8.055	96.04	113.52	
(17) 17	4.893	115.14	55.56	
(22) 23	1.116	113.38	19.13	
[04]				
<hr/>				
(xx)	= indicated clamping force at joint before loading			
xx	= indicated clamping force during loading. This value was used as the actual clamping force in data reduction			
[xx]	= indicated clamping force when joint is unclamped			
***	= data lost during processing			

Table D-34

Mark II Test 8B EXPDATA.m Results (10Hz)

Clamping Force (lbs)	ED $\times 10^{-2}$ (lbs-in)	Peak Force (lbs)	Peak Displacement (in)	Friction Coefficient μ
16	4.126	.9125	.0236	-.0262
24	3.872	.9712	.0168	.1373
31	2.486	1.256	.0067	.3757
16	2.995	.9433	.0122	.2929
22	.8542	1.120	.0033	.4995
31	.0620	1.123	.0008	.4162
15	2.556	1.071	.0087	.4900
21	.4880	1.140	.0021	.5552
35	.0438	1.101	.0006	.3700
15	1.172	1.112	.0041	.6441
22	.6199	1.153	.0023	.5375
30	***	***	***	***
9	2.244	.8505	.0123	.3413
15	1.972	1.003	.0078	.4688
21	1.250	1.150	.0036	.5282
8	4.076	.9723	.0237	.0083
16	3.820	1.153	.0159	.3315
22	2.257	1.168	.0065	.4583
11	2.561	.9604	.0090	.5030
17	1.556	1.151	.0044	.6023
23	.3548	1.134	.0015	.5241

Mean Values: Peak Force (F_0) = 1.0720 lbs
 μ (all values) = 0.4029
(excluding the negative μ and the near
zero μ value of .0083) = .4487

Appendix E: Mark I Damping Model Slope Calculation

The Mark I Damping model is a linearized rotational macroslip damping model developed in Section 2.3.1. and is very similar to the translational damping model presented in Section 2.1.1.. The slope of the envelope of decay due to Coulomb damping for the translational system is the decrease in each successive peak displacement divided by the time between cycles, or

$$\frac{4 \frac{\bar{f}_d}{k}}{\frac{2\pi}{\omega_n}} = \frac{2 f_d \omega_n}{k\pi}$$

The term which defines the envelope of decay is the f_d/k term, and can be found in the equation of motion for translation motion below.

$$x(t) = \pm \frac{\bar{f}_d}{k} (1 - \cos \omega_n t) + x(0) \cos \omega_n t + \frac{\dot{x}(0)}{\omega_n} \sin \omega_n t$$

Similarly, the linearized equation of motion for rotational motion is

$$u(t) = \pm \frac{M_{gross} L}{I_o \omega_n^2} (1 - \cos \omega_n t) + u(0) \cos \omega_n t + \frac{\dot{u}(0)}{\omega_n} \sin \omega_n t$$

where M_{gross} includes the moment friction due to both the joint

and the bolt shank. The term which characterizes the envelope of decay is

$$\frac{M_{gross}L}{I_o\omega_n^2}$$

and when multiplied by 4 and divided by the time between cycles, yields

$$\frac{2M_{gross}L}{I_o\omega_n\pi}$$

as the magnitude of the slope of linear decay. The equation above was used to calculate the theoretical slopes in MARKPLOT.m. Refer to Figures 5-1 and 5-3 in Chapter 5 for examples.

Refer to Sections 2.1.1. and 2.3.1. for development of the equations of motions, and for definitions of the variables presented above.

Bibliography

1. Crawley, E. F., Sarver, G. L., and Mohr, D. G., "Experimental Measurement of Passive Material and Structural Damping for Flexible Space Structures," Acta Astronautica, Vol. 10, No. 5-6: 381-393, 1983.
2. Ashley, H., "On Passive Damping Mechanisms in Large Space Structures," Journal of Spacecraft, Vol 21(5): 448-455, 1984.
3. Beards, C. F., "Damping in Structural Joints," Shock and Vibration Digest, Vol 11(9): 35-41, 1979.
4. Donnelly, Capt. Robert P., The Effects of Energy Dissipation Due to Friction at the Joint of a Simple Beam Structure, MS Thesis, AFIT/GAE/AA/85D-5, School of Engineering, Air Force Institute of Technology (AU), Wright-Patterson AFB OH, December 1985.
5. Leiker, Capt. Gregory L., Improved Modeling of Structural Joint Damping, MS Thesis, AFIT/GAE/AA/86D-9, School of Engineering, Air Force Institute of Technology, (AU), Wright-Patterson AFB OH, December 1986.
6. Beards, C. F., "Some Effects of Interface Preparation on Frictional Damping in Joints," International Journal of Machine Tool Design and Research, Vol 15: 77-85, 1975.
7. Beards, C. F., and Williams, J. L., "The Damping of Structural Vibration by Rotational Slip in Joints," Journal of Sound and Vibration, Vol 53(3): 333-340, 1977.
8. Srinivasan, A. V., Cassent, B. N., and Cutts, D. G., "Characteristics of Dry Friction Damping," AFWAL Vibration Damping 1984 Workshop Proceedings.
9. Den Hartog, J. P., "Forced Vibrations with Combined Couloumb and Viscous Friction," Transactions ASME, Vol. 53: 107-115, 1931.
10. Pratt, T. K., and Williams, R., "Non-Linear Analysis of Stick/Slip Motion," Journal of Sound and Vibration, Vol.74(4): 531-542, 1981.
11. Ungar, E. E., "The Status of Engineering Knowledge Concerning the Damping of Built-Up Structures," Journal of Sound and Vibration, Vol. 26(1): 141-154, 1973.

12. Earles, S. W. E., and Philpot, M. G., "Energy Dissipation at Plane Surface in Contact," Journal of Mechanical Engineering Science, Vol. 9: 86-97, 1967.
13. Panovko, Ya. G. , Goltzev, D. I., and Strakov, G. N., "Elementary Problems of Structural Hysteresis," Voprosy Dinamiki i Prochnosti V. Riga, p. 5, 1958.
14. Goodman, L. E., "A Review of Progress in Analysis of Interfacial Slip Damping," Structural Damping, Ed. J. Ruzicka, ASME, New York, pp 35-48, 1960.
15. Craig, R. R. Jr., "Recent Literature on Structure Modeling Identification, and Analysis," Mechanics and Control of Large Flexible Structures, Progress in Astronautics and Aeronautics, Vol. 129: 3-29, 1990.
16. Richardson, R. S. H., and Nolle, H., "Energy Dissipation in Rotary Structural Joints," Journal of Sound and Vibration, Vol. 54(4): 577-588, 1977.
17. Steidel, R. F. Jr., An Introduction to Mechanical Vibrations, Third Edition, New York, John Wiley & Sons, Inc., 1989.
18. Greenwood, D. T., Principles of Dynamics, New Jersey, Prentice-Hall, Inc., 1965.
19. Reid, J. G., Linear System Fundamentals, Continuous and Discrete, Classic and Modern, USA, McGraw-Hill, Inc., 1983.
20. Clark, S. K., Dynamics of Continuous Elements, New Jersey, Prentice-Hall, Inc., 1972.
21. Griffel, W., Beam Formulas, Frederick Ungar Publishing Co., New York, 1970.
22. Stokey, W. F., "Vibration of Systems Having Distributed Mass in Elasticity," Shock and Vibration Handbook, Third Edition, McGraw-Hill Book Co., 1988.
23. Bagley, R.L., Class Notes MECH 610, Structural Vibrations. School of Engineering, Air Force Institute of Technology (AU), Wright-Patterson AFB OH, June 1992.
24. Ferri, A.A., Heck, B.S., "Active and Passive Joints for Damping Augmentation of Large Space Structures", Proceedings of the 1990 American Control Conference, 9th, San Diego, CA, Vol 3: 2978-2983, 1990.

25. NASA Tech Briefs, MSC-21786, "Torque, Tension, and Friction in Bolts", Technical Support Package, Lyndon B. Johnson Space Center, Houston, Texas, 77058.
26. Williamson, J.B.P., "The Shape of Surfaces", CRC Handbook of Lubrication (Theory and Practice of Tribology), Vol II, CRC Press Inc., Boca Raton, Florida: 3-16, 1983.
27. Ballinger, R.S., Finite Element Analysis of Frictional Damping Forces in Structural Joints Subjected to Flexural Vibration, Phd Dissertation, College of Engineering, University of Cincinnati, Cincinnati, OH, 1990.
28. Vasarhelyi, D.D., and Chiang, K.C., "Coefficient of Friction in Joints of Various Steels", Journal of the Structural Division, Proceedings of the American Society of Civil Engineers, 93(ST4):227-243, 1967.
29. Ludema, K.C., "Friction", CRC Handbook of Lubrication (Theory and Practice of Tribology), Vol II, CRC Press Inc., Boca Raton, Florida: 31-48, 1983.
30. Groper, M., "Microslip and Macroslip in Bolted Joints", Journal of the Society for Experimental Mechanics, Inc (SEM), Experimental Mechanics, 25(2): 171-174, June 1985.
31. Fuller, D.D., "Friction", Mark's Standard Handbook for Mechanical Engineers, Eight Edition, New York, McGraw-Hill Book Company: 3-24 to 3-32, 1978.
32. Armstrong-Helouvry, B., Control of Machines with Friction, Boston, Kluwer Academic Publishers, 1991.
33. Unholtz-Dickie Corporation. Operation and Maintenance Manual for Model 5PM Shaker, Model TA30 Power Amplifier, and Oscillator-Servo-Programmer (OSP-4). Wallingford, Connecticut.
34. ENDEVCO Dynamic Instrument Division. Specifications sheet for the ENDEVCO Accelerometer Model 2235C. Pasadena, California.
35. PCB Piezotronics, Inc. Operating Guide for PCB Force Transducer Model 208A02 and PCB Battery Power Unit Amplifier Model 480C06. Buffalo, New York.
36. Mechanical Technology Incorporated. MTI Fotonic Sensor Instruction Manual. Latham, New York.

37. Measurements Instruments Division. Nicolet Multipro Data Acquisition Systems Operation Manual. Madison, Wisconsin.
38. Rank Taylor Hobson Limited. Surtronic 3 Operation and Calibration Manual. Tritek Machinery, Cincinnati, OH.
39. Carron & Company. Specification Sheet on Miniature Modular Transducer. Inkster, Michigan.
40. Eaton Corporation. Lebow Load Cell And Torque Sensor Handbook No. 570. Troy, Michigan.

Vita

John P. Santacroce was born on 17 March 1961 in Wichita Falls, Texas. John enlisted in the Air Force in December 1983 while attending the University of Texas at Austin, where he obtained his Bachelor of Science Degree in Aerospace Engineering in December 1984. After earning his commission at the Officer Training School in 1985, John's first assignment was to Sunnyvale AFS (currently Onizuka AFB) California, where he worked as a Satellite Operations Engineer performing on-orbit command and control of satellites. John's next assignment was to Falcon AFB Colorado performing the same mission. After four years, he left Falcon AFB to attend the Air Force Institute of Technology at Wright-Patterson AFB Ohio to complete a Master of Science degree in Astronautical Engineering.

He married Miss Denise A. DeFord of Houston Texas in 1984. They have two children: Zachary Patrick and Christopher Travis.

Permanent Address: 9607 Caney Creek
San Antonio, Texas 78245
(513) 673-7755

